Thermal Diffusion in Liquid Mixtures and Polymer Solutions by Molecular Dynamics Simulations

Vom Fachbereich Chemie
der Technischen Universität Darmstadt

zur Erlangung des akademischen Grades eines
Doctor rerum naturalium (Dr. rer. nat.)

genehmigte
Dissertation

vorgelegt von

Dipl.-Ing. Meimei Zhang
aus Zhe Jiang, China

Berichterstatter:	Professor Dr. Florian Müller-Plathe
Mitberichterstatter:	Professor Dr. Rolf Schäfer
Tag der Einreichung:	12. 12. 2006
Tag der mündlichen Prüfung:	05. 02. 2007

Darmstadt 2006

D17

ACKNOWLEDGMENTS

I would like to thank my thesis advisor, Professor Dr. Florian Müller-Plathe for his support, his guidance and his patience to make this thesis possible.

I would also like to thank my colleagues, Dr. Sudip Roy, Dr. Hossein Eslami, and Dr. Volker Weiss, for the English correction of the thesis. Thanks to Dr. Bernd Schilling for the format help.

Special thanks to my colleague Mr. Thomas Müller and our secretary Ms. Gabriele General for the German language help.

I also want to thank Professor Dr. Giuseppe Milano at the University of Salerno for helpful discussion in my research.

Thanks to Professor Dr. Rolf Schäfer and the other defense committee members for showing interests to this thesis.

Thanks to all the members in the research group for giving me friendship and happiness.

Finally, I would thank my family for their endless support.

Contents

List of Figures

List of Tables

Zusammenfassung

Diese Arbeit beschäftigt sich mit der Simulation von Transportprozessen von Wärme oder Materie in binären isotropen Flüssigkeiten unter einem so schwachen Temperaturgradienten, dass für das System die Lineare-Antwort-Theorie angewendet werden kann. Als weitere Einschränkung tritt keine Konvektion und kein viskoser Fluss auf. Unter diesen Bedingungen werden folgende vier Transportparameter des Systems mit Molekulardynamik-Simulation untersucht:
- die Wärmeleitfähigkeit,
- der Diffusionskoeffizient des Teilchentransports,
- der Soret-Koeffizient,
- der Wärmediffusionskoeffizient der Interaktion zwischen Wärme- und Massentransport.

Zur Berechnung der Wärmeleitfähigkeit und des Soret-Koeffizienten wird die "Reverse non-equilibrium molecular dynamics" (RNEMD) Methode eingesetzt, während konventionelle Molekulardynamik Simulationen benutzt werden um den Massendiffusionskoeffizienten zu bestimmen, der zur Berechnung des Thermodiffusionskoeffizienten benötigt wird.

Für Benzol, Cyclohexan und verschiedene Mischungen dieser beiden Substanzen wurde der Einfluss verschiedener Simulationsparameter auf die verschiedenen Varianten von Simulationen untersucht. Die varierten Parameter waren die Intensität der am System angelegten Störung (inklusive der Störungsintensität der RNEMD Methode), die Länge der cutoff-Radien, die Systemgrösse und die Verwendung eines Thermostaten. Die Moleküle wurden jeweils durch ein vollständiges "all-atom"-Modell dargestellt. Zusammenfassend können die Ergebnisse wie folgt charakterisiert werden: Während die Störungsintensität nur einen geringen Einfluss auf die Wärmeleitfähigkeit hat, beeinflusst sie den Soret-Koeffizienten markant. Eine Vergrösserung des cutoff-Radius führt oberhalb einer gewissen Länge zu keiner signifikanten Veränderung des Soret-Koeffizienten. Ein System mit einigen hundert bis wenigen tausend Molekülen, das eine Simulationsbox mit ein paar Nanometern Seitenlänge aufweist, genügt, um Grösseneffekte in der Berechnung der Wärmeleitfähigkeit und des Massendiffusionskoeffizienten vermeiden. Ausserdem hat die Verwendung eines Berendsen-Thermostaten keinen nennenswerten Einfluss auf die Wärmeleitfähigkeit. Das Kraftfeld hingegen kann die Resultate entscheidend beeinflussen. Zwei Kraftfelder, die sich nur leicht in den Parametern der nicht bindenden Kräfte unterschieden, führten zu einer Abweichung von 30% bei der Wärmeleitfähigkeiten von Cyclohexan und von 20% beim Soret-Koeffizienten von Benzol-Cyclohexan-Mischungen. Auch die Freiheitsgrade der verwendeten Modelle haben entscheidenden Einfluss auf die Wärmeleitfähigkeit. Die Eliminierung der Bindungsschwingungen bei aliphatischen und aromatischen Wasserstoffen führt zu Wärmeleitfähigkeiten, die näher am experimentellen Wert liegen. Die meisten der berechneten Wärmeleitfähigkeiten weichen 30-50% von experimentellen Werten ab. Solche Abweichungen sind jedoch für Berechnungen von Transportparametern nicht

unüblich. Und auch wenn die Soret-Koeffizienten (3-5) × 10^{-3} K^{-1} grösser sind als die experimentellen Werte, sind die Resultate dieser Rechnungen deutlich besser als jene früherer Simulationen. Überdies reproduzieren unsere Resultate die Abhängigkeit des Soret-Koeffizienten vom Molenbruch und der Temperatur.

Ebenfalls wurde im Rahmen dieser Arbeit die Thermodiffusion in verdünnten Polymerlösungen zum ersten Mal mit der RNEMD Methode untersucht. Die Polymere wurden dabei durch ein allgemeines Kugel-Feder-Modell dargestellt. Zunächst wurde der Einfluss der Qualität des Lösungsmittels auf den Soret-Koeffizienten untersucht. Bei konstanter Temperatur und Polymeranteil führt eine bessere Qualität des Lösungsmittels zu einer Akkumulation des Polymers in der kälteren Region des Systems. Die kann sogar zu einer durch die Thermodiffusion bedingten Phasenseparation führen. Die von Experimenten her bekannte Unabhängigkeit des Thermodiffusionskoeffizienten vom Molekülgewicht der Polymere wurde durch Berechnung für drei verschiedene Gruppen von Polymeren mit unterschiedlicher Steifheit der Ketten bestätigt. Die Thermodiffusionskoeffizienten erreichen einen konstanten Wert, wenn die Länge des Polymers dem 2-3 fachen der Persistenzlänge entspricht. Überdies wurde gezeigt, dass starre Polymere einen höheren Soret-Koeffizienten und höhere Thermodiffusionskoeffizienten aufweisen als flexible Polymere.

Unsere Simulationen bestätigen die Anwendbarkeit der RNEMD Methode zur Untersuchung von Wärmeleitung und Massentransport. Auf dieser Grundlage kann sie auch auf weitere Systeme angewendet werden, um dort mikroskopische Mechanismen von Transportprozessen zu untersuchen.

Abstract

This thesis is focused on simulating the transport processes of heat and matter under a sufficiently weak temperature gradient where the system linearly responds. The systems we are interested in are binary isotropic liquids with no convection and no viscous flows. Four related transport coefficients of the systems, the thermal conductivity of heat conduction, the diffusion coefficient of matter transfer, the Soret coefficient and the thermal diffusion coefficient of the cross effect between the heat and mass transfer, are investigated by the method of molecular dynamics. The reverse non-equilibrium molecular dynamics (RNEMD) method is the tool to compute the thermal conductivity and the Soret coefficient, while the equilibrium molecular dynamics is used to obtain the mutual diffusion coefficient which is needed for the calculation of the thermal diffusion coefficient.

The influences of the simulation parameters are investigated in benzene, cyclohexane and their mixtures. These parameters include the perturbation intensity of the RNEMD method, the cutoff length, the system size, and the presence of a thermostat. These molecules are represented with all-atom models. The perturbation intensity has only a small impact on the thermal conductivity, while it affects the Soret coefficient significantly. Above a certain value, longer cutoff length does not yield substantial difference for the Soret coefficients. A system of several hundred to some thousand molecules and of several nanometers in length is sufficient to avoid size effects in the calculations of the thermal conductivity and the mutual diffusion coefficient. The presence of the Berendsen thermostat is harmless for the calculation of the thermal conductivity. The force field potentially affects the results largely. Two groups of force fields slightly different in the non-bonded parameters produce thermal conductivities for cyclohexane which differ by 30%, and lead to about 20% deviation for the Soret coefficient of a benzene-cyclohexane mixture. The degrees of freedom of the model are found to affect the thermal conductivity significantly. Eliminating the vibrational freedom of the aliphatic and aromatic hydrogens yields thermal conductivities closer to the experimental values.

Most of the thermal conductivities we obtain have deviations at around 30-50% from the experimental values. Such deviations are quite common in the calculations of transport coefficients. Although the Soret coefficients were (3-5) $\times$ 10^{-3} K^{-1} larger than the experimental values, our simulation yielded the best results compared to previous simulations. Furthermore, our results reproduced the dependence of the mole fraction and the temperature of the Soret coefficients. Thermal diffusion in dilute polymer solutions has also been studied for the first time by the RNEMD method. The polymers are represented by a generic bead-spring model. The influence of the solvent quality on the Soret coefficient is investigated. At constant temperature and monomer fraction, a better solvent quality causes a higher affinity for the polymer to the cold region. This may even go to thermal-diffusion-induced phase separation. The experimentally known independence of the thermal diffusion coefficients of the

molecular weight is reproduced for three groups of polymers with different chain stiffnesses. The thermal diffusion coefficients reach constant values at chain lengths of around 2-3 times the persistence length. Moreover, rigid polymers have higher Soret coefficients and thermal diffusion coefficients than more flexible polymers.

Our simulations validate the applicability of the RNEMD methods to investigate heat conduction and matter transport. Potentially, the method can be extended to more systems to study the microscopic mechanisms of transport processes.

1. Introduction

Transport processes, such as heat conduction, electrical conduction and diffusion, are universal phenomena and play an important role in understanding the properties of fluids. When two or more irreversible transport processes happen simultaneously, they may interfere with each other. In this thesis, thermal diffusion or the coupling between heat conduction and mass transfer is the major topic. Thermal diffusion can be characterized quantitatively by thermal diffusion coefficient (D_T) or the Soret coefficient (S_T).

1.1 Definition and significance of the research in thermal diffusion

Thermal diffusion or the Ludwig-Soret effect was initially discovered by Ludwig [1] in the study of sodium-sulfate solution in 1856. He found a small difference in the concentration profile when the solution was heated from below: the salt was more concentrated near the cold end than near the hot end of the tube. About twenty years later, Soret made the first systematic investigation in electrolyte solutions [2]. From their observations, thermal diffusion is defined as a flux of matter driven by a temperature gradient resulting in a concentration gradient in steady-state conditions.

The Soret effect is ubiquitous in nature. It is a side-effect when the thermal conductivity is measured in mixtures of fluids. It happens in the operation of solar ponds [3], in the formation of the salt concentration in different layers of oceans [4], in the natural gas and petroleum reservoirs [5,6], in the mass transport across biological membranes induced by small temperature gradients in living tissue [7], and perhaps even in the convection within stars [8]. The active application of thermal diffusion is limited to some specific important fields. An early application was the separation of the uranium isotopes using thermal gradient column in 1940s [9]. The most important remaining application of the Soret effect is to optimize exploitation of oil reservoirs; however, a perfect knowledge of the fluid physics in crude oil reservoirs is still a challenge. Technically and analytically, the Soret effect can also be used in macromolecules fractionation [10].

One important motivation of Soret effect research in condensed matters is pure scientific challenge. “It is the only hydrodynamic transport mechanism that lacks a simple physical explanation” [11]. Until now, for this transport coefficient, no approximate prediction could be made even for closely related systems. However, in recent years, the development of experimental and simulation techniques has brought about a growing interest in Soret effect.

1.2 Historical background of thermal diffusion research

1.2.1 Theoretical studies

In the 1910s, Enskog [12] and Chapman [13] developed a kinetic theory that successfully predicted the thermal diffusion in dilute gases by giving a solution of Boltzmann's equation. According to this theory, the thermal diffusion coefficient of gas mixture is related to the masses, the sizes, and the composition of the species. The theory was proved experimentally by Chapman and Dootson [14]. In 1922, Enskog proposed a so-called the Standard Enskog Theory (SET) for a simple dense hard-sphere fluid [15]. In the 1970s, van Beijeren and Ernst [16] extended the SET for simple fluids to the Revised Enskog Theory (RET), where they gave a general form of the solutions of their kinetic equations for the dense multi-component mixtures. Later, López de Haro et al. derived explicit expressions for the transport coefficients in terms of the diameters, masses, and concentrations [17-18]. The RET is strictly valid only for hard-sphere mixtures. The theory derived some trends for the thermal diffusion coefficient of hard-sphere mixtures: (i) in mixtures of species of different masses, the heavier component migrates to the cooler region; (ii) if the species have the same mass, then the larger component diffuses into the cooler region. However, the kinetic theory is no longer valid if soft interactions are involved. In the 1930s, Onsager [19] proposed his "reciprocity relations" for a phenomenological description of irreversible transport processes, especially of the thermal diffusion and other cross effects, such as the coupling between the heat conduction and electrical current, and the heat conduction under a concentration gradient (Dufour effect). It states a linear coupling of the interference of two or more related transport processes in a thermodynamic system. On the basis of Onsager's theory and the binary Liouville equation, Bearman et al. [20] derived microscopic expressions for the Soret coefficient, which consist of the interaction potentials in molecular mixtures. However, the results of this work are not in a form that allows a direct comparison with experiments.

Due to the failure of the kinetic theory for dense realistic fluids where soft interactions exist, thermodynamic contributions were accounted for in newer theories. There are mainly two approaches to introduce the thermodynamic contributions. The first approach is the so-called phenomenological approach, where phenomenological equations of irreversible thermodynamics related to molar enthalpy and chemical potential of components are used. Hasse's [21] and Kemper's [22] models are based on this approach. The second one is the so-called kinetic approach, where the Soret coefficient is related to the activation energy of molecular motion. Rutherford's [23], Dougherty and Drickamer's [24], as well as Shukla and Firoozabadi's [25] models employed this concept. In these two approaches the estimation of the thermodynamic properties such as partial molar enthalpy, chemical potentials, activation energies in mixtures are approximated, which lowered their predictive power. There are also several models developed for the thermal diffusion of macromolecules. For example, based on the Smoluchowski equation for a single polymer chain, Khazanovich [26] formulates D_T as proportional to the polymer segmental diffusion coefficient and the solvent activation energy for viscous flow, and as inversely proportional to the temperature. Schimpf and Semenov's thermophoresis theory [27] predicts that D_T is

related to the properties of the solvent and the effective segmental size of polymer chains. Luettmer-Strathmann [28] proposed a two-chamber (with different temperatures) lattice model. By measuring the partition of the polymers and solvents in the two chambers she could calculate the Soret coefficient. This model predicts the sign change of the Soret coefficient in polyethylene oxide (PEO)-water-ethanol solutions. Very recently, Dhont [29] developed a microscopic approach to thermodiffusion in colloidal solutions. In this approach the contribution of inter-colloidal interactions to the thermal diffusion coefficient are considered, which explained the sign changes of the Soret coefficient with temperature and/or concentration under appropriate conditions. Although, the theoretical models can predict the thermal diffusion qualitatively, they perform poorly with quantitative accuracy in most cases.

1.2.2 Experimental studies

The experimental instruments for measuring the Soret effect can be divided into convective and nonconvective. The best known convective one is the thermo-gravitational column [30]. In this kind of instruments, the convection processes enhance the separation of species of different masses. They disappear after a stable concentration profile is formed. The main nonconvective ones include techniques of diffusion cell [31] (the standard Soret cell and the beam deflection technique), thermal field flow fractionation (TFFF), and the thermal diffusion forced Rayleigh scattering (TDFRS) [32]. This kind of instruments intends to establish stable thermal and mechanical conditions and to avoid convection processes which lead to a re-mixing of the components.

In thermogravitational columns [30], the liquid is kept within the narrow space between two concentric vertical pipes. The lighter component concentrates near the hot wall and the heavier one near the cold. Due to convection, the lighter one would migrate to the top of the column and the heavier one stays at the bottom. In this method, convection amplifies the separation effect, and this can be utilized in the separation of isotopes [9], and for polymer fractionation [33]. Modern state-of-the-art gravitational columns have typical lengths between 30 and 50 cm. [30]. The Soret coefficient can be obtained by measuring the concentration difference between the bottom and the top, then excluding the separation effect due to gravity.

The diffusion cell [31] consists of two horizontal rigid planar plates, which are maintained at different temperatures in order to create a vertical temperature gradient in a parallelepipedic working space. The system is heated usually from above in order to avoid free convection. The refractive index gradient induced by the concentration gradient can be read out by the deflection of a laser beam crossing the liquid layer horizontally when the two opposite lateral layers are made of glass of good optical quality, or by extracting small amount of the samples at different isothermal layers and analyzing them with refractometer or densimeter. The technique with the former read-out method is the beam deflection technique, and the later one is named the standard Soret cell.

Thermal field flow fraction [10] (TFFF) is a liquid chromatography technique for chemical fractionation of macromolecules, which employs a temperature gradient perpendicular to a narrow flow channel with a parabolic flow profile of solvents. Therefore, the macromolecules next to the channel wall region have a lower velocity to flow out. Differential retention makes it possible to measure thermal diffusion parameters for various macromolecules and colloids by using the characteristic thickness of the solute layer calculated from their retention time.

TDFRS, or "holographic grating technique", is probably the newest technique to measure thermal diffusion. In TDFRS [32], a first laser beam split into two beams of equal intensity crosses the fluids in a glass container. At the intersection of the two laser beams, interference fringes are created and by putting some chemically inert dye in the mixture a temperature grating is produced. This periodic temperature field induces via the Soret effect a periodic concentration profile. Both the temperature grating and the concentration grating create an index of refraction grating, which is read out by a second laser by Bragg diffraction.

In 1938, Clusius and Dickel [34] initially applied a thermogravitational column method in salt solutions to study the Soret effect. In 1950s, Prigogine et al. [35] measured for the first time the Soret coefficient in molecular fluids (cyclohexanol-cyclohexane) by the same thermogravitational method. They reported a large change with composition, not only of the magnitude, but also of the sign. They also tried a qualitative explanation using free energy and entropy considerations. Later, Tichacek [36] measured the thermal diffusion in water-ethanol mixtures, and also observed a sign change with composition. In 1988, Kolodner et al. [37] confirmed this observation of Tichacek, and obtained more reliable Soret coefficients by using the beam-deflection technique. Although there are many data obtained by different groups on different systems, it took until the 1990s to obtain mutually consistent results for toluene-*n*-hexane [38, 39] and water-ethanol mixtures [37, 38]. Recently, mutual agreement of various techniques has been reached in a benchmark test on binary mixtures of dodecane, isobutyl benzene and tetralin [40]. With the development of modern techniques, such as the optical method TDFRS, research on measuring the thermal diffusion coefficient became more popular over the last few years. This technique was used also in *n*-pentane-*n*-decane [41], benzene-cyclohexane [42, 43], isotopically substituted dibromohexane-cyclohexane [43] alkane-benzene [44] mixtures, and even for polymer solutions [45-47]. The new techniques did away with convection in the sample and assured the reliability of the results. One major finding of this set of experiments is that quite a number of liquid mixtures change their thermal diffusion behaviour substantially with the composition. For example, a sign change of the Soret coefficient with composition was observed in cyclohexanol-cyclohexane [35], water-alcohols [37] alkane-benzene [44], isotopically substituted dibromohexane-cyclohexane [43], benzene-cyclohexane mixtures [43], as well as even ternary octane-decane-1-methylnaphthalene [48] mixture. More recently, it has also been observed that the temperature dependence of the Soret coefficient depends on the composition [43, 44]. The other important finding is that the Soret coefficient can be split into additive contributions from different parts of the molecular architecture: the mass effect, which comprises the mass and the moment of inertia difference of the species, and a *so-called* chemical effect, which depends on the interactions among the species (the composition effect belongs to this part). This has

been observed by Debuschewitz et al. in the benzene-cyclohexane system [42]. However, there is still no microscopic understanding of the results.
Different from low molecular weight mixtures, unusual thermal diffusion properties were found in polymer solutions. Schimpf et al. [49] were the first to prove that the thermal diffusion coefficient was independent of chain length and branching topology by testing twenty-nine dilute polystyrene-ethylbenzene solutions with the ThFFF method. Later, the same phenomenon was observed in polystyrene-ethylacetate system [50]. Recently, It has been found that in dilute, semi-dilute, and concentrated polystyrene-toluene solutions [51], the thermal diffusion coefficients are molar mass independent over the entire concentration range. Furthermore, dependence of the sign of the Soret coefficient on the solvent quality was found for polymer solutions. In 1977, Giglio and Vendramini [52] unexpectedly observed a negative Soret coefficient for poly (vinyl alcohol) in water, which was very close to poor solvent condition. Later, Wiegand et al.[40, 46, 47] investigated the PEO-water-ethanol system, and found the sign of Soret coefficient changed with the composition of water. The sign change of Soret coefficient with solvent quality has also been observed in dilute charged colloids solutions [53, 54], and in poly (N-isopropylacrylamide)-ethanol solutions [55], where the phase transition is thermal induced. Above all, in polymer solutions, the interactions between solute and solvent are very important, so that the solvent quality determines the value and even the sign of Soret coefficient. Such interactions include hydrogen bonding, electrostatic effects according to the types of the solutions.

1.2.3 Simulation studies

Molecular dynamics (MD) simulations have become an important tool in the investigation of transport processes in molecular liquids [56]. The advantages of molecular dynamics over the experiments in thermal diffusion studies are twofold: first, in molecular dynamics, each parameter that affects the thermal diffusion, such as mass, size, moment of inertia, and interaction potential, can be tuned independently and even unphysically; second, molecular dynamics helps to understand the mechanism of thermal diffusion microscopically, as the motion of each particle can be followed. During the 1980s, many approaches based on irreversible thermodynamics and nonequilibrium statistical mechanics have been developed to compute the Soret coefficient in binary mixtures using molecular dynamics methods. There are generally three molecular dynamics methods to simulate thermal diffusion: equilibrium molecular dynamics (EMD) which uses the Green-Kubo relations to calculate the transport coefficients [57,58], synthetic (homogeneous) molecular dynamics, where the system is locally driven out of equilibrium through an external force [59-61], and direct (boundary driven) non-equilibrium molecular dynamics [11], which mimics the real thermal diffusion experiment by modifying the conditions at the boundaries of the simulation box. The details of the different molecular dynamics methods will be introduced in Section 2.

Compared to the experimental methods, simulations were performed quite late in the thermal diffusion study. Most of the work has been devoted to improving the methods and was applied to Lennard-Jones liquids because they are relatively simple to model [62-66]. In 1986, MacGowan and Evans [66] for the first time calculated the Soret

coefficient of a dense argon-krypton mixture with a synthetic non-equilibrium molecular dynamics (S-NEMD) simulation. The results were confirmed later by Paolini and Ciccoti [64]. Hoheisel et al. estimated the Soret coefficients roughly for CH_4-CF_4 [67], and benzene-cyclohexane mixtures [68] using rigid-body models with EMD simulations. These results remained qualitative because of large uncertainties. In early 1990s, Kincaid and Hafskjold [11, 69, 70] developed a direct non-equilibrium molecular dynamics algorithm and tested it for the high density Ar-Kr fluids. More recently, the algorithm has been modified and utilized in simulations of different Lennard-Jones fluids [62, 63, 66, 71]. The simulations proved that larger mass, smaller size, as well as higher depths of the interaction potentials (higher cohesion) helps the species migrate to the colder side; and the contributions of these three parameters to thermal diffusion are additive. For application to petroleum reservoirs, the algorithm was also utilized together with a more realistic united atom model to simulate *n*-alkanes [41, 72]. It was also extended to associating fluids, such as water plus methanol, ethanol, acetone, and dimethyl sulfoxide, by Nieto-Draghi et al. [73] and Rousseau et al. [74]. They studied the sign change related to the composition. Besides to bulk fluids, the direct NEMD method was also employed to simulate the thermal diffusion in porous media [75, 76]. Around 2002, Perronace et al. [41] did the first verification between the experimental data and the simulation results for *n*-pentane-*n*-decane mixture. They compared the experimental data and the simulation results of both EMD and NEMD simulations. All these explorations still could not establish whether molecular dynamics is reliable enough to give a significant improvement to thermal diffusion studies.

The introduction above shows that the microscopic mechanism of thermal diffusion is far from being explained clearly and the prediction of precise amount of thermal diffusion still needs a good exploration.

1.3 Aim and layout of the thesis

This research aims at two major goals. The first one is to extend the applicability of the reverse non-equilibrium molecular dynamics (RNEMD), one of the direct NEMD algorithms, to more realistic molecular fluid systems and to polymer solutions. Previous research showed that the usefulness of the direct NEMD for simulating thermal diffusion in realistic molecular fluid was only shown for a limited number of systems such as water-alcohol and *n*-alkane mixtures; and there were barely any simulation studies for polymer solutions.

The second goal is to explore the molecular origin of the thermal diffusion behavior. Specifically, we are mainly interested in two features observed. The first one is that thermal diffusion depends, sometimes strongly, on composition [35, 36, 42, 73]. We choose one group of realistic molecular fluids, benzene-cyclohexane mixture, to study this topic. The second one is unique for polymer solutions: thermal diffusion coefficient is independent of the chain length [49, 50], but the solvent quality affects the thermal diffusion strongly. Model polymer solutions are investigated.

In Section 1, we introduce the background theory of irreversible transport processes, including the relationship between the transport coefficients of heat conduction and mass transfer described by Onsager reciprocal relations. Equations, with which different molecular dynamics methods calculate the Onsager transport coefficients, are also introduced. The reverse non-equilibrium molecular dynamics algorithm is described in detail.

Thermal diffusion is much related to heat conduction, and the thermal conductivity as well as the Soret coefficient can be calculated from the same simulation for given system. The thermal conduction is a diagonal transport mode in the Onsager picture. Therefore, it is a much more pronounced effect than the off-diagonal Soret effect. As a result, it has a much better signal-to-noise ratio and much shorter sampling simulations are needed for a satisfactory statistical accuracy. Hence, in Section 2 we investigate the impact of molecular models and the RNEMD algorithm parameters on thermal conductivity in systems of benzene, cyclohexane, and their mixtures. The algorithm variants and simulation parameters, such as different exchange frequencies, different force field parameters, and presence versus absence of a thermostat, are varied and tested.

Section 3 deals with the concentration dependence of the thermal diffusion coefficient and the Soret coefficient in benzene-cyclohexane mixtures. Except for the influence of the algorithm parameters and molecular models, the capability of the method when applied to molecular fluids is also tested by comparing to the experimental results.

In Section 4, we show the simulation results about the thermal diffusion in dilute polymer solutions. In the first part, the influence of the solvent quality on thermal diffusion is investigated. Further systems of varying chain lengths are simulated to learn whether the algorithm and the model can reproduce the chain-length independence of the thermal diffusion coefficient. The impact of the chain stiffness and the monomer mole fraction on the thermal diffusion is also investigated.

The final part of the thesis is a summary and outlook for the whole research work.

References

[1] C. Ludwig, Sitz.ber. Akad. Wiss. Wien Math.-naturw. Kl. **20**, 539 (1856).
[2] C. Soret, Arch. Geneve **3**, 48 (1879).
[3] W. Weinberger, Sol. Energy **8**, 45 (1964).
[4] M. Gregg, Sci. Am. **228**, 65 (1973).
[5] F. Montel, Entropie **184–185**, 86 (1994).
[6] F. Montel, Entropie **214**, 7 (1998).
[7] F. J. Bonner and L. O. Sundelöf, Z. Naturforsch. C **39**, 656 (1984).
[8] E. A. Spiegel, Annu. Rev. Astron. Astrophys. **10**, 261 (1972).
[9] F. G. Gosling, *The Manhattan Project: Making the Atomic Bomb* (DOE/MA-0001) (History Division, Department of Energy, Washington, 1999).
[10] J. C. Giddings, K. D. Caldwell, M. N. Myers, Macromolecules **9**, 106 (1976).

[11] B. Hafskjold, T. Ikeshoji, and S. K. Ratkje, Mol. Phys. **80**, 1389 (1993).
[12] D. Enskog, Ann. Phys. **36**, 731 (1912).
[13] S. Chapman, Philos. Trans. R. Soc. London Ser. A **217**, 115 (1917).
[14] S. Chapman and F. Dootson, Philos. Mag. **33**, 248 (1917).
[15] S. Chapman and T. G. Cowling, *The mathematical theory of non-uniform gases* (Cambridge University, Cambridge, 1952).
[16] H. van Beijeren and M. H. Ernst, Phys. Lett. A **43**, 367 (1973).
[17] M. López de Haro, E. G. D. Cohen, and J. M. Kincaid, J. Chem. Phys. **78**, 2746 (1983).
[18] M. López de Haro and E. G. D. Cohen, J. Chem. Phys. **80**, 408 (1984).
[19] L. Onsager, Phys. Rev. **37**, 405 (1931).
[20] R. J. Bearman, J. G. Kirkwood, and M. Fixman, Adv. Chem. Phys. **1,** 1 (1958).
[21] R. Hasse, Z. Phys. A **127**, 1 (1949).
[22] L. J. T. M. Kempers, J. Chem. Phys. **115**, 6330 (2001).
[23] Rutherford, W. M. and Roof, J. G. J. Phys. Chem. **1959**, *63*, 1506,
[24] E. L. Dougherty and H. G. Drickamer, J. Phys. Chem. **59**, 443 (1955).
[25] L. Shukla and A. Firoozabadi, Ind. Eng. Chem. Res. **37**, 3331 (1998).
[26] T. N. Khazanovich, J. Polym. Sci. C **16,** 2463 (1967).
[27] M. E. Schimpf and S. N. Semenov, J. Phys. Chem. B **104,** 9935 (2000).
[28] J. Luettmer-Strathmann, J. Chem. Phys. **119**, 2892 (2003).
[29] J. K. G. Dhont, J. Chem. Phys. **120,** 1632 (2004).
[30] M. M. Bou-Ali, O. Ecenarroy, J. A. Madariaga, C. M. Santamaría and J. J. Valencia, J. Phys.: Condens. Matter **10,** 3321(1998).
[31] J. Platten, J. Appl. Mech. **73**, 5 (2006).
[32] S. Wiegand and W. Köhler, in *Thermal Nonequilibrium Phenomena in Fluid Mixtures*, Lecture Notes in Physics Vol. 584, edited by W. Köhler and S. Wiegand (Springer, Verlag, 2002) p189.
[33] O. Ecenarro, J. A. Madariaga, J. L. Navarro, C. M. Santamaria, J. A. Carrion, and J. M. Saviron, Macromolecules **27**, 4968 (1994).
[34] K. Clusius and G. Dickel, Naturwissenschaften **26**, 546 (1938).
[35] I. Prigogine, L. de Broukere, and R. Amand, Physica **16**, 577 (1950).
[36] L. Tichacek, W. Kmak, and H. Drickamer, J. Phys. Chem. **60**, 660 (1956).
[37] P. Kolodner, H. Williams, and C. Moe, J. Chem. Phys. **88**, 6512 (1988).
[38] K. Zhang, M. Briggs, R. Gammon, and J. Sengers, J. Chem. Phys. **104**, 6881 (1996).
[39] W. Köhler and B. Müller, J. Chem. Phys. **103**, 4367 (1995).
[40] J. K. Platten, M. M. Bou-Ali, P. Costesèque, J. F. Dutrieux, W. Köhler, C. Leppla, S. Wiegand, and G. Wittko, Philos. Mag. **83**, 1965 (2003).
[41] A. Perronace, C. Leppla, F. Leroy, B. Rousseau, and S. Wiegand, J. Chem. Phys. **116**, 3718 (2002).
[42] C. Debuschewitz and W. Köhler, Phys. Rev. Lett. **87**, 055901-1 (2001).
[43] G. Wittko and W. Köhler, in *Thermodiffusion: Basics & Applications*, Edited by M. M. Bou-Ali and J. K. Platten (Mondragon Unibertsitatea, 2006) p399.
[44] P. Polyakov and S. Wiegand, in *Thermodiffusion: Basics & Applications*, Edited by M. M. Bou-Ali and J. K. Platten (Mondragon Unibertsitatea, 2006) p399.
[45] B.-J. de Gans, R. Kita, B. Müller, and S. Wiegand, J. Chem. Phys. **118**, 8073 (2003).
[46] B.-J. de Gans, S. Wiegand, and J. Luettmer-Strathmann, Phys. Rev. Lett. **91**, 245501 (2003).

[47] R. Kita, S. Wiegand, and J. Luettmer-Strathmann, J. Chem. Phys. **121**, 3874 (2004).
[48] A. Leahy-Dios, M. M. Bou-Ali, J. K. Platten, and A. Firoozabadi, J. Chem. Phys. **122**, 234502 (2005).
[49] M. Schimpf and J. Giddings, Macromolecules **20**, 1561 (1987).
[50] P. Rossmanith and W. Köhler, Macromolecules **29**, 3203 (1996).
[51] J. Rauch and W. Köhler, J. Chem. Phys. **119**, 11977 (2003).
[52] M. Giglio and A. Vendramini, Phys. Rev. Lett. **38**, 26 (1977).
[53] R. Piazza and A. Guarino, Phys. Rev. Lett. **88**, 208302-1 (2002).
[54] H. Ning, J. Buitenhuis, and S. Wiegand, in *Thermodiffusion: Basics & Applications*, Edited by M. M. Bou-Ali and J. K. Platten (Mondragon Unibertsitatea, 2006) p389.
[55] R. Kita, G. Kircher, and S. Wiegand, J. Chem. Phys. **121**, 9140 (2004).
[56] M. Allen, D. Tildesley, *Computer Simulation of Liquids* (Oxford University Press, Oxford, 1987).
[57] M. Schoen and C. Hoheisel, Mol. Phys. **52**, 33 (1984).
[58] M. Schoen and C. Hoheisel, Mol. Phys. **52**, 1042 (1984).
[59] D. J. Evans and G. P. Morriss, *Statistical mechanics of nonequilibrium liquids* (Academic Press, London, 1990).
[60] P. T. Cummings and D. J. Evans, Ind. Eng. Chem. **31**, 1237 (1992).
[61] G. V. Paolini, G. Ciccotti, Phys. Rev. A **35**, 5156 (1987).
[62] D. Reith and F. Müller-Plathe, J. Chem. Phys. **112**, 2436 (2000).
[63] P. Bordat, D. Reith, and F. Müller-Plathe, J. Chem. Phys. **115**, 8978 (2001).
[64] A. Perronace, G. Ciccotti, F. Leroy, A. Fuchs, and B. Rousseau, Phys. Rev. E **66**, 031201 (2002).
[65] D. MacGowan and D. Evans, Phys. Rev. **34**, 2133 (1986).
[66] G. Galliéro, B. Duguay, J.-P. Caltagirone, and F. Montel, Philos. Mag. **83**, 2097 (2003).
[67] H. M. Schaink and C. Hoheisel, Physica A **184**, 451 (1992).
[68] H. M. Schaink, H. Luo, and C. Hoheisel, J. Chem. Phys. **99**, 9912 (1993).
[69] B. Hafskjold and T. Ikeshoji, Mol.Phys. **81**, 251 (1994).
[70] B. Hafskjold and S. Ratkje, J Stat. Phys. **78**, 463 (1995).
[71] S. Yeganegi, J. Phys. Soc. Japan **72**, 2260 (2003).
[72] J.-M. Simon, D. Dysthe, A. Fuchs, and B. Rousseau, Fluid Phase Equilibr. **150-151**, 151 (1998).
[73] C. Nieto-Draghi, *Transport and structural properties of aqueous solutions of organic solvents*, Thesis Universitat Rovira i Virgili, Tarragona, 2003.
[74] B. Rousseau, C. Nieto-Draghi, and J. Bonet Avalos, Europhys. Lett. **67,** 976 (2004).
[75] J. Colombani, G. Galliéro, B. Duguay, J.-P. Caltagirone, F. Montel, and P.A. Bopp, Phys. Chem. Chem. Phys. **4**, 313 (2002).
[76] G. Galliéro, J. Colombani, B. Duguay, J.-P. Caltagirone, and F. Montel, Entropie **239–240**, 98 (2002).

2. Theory of heat conduction and matter transport in binary liquids

2.1 Definition of transport coefficients in Onsager reciprocal relations

In irreversible processes which are not so far from equilibrium, a system is divided into small subsystems and local equilibrium is assumed [1]. That is, every "small" volume element δV fulfills microscopic reversibility. Furthermore, the amount of particles inside δV is sufficient to define thermodynamic properties, such as entropy and temperature. In the whole system, the macroscopic irreversible processes are assumed to obey the same laws as the average regressions of fluctuations in the microscopic equilibrium systems.

In order to achieve local equilibrium, several conditions should be satisfied [1]: first, the thermodynamic forces should be sufficiently small to hold the linear response of the field conjugated flux; second, the whole system should be sufficiently close to equilibrium; third, the characteristic distances over which the thermodynamic forces vary should be sufficiently large so that these forces can be viewed as being constant over the microscopic length scale required to properly define a local thermodynamic state; fourth, the characteristic times over which the thermodynamic forces vary should be sufficiently long that these forces can be viewed as being constant over the microscopic times required to properly define a local thermodynamic state.

A single transport process in linear response to an imposed field, where the conjugated flux is proportional to the corresponding thermodynamic force, can be described by equations proposed more than one century ago [2]:

$$\vec{J} = -L\vec{X} \tag{2.1}$$

where $\vec{J}$ is the flux, $\vec{X}$ the thermodynamic force, and L a proportionality constant, or transport coefficient. For example, Fourier's law describes the first relation of such a type [3]:

$$\vec{J}_q = -\lambda\vec{\nabla}T \tag{2.2}$$

Here the heat flux $\vec{J}_q$ is related to a temperature gradient $\vec{\nabla}T$ with the proportionality constant λ, which is termed the "thermal conductivity" and characterizes the capability of the material to transport heat through the system. Fick's first law [3] is another example for the flux of matter $\vec{J}_m$ (the amount passing through unit area in unit time) caused by the molar concentration gradient $\vec{\nabla}c$:

$$\vec{J}_m = -D\vec{\nabla}c \tag{2.3}$$

where D is the diffusion coefficient in a common unit such as "$cm^2\ s^{-1}$". In an incompressible binary system regarding only the translational diffusion, we choose a reference frame where the flux of two species has the relation $\vec{J}_{m1} + \vec{J}_{m2} = 0$. When the molar concentration of the two species c_1+c_2 = const, the D of species 1 and species 2 are of the same value and satisfy:

$$\vec{J}_{m1} = -D\vec{\nabla}c_1 \quad \text{and} \quad \vec{J}_{m1} = -D\vec{\nabla}c_2 \tag{2.4}$$

Therefore, the system is characterized by one single diffusion coefficient, which is commonly notated as "mutual diffusion coefficient" D_{12}. Note that the value for D_{12} can be equally assigned in different frames of reference (e.g. mass-fixed, mole-fixed, …) [3]. In the following discussion, we will use the "mass-fixed frame of reference", where no net transfer of total mass crosses a fixed reference plane, to connect Onsager's relation with Fick's law.

Two or more transport processes may happen simultaneously and interfere with each other. Onsager reciprocal relations [4, 5] describe such coupling between irreversible transport processes, where the macroscopic flux is expressed as a linear combination of different forces. Therefore, the coupling processes of heat conduction and matter transfer in a multi-component mixture can be written in the following way.

$$\vec{J}_i = \sum_{j=1}^{n-1} L_{ij}\vec{X}_j + L_{iq}\vec{X}_q, \qquad i = 1, \ldots, n\text{-}1$$

$$\vec{J}_q = \sum_{j=1}^{n-1} L_{qj}\vec{X}_j + L_{qq}\vec{X}_q \tag{2.5}$$

where n denotes the total number of species, $\vec{X}_j$ the field (thermodynamic force) which drives the mass flux of species j, $\vec{X}_q$ the field which drives the heat flux, and $L_{\alpha\beta}$ the Onsager coefficients with $\alpha, \beta = (j, q)$. We will introduce their specific representations below. Note that this representation assumes that the flux is parallel to the driving force, otherwise each $L_{\alpha\beta}$ has to be a 3 × 3 tensor. In this work, only binary isotropic media are studied, where the driving force is always parallel to the flux. Hence, without loss of generality, we can use the scalar form to represent the Onsager relation in a binary system:

$$J_1 = L_{11}X_1 + L_{1q}X_q$$

$$J_q = L_{q1}X_1 + L_{qq}X_q \tag{2.6}$$

where the chemical-potential gradient and the temperature gradient are the thermodynamic forces:

$$X_1 = -\nabla_T[(\mu_1 - \mu_2)]/T \tag{2.7}$$

$$X_q = \nabla T / T^2 \tag{2.8}$$

Here μ_i is the chemical potential of species i (note the chemical potential here is defined in "J/g" instead of "J/mol" as the "mass-fixed frame of reference" is used). $\nabla_T\mu$ denotes a chemical potential gradient at constant temperature.

Of the two diagonal elements in equation (2.6), L_{11} is related to diffusion under a concentration gradient; and L_{qq} is connected to heat conduction under a temperature gradient. Of the two off-diagonal elements, L_{1q} is related to thermal diffusion, the diffusion of mass under a temperature gradient and L_{q1} is related to the Dufour effect, the heat transport under a concentration gradient. The assumption of microscopic reversibility of the system requires a general reciprocal relation to hold for equilibrium fluctuations as well as the macroscopic irreversible processes which obeys the same laws of fluctuation regression [4, 5]. According to the reciprocal relation, the two off-diagonal elements are equal: $L_{1q} = L_{q1}$. In the following discussion, we shall link the Onsager coefficients to the transport coefficients shown in equations (2.2) and (2.3).

First, if we assume the steady state of the non-equilibrium system is reached where the mass flux is zero, the relation between the thermal conductivity and Onsager coefficients can be derived from equations (2.2), (2.6) and (2.8):

$$\lambda_{J_1=0} = \frac{1}{T^2}\left[L_{qq} - \frac{L_{1q}^2}{L_{11}}\right] = -\left(\frac{J_q}{\nabla T}\right)_{J_1=0} \tag{2.9}$$

When the temperature gradient disappears, the mass diffusion of the system is only caused by the chemical potential gradient, i. e.,

$$J_1\big|_{\nabla T=0} = -L_{11}\frac{\nabla_T(\mu_1 - \mu_2)}{T} \tag{2.10}$$

If the "mass fixed frame of reference" is used in equation (2.3), and the unit of the mutual diffusion coefficient is kept as "$cm^2\ s^{-1}$", the molar concentration gradient may be replaced by the dimensionless weight fraction of species 1, w_1, and equation (2.3) can be rewritten as:

$$J_1\big|_{\nabla T=0} = -\rho D_{12}\nabla w_1 \tag{2.11}$$

where ρ is the overall mean density of the system given in "g/cm^3". It can be assumed to be a constant property since the system is close to equilibrium. Combining the two equations, we obtain the expression for the mutual diffusion coefficient as:

$$D_{12} = L_{11}\frac{\nabla_T(\mu_1 - \mu_2)}{\rho T\nabla w_1} \tag{2.12}$$

According to the Gibbs-Duhem relation [6], at constant temperature and pressure, the chemical potential of a multicomponent system has the following relation:

$$\sum_i w_i d\mu_i = 0 \tag{2.13}$$

Note that we also use dimensionless weight fraction of species i, w_i, to replace the normally used particle number to be consistent with the special definition of chemical potential here. Hence, in a binary system, the chemical potential gradient can be expressed as:

$$\nabla_T(\mu_1 - \mu_2) = \frac{1}{(1-w_1)}\frac{\partial\mu_1}{\partial w_1}\nabla w_1 \tag{2.14}$$

Combining equations (2.12) and (2.14), the relation between D_{12} and L_{11} is written as:

$$D_{12} = \frac{L_{11}}{\rho(1-w_1)T}\frac{\partial \mu_1}{\partial w_1} = \frac{L_{11}}{\rho T}\frac{1}{w_1(1-w_1)}\left(\frac{\partial \ln w_1}{\partial \mu_1}\right)^{-1} \tag{2.15}$$

The remaining question is how to link the transport coefficients for thermal diffusion with the Onsager coefficients. Phenomenologically, the law of thermal diffusion is defined as [7]:

$$J_1 = -D_{12}\rho\nabla w_1 - D_T \rho w_1(1-w_1)\nabla T \tag{2.16}$$

Comparing to equation (2.6), we obtain the link between D_T and L_{1q}:

$$D_T = \frac{1}{\rho T^2}\frac{1}{w_1(1-w_1)}L_{1q} \tag{2.17}$$

Finally, the definition of Soret coefficient is obtained for a system in the steady state, where $J_1 = -J_2 = 0$:

$$S_T = \frac{D_T}{D_{12}} = -\frac{1}{w_1(1-w_1)}\frac{\nabla w_1}{\nabla T} \tag{2.18}$$

2.2 Molecular dynamics calculation of transport coefficients

As mentioned in Section 1, there are three types of molecular dynamics methods to calculate the transport processes in liquids [1, 8-13]: equilibrium molecular dynamics (EMD), synthetic non-equilibrium molecular dynamics (NEMD), and direct (or boundary driven) NEMD. In the following the calculation of the Onsager transport coefficients with these methods is briefly introduced.

2.2.1 Equilibrium molecular dynamics (EMD)

The existence of the microscopic local fluctuation in equilibrated system makes EMD a possible way to test the transport processes in a microscopic view. In EMD, computation of the transport coefficients is relying on time correlation functions, which can be obtained by measuring the decay of spontaneous fluctuations of the flux (Green-Kubo (GK) relations [14-16]), or by measuring the accumulated displacements in properties over time (the integrated form of the GK relations, called Einstein relations). The GK relation of Onsager coefficient for isotropic system is in the form of [9]:

$$L_{\alpha\beta} = \frac{V}{3k_B}\int_0^\infty dt\left\langle \vec{J}_\alpha(t)\cdot\vec{J}_\beta(0)\right\rangle \tag{2.19}$$

where the angle brackets denote averaging over ensemble and over time, V is the volume of the system, and k_B the Boltzmann constant. In the form of Einstein relations, the Onsager transport coefficient is given by [2, 9]:

$$L \propto \lim_{t\to\infty} \frac{\left\langle [F(t)-F(0)]^2 \right\rangle}{t} \tag{2.20}$$

Here F is related to the corresponding flux with

$$\vec{J} = \frac{d\vec{F}}{dt} \tag{2.21}$$

We have introduced the concept of mutual diffusion coefficient D_{12} in Section 2.1. Different from mutual diffusion, self-diffusion is defined as the diffusion of a labeled particle among solvent particles which may be identical. Both self-diffusion coefficients and mutual diffusion coefficients can be calculated with the GK relation by using the relaxation time of the velocity-velocity autocorrelation function [2, 17]. For the self-diffusion coefficient of species i, the equation is:

$$D_i = \frac{1}{3}\int_0^\infty \left\langle \vec{v}^{\,i}(t)\cdot\vec{v}^{\,i}(0)\right\rangle dt \tag{2.22}$$

where $\vec{v}^{\,i}$ is the velocity vector of an individual particle of species i, and the averaging is performed over time origins and over all n_i particles. The mutual diffusion coefficient of a binary system can be calculated as follows [17, 18]:

$$D_{12} = \frac{Nx_1x_2}{3}\left(\frac{1}{x_1M_1}+\frac{1}{x_2M_2}\right)^2 (x_iM_i)\int_0^\infty \left\langle \vec{v}^{\,i}_{cms}(t)\cdot\vec{v}^{\,i}_{cms}(0)\right\rangle dt \tag{2.23}$$

where $\vec{v}^{\,i}_{cms}$ is the velocity vector of the center of mass of all particles of species i ($\vec{v}^{\,i}_{cms} = \frac{1}{n_i}\sum_{j=1}^{n_i}\vec{v}^{\,i}_j$), N the total number of particles in the system, n_i the number of particles of species i, M_i the molar mass of species i, and x_i its mole fraction. Here, the averaging is only performed over all time origins, since D_{12} is a collective quantity. The prefactor before the auto correlation function ensures that the mutual diffusion coefficients calculated from the motions of both species are of the same value.

One can also calculate the self-diffusion coefficient and mutual diffusion coefficient with Einstein equations, i. e. [18, 19],

$$D_i = \lim_{t\to\infty}\frac{1}{6t}\left\langle \left|\vec{r}^{\,i}(t)-\vec{r}^{\,i}(0)\right|^2\right\rangle \tag{2.24}$$

and

$$D_{12} = \frac{Nx_1x_2}{6t}\left(\frac{1}{x_1M_1}+\frac{1}{x_2M_2}\right)^2 (x_iM_i)\lim_{t\to\infty}\left\langle \left|\vec{r}^{\,i}_{cms}(t)-\vec{r}^{\,i}_{cms}(0)\right|^2\right\rangle \tag{2.25}$$

where $\vec{r}$ is the position vector. The subscripts and superscripts have the same meaning as in the GK relations. The mean squared displacement replaces the integrals of auto correlation function of velocity when Einstein relations are used.

The thermal conductivity λ is usually calculated with a GK relation by measuring the regression of equilibrium fluctuations of the heat flux [19]:

$$\lambda = \frac{1}{3k_B VT^2}\int_0^\infty \left\langle \vec{J}_q(0)\cdot\vec{J}_q(t)\right\rangle dt \tag{2.26}$$

In principle, the thermal diffusion coefficient can be calculated by a GK relation as [11, 20, 21]:

$$D_{\mathrm{T}} = \frac{V}{3k_B T^2 \rho w_1(1-w_1)}\int_0^\infty \left\langle \vec{J}_1(t)\cdot\vec{J}_q(0)\right\rangle dt \tag{2.27}$$

where a cross correlation function of two different fluxes is contained. Nevertheless, in practice the weak correlation between $\vec{J}_1$ and $\vec{J}_q$ in equilibrium system make it less efficient to calculate the cross coefficients. Equations (2.26) and (2.27) show that the calculation of the thermal conductivity and the thermal diffusion coefficient by GK relations need a microscopic definition of an instantaneous heat flux $\vec{J}_q(t)$ of the system. Of the many definitions and terminologies of the heat flux and energy flux, we use the one of Hafskjold et al. [12] with $\vec{J}_q$ denoting the "heat flux" and $\vec{J}_U$ the "internal energy flux":

$$\vec{J}_q = \vec{J}_U - \sum_{i=1}^{n-1}(h_i - h_n)\vec{J}_i \tag{2.28}$$

where h_i is the partial specific enthalpy of species i. There is no microscopic definition of h_i. The h of species n acts as the reference frames. In an ideal mixture, h_i is equal to that of the pure species i and does not dependent on the composition [12]. The microscopic internal energy flux can be expressed using the Irving-Kirkwood definition [9-12, 22]:

$$\vec{J}_U = \frac{1}{V}\sum_{i\in CV}\left(\left[\frac{1}{2}m_i(\vec{v}_i-\vec{v}_0)^2+\phi_i\right](\vec{v}_i-\vec{v}_0) - \frac{1}{2}\sum_{j=1}^{N}\left[(\vec{v}_i-\vec{v}_0)\cdot\vec{F}_{ij}\right]\vec{r}_{ij}\right) \tag{2.29}$$

where $i \in CV$ means the summation over all the particles in the controll volume, v_i is the velocity of particle i, v_0 the velocity of the reference frame, ϕ_i the potential energy of particle i in the field of all other particles, $\vec{F}_{ij}$ the force exerted on particle i by particle j, and $\vec{r}_{ij}$ the distance vector from i to j. Equation (2.29) suggests three contributions to the internal energy flux: the kinetic energy, the potential energy flux carried by each particle, and the energy transferred through intermolecular soft interactions. The negative sign in front of the third term means that the energy is transferred from i to j if i moves toward j against a repulsion from j. In the third term on the right hand side of equation (2.29), the factor ½ is not a symmetry factor, but a geometrical factor indicating the average spatial distribution of the intermolecular energy transfer [12].

The advantage of equilibrium molecular dynamics is that all quantities of the system can be obtained in a single simulation. Nevertheless, there are several disadvantages of EMD. First, the fluctuations naturally occurring in the system are quite small, leading to an unfavorable signal-to-noise ratio, and the Green-Kubo correlation functions decay in a slow algebraic fashion ($t^{-2/3}$ in three dimension) [23], and the long

time tail which may determine a considerable part of the transport coefficients might be hard to obtain due to the presence of noise. Second, the finite system size may cause a limit on the maximum time for which reliable correlations can be calculated. Third, the partial molar enthalpies of the different species for the calculation of the heat current $\vec{J}_q(t)$ are difficult to obtain in simulations.

2.2.2 Synthetic non-equilibrium molecular dynamics (S-NEMD)

The method is called "synthetic", because the mechanical perturbation created does not exist in nature. A *fictitious* external field interacts with the system to precisely mimic the linear thermal transport process. The S-NEMD algorithm is notationally complex. For detailed and precise formulation, the readers can refer to reference 1, 9 and 10. In S-NEMD, a perturbation field $\vec{F}_{ext}$ is added into the Hamiltonian motion of the system and drives the conjugate thermodynamic flux $\vec{J}$. The perturbation can remain constant starting from the beginning of the simulation, or occur as a pulse, or oscillate periodically. The applied field should not only be consistent with the periodic boundary conditions to ensure the homogeneous system, but also to ensure that the transport coefficient can be calculated from constitutive relation $L = \lim_{X\to 0}\lim_{t\to\infty} J/F_{ext}$. The reason of the second requirement is that in many cases the value of the transport coefficient at nonzero fields has no physical meaning due to the fictitious flux [8]. When the external field is applied, the Hamiltonian becomes [23]:

$$H = H_0 + A(\vec{r},\vec{p})\cdot\vec{F}_{ext}(t) \tag{2.30}$$

H_0 is the unperturbed Hamiltonian, $A(\vec{r},\vec{p})$ a function of particle positions and momenta, and $\vec{F}_{ext}(t)$ the time-dependent applied field. The translational equations of motion of particle *i* for the new Hamiltonian are given by:

$$\dot{\vec{r}}_i = \frac{\dot{\vec{p}}_i}{m} + \overleftrightarrow{C}_i\vec{F}_{ext}(t) \tag{2.31}$$

and

$$\dot{\vec{p}}_i = \vec{F}_i + \overleftrightarrow{D}_i\vec{F}_{ext}(t) \tag{2.32}$$

where the time derivatives are denoted by dots, $\overleftrightarrow{C}_i$ and $\overleftrightarrow{D}_i$ are phase space functions of suitable tensorial nature, and H_0 is the unperturbed Hamiltonian. In the absence of an external field and a thermostat, H_0 is the total energy and is therefore a constant of the motion. The rate of change of internal energy due to the external field is:

$$\dot{H}_0 = -\sum_{i=1}^{N}\left[-\overleftrightarrow{D}_i\cdot\frac{\dot{\vec{p}}_i}{m} + \overleftrightarrow{C}_i\cdot\vec{F}_i\right]\vec{F}_{ext}(t) = -V\vec{J}\cdot\vec{F}_{ext}(t) \tag{2.33}$$

where $\vec{J}$ is called the dissipative flux. $\vec{J}$ can be one of the fluxes appearing in the GK relations [9]. The idea of S-NEMD is to design $\vec{\vec{C}}_i$ and $\vec{\vec{D}}_i$ so as to satisfy $\dot{H}_0 = -V\vec{J} \cdot \vec{F}_{ext}(t)$.

According to linear response theory the flux $\vec{J}_\alpha$ one of the phase variables, at weak non-equilibrium steady state can be evaluated with [1, 24]:

$$\left\langle \vec{J}_\alpha(t) \right\rangle_{neq} = \left\langle \vec{J}_\alpha(0) \right\rangle_{eq} - \frac{V}{k_B T} \int_0^t \left\langle \vec{J}_\alpha(t-s) \vec{J}_\beta(0) \right\rangle_{eq} \cdot \vec{F}_{ext}(s)\, ds \tag{2.34}$$

Here $\left\langle \vec{J}_\alpha(0) \right\rangle_{eq}$ is assumed to be zero, which denotes the ensemble average of $\vec{J}_\alpha$ at time origin when the external field starts to be imposed. $\vec{J}_\beta$ is the dissipative flux. By monitoring $\left\langle \vec{J}_\alpha(t) \right\rangle_{neq}$ for the resulting non-equilibrium steady state, the GK relation can be evaluated from the equation above. Comparing equation (2.19) and (2.34), the expression of the equilibrium transport coefficients is [24]:

$$L_{\alpha\beta} = \lim_{F_e \to 0} \frac{T \left\langle J_\alpha(t) \right\rangle_{neq,\infty}}{F_e} \tag{2.35}$$

where the average $\langle\ \rangle_{neq,\infty}$ means an infinite time average over a non-equilibrium steady state distribution. The limit $F_{ext} \to 0$ can be performed by choosing either a very small value of the field or by extrapolation to zero field.

Because in S-NEMD the motion of particles is modified by the external field, the signal-to-noise ratio of the flux is much higher. This is the main advantage of S-NEMD over EMD. However, the S-NEMD method still requires a microscopic definition of the heat flux for calculating the transport coefficients such as thermal conductivity and thermal diffusion coefficient. Therefore, the deficiency of the microscopic definition of partial specific enthalpy makes it not so easy.

2.2.3 Direct (boundary driven) non-equilibrium molecular dynamics

In Direct non-equilibrium molecular dynamics (D-NEMD), the perturbation is imposed only on the boundaries of the system to mimic the physical phenomenon [12,13]. The transport coefficients can be directly calculated with linear response equations listed in Section 2.1, and in the case of the thermal conductivity, only the macroscopically defined heat flux is needed. There are two types of this method: The Norton-ensemble where the flux is constant, and the more conventional Thévenin-ensemble where the applied perturbation (force) is fixed. The D-NEMD algorithm in this research is called the reverse non-equilibrium molecular dynamics (RNEMD) method [13, 25], and it uses the Norton-ensemble. Although the RNEMD method can also be performed to calculate shear viscosities [26, 27], we will only discuss the version related to the thermal conductivity and the Soret coefficient, which is the topic of this thesis.

Reverse Non-equilibrium Molecular Dynamics

The word "reverse" comes from the fact that in the algorithm the roles of the flux and the field are reversed way in comparison with real experiments. In the experiments, the temperature gradient is firstly imposed on the system to produce the heat flux; while in our simulations, the heat flux is firstly created to induce the temperature gradient. The algorithm we use in the following Sections is divided into two types of small difference: a) the atomic exchange algorithm and b) the molecular exchange one. The former one is used in fluid containing only atomic or fully flexible molecules. The latter one is for molecules with inner constraints (bond, angle, …). For both algorithms, periodic boundary conditions [28] are employed. This is a good method to reduce the simulation system size. In small systems, the number of particles near container walls would be disproportionate, affecting the simulation results a lot. In periodic boundary conditions, no container wall exists and each particle acts like in bulk fluid. This condition is realized by dividing the system into one central box and an infinite number of image boxes; any particle leaving the central box during the simulation will be replaced by an image particle that enters from the opposite side. So the total number of particles in the central box is kept constant (Figure 2.1).

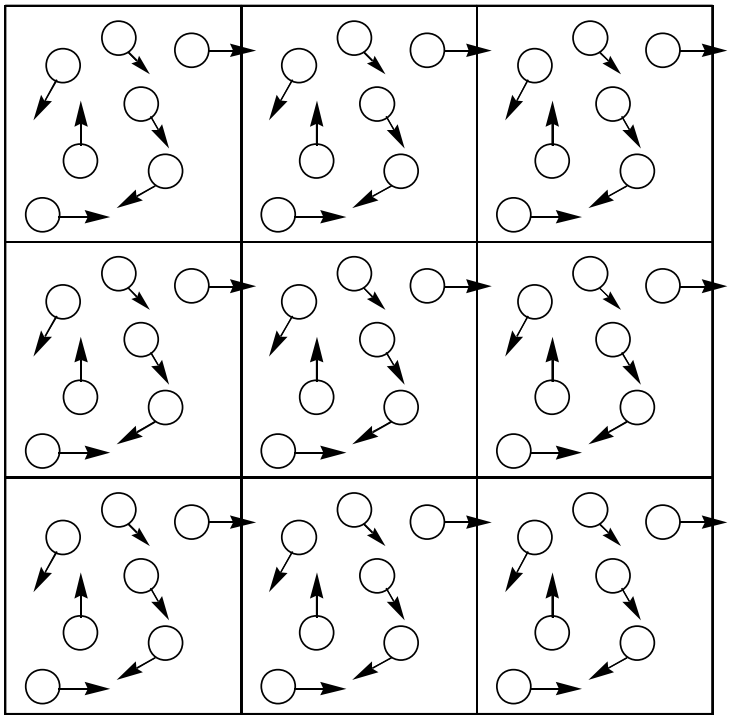

Figure 2.1. Schematic representation of periodic boundary conditions in two dimensions.

a) Atomic exchange algorithm

The periodic system (simulation box) is partitioned into n slabs along, say, the z direction. Of these slabs, the two at the beginning and the end of the simulation box are designated as the "hot" slab, the one at the center of the box as the "cold" slab. This arrangement is for keeping the continuity of the temperature gradient along the

whole system. The non-equilibrium algorithm moves, in an artificial manner, energy from the cold slab to the hot slab, i.e. against the temperature gradient ($\partial T / \partial z$). Since energy is conserved, it flows back through the liquid by physical transport mechanisms, resulting in an energy flux j_z in the z direction. When the steady state has been reached, J_z is equal in magnitude but opposite in direction of the known imposed artificial energy flow. The RNEMD algorithm comprises two ingredients, both of which require modification when going from atomic to molecular fluids: A means to move energy from the cold to the hot slab and a way of calculating the temperature gradient. For atomic liquids or fluids of fully flexible molecules, the appropriate energy exchanges are applied to individual atoms. The energy transfer mechanism uses a Maxwell demon, which, every so many MD time steps, determines the atomic velocities (or momenta) of all atoms in the two slabs. It then selects the hottest atom of the cold slab and the coldest atom of the hot slab and swaps their Cartesian velocity vectors. Other schemes are possible, which do not use the hottest and the coldest atoms, respectively, but two other atoms with a smaller difference in kinetic energy, and which exchange velocities more often. The details are relatively unimportant, as long as energy is moved from the cold to the hot slab. This is always possible, as the Maxwell-Boltzmann distribution of atomic velocities is much wider than the difference between the average velocities in the two slabs. It can be shown that, if velocities are exchanged between atoms of like mass, the algorithm conserves both total energy and total linear momentum up to a negligible error coming from the discretization of the equations of motion. Note that there is also a recent variant of the RNEMD schemes which allows velocity exchange between objects of different masses [29]. The energy flux is given by the sum of all energy transfers per time per area.

$$J_z = \frac{1}{2tA} \sum_{transfers} \frac{m}{2} \left(v_{hot}^2 - v_{cold}^2 \right) \tag{2.36}$$

Here, t is the length of the simulation, A is the cross sectional area of the simulation box perpendicular to the flow direction z, v_{hot} and v_{cold} denote the velocities of the hot and the cold atom of like mass m, whose velocities are exchanged, and the factor 2 arises from the symmetry of the problem. In our implementation, the strength of the non-equilibrium perturbation is governed by the period W, with which velocity swaps are executed, a larger W meaning a smaller perturbation.

The second task is the calculation of the temperature gradient. To this end, one analyzes the intervening slabs, where no velocity exchange is performed and where unperturbed Newtonian dynamics takes place. One evaluates the temperature T_{slab} within each slab as:

$$\frac{3Nk_B T_{\text{slab}}}{2} = \frac{1}{2} \left\langle \sum_{\substack{\text{atoms } i \\ \text{in slab}}}^{N} m_i v_i^2 \right\rangle \tag{2.37}$$

where the number of atoms in the slab is N, and k_B is Boltzmann's constant. The angle brackets denote time-averaging over the atoms in the slab. For a small enough perturbation (large W), linear response holds and the temperature profile is linear. Its slope ($\partial T / \partial z$) is extracted by a linear regression.

b) Molecular exchange algorithm

For molecular models with holonomic constraints, the atom exchange method has to be amended if energy and momentum conservation are to be maintained [30, 31]. The description that follows is our implementation in the atomistic MD program YASP [32]. The velocity exchange is now done between molecules of like mass, rather than between atoms. Otherwise, the atomic velocities after exchange would not comply with the constraints. The selection of the two molecules, whose velocities are to be swapped, is based on their centre-of-mass momenta.

$$\vec{P} = \sum_{\substack{\text{atoms } i \text{ in} \\ \text{molecule}}} m_i \vec{v}_i = \vec{v}_{cms} \sum_{\substack{\text{atoms } i \text{ in} \\ \text{molecule}}} m_i \tag{2.38}$$

To establish a temperature gradient, the Maxwell demon selects the translationally hottest and coldest molecules in the cold and hot slabs, respectively. The translational kinetic energy of a molecule is defined as $\frac{1}{2} v_{cms}^2 \sum_{\substack{\text{atoms } i \text{ in} \\ \text{molecule}}} m_i$, with $\vec{v}_{cms}$ its centre-of-mass velocity vector from equation (2.38). The entire Cartesian centre-of-mass velocity vectors of the two selected molecules are exchanged. Thus, the velocity $\vec{v}_i'$ of atom *i* of the molecule *a* after the exchange is given in terms of velocities before the exchange:

$$\vec{v}_i' = \vec{v}_i - \vec{v}_{cms}^{\,a} + \vec{v}_{cms}^{\,b} \tag{2.39}$$

Here the superscripts *a* and *b* represent the two molecules with their velocity vectors exchanged. As only centre-of-mass velocities are exchanged, the relative velocities of atoms within each molecule remain unchanged. Hence, the velocities after the exchange are compatible with the application of a constraint algorithm. The exchange of molecular centre-of-mass velocities instead of atomic velocities is referred to as *molecular* exchange. It can, of course, also be applied to flexible molecules, even if it is not necessary in this case.

The presence of constraints complicates the calculation of the temperature profile, too. The temperature in a molecular dynamics simulation with constraints is given by the equipartition theorem

$$\left(\frac{3N - C}{2} \right) k_B T = \frac{1}{2} \left\langle \sum_{\text{atoms } i} m_i v_i^2 \right\rangle \tag{2.40}$$

where *C* is the number of constraints in the system. If a local (slab) temperature is to be determined, the angle brackets denote time averaging only over the *N* atoms within the slab, and *C* refers to the number of constraints in the slab. This number can be estimated analytically only if the constraints are assumed to be distributed uniformly throughout the system. This is only the case if (i) the density is uniform (small perturbation) and (ii) the composition is uniform (only one molecular species or Soret effect negligible). In all other cases, the local *C*'s must be evaluated in the simulation. In our algorithm, bond constraints are solved for by a modified SHAKE procedure [28, 33], the performance of which will be introduced in Section 3.2. The constraints are stored as a list of pairs of atoms whose distance is to be kept constant. The program uses this list to determine, in which slab(s) the two atoms defining a constraint reside.

For every atom, the constraint counter in its slab is incremented by 1/2. If an atom is part of c constraints its contribution to the constraints in the slab is $c/2$. In this way, constraints spanning two slabs are split between the slabs. As a consequence, the scheme also allows for molecules extending over several slabs.

For both types of the RNEMD methods, the macroscopic energy flux J_z is known. As said above, in a multi-component fluid, the heat flux may contain diffusional mass fluxes of the components weighted with their partial molar enthalpies (equation 2.28). In the simulations, when the concentration profile becomes stable at steady state, the net mass flux in the system is equal to zero. Hence, the heat flux is $J_{qz} = J_z$. The thermal conductivity can be calculated by combining Fourier's relation with equation (2.36):

$$\lambda = \frac{-J_{qz}}{\nabla T} = \frac{-\sum_{transfers} \frac{m}{2}\left(v_{hot}^2 - v_{cold}^2\right)}{2At\left(\partial T / \partial z\right)} \tag{2.41}$$

The Soret coefficient of a binary mixture can be obtained with equation (2.18) by measuring both the concentration gradient and temperature gradient in the z direction at the steady state:

$$S_T = -\frac{1}{w_1\left(1-w_1\right)} \frac{\left(\partial w_1 / \partial z\right)}{\left(\partial T / \partial z\right)} \tag{2.42}$$

References

[1] D. J. Evans and G. P. Morriss, *Statistical mechanics of nonequilibrium liquids* (Academic, London, 1990).

[2] D. Reith, *Thermal diffusion in binary Lennard-Jones liquids*, Diploma Thesis, Max-Planck-Institute for Polymer Research, Mainz, 1998.

[3] E. L. Cussler, *Diffusion: mass transfer in fluid systems*, (Cambridge University Press, Cambridge, 1984).

[4] L. Onsager, Phys. Rev. **37**, 405 (1931).

[5] L. Onsager, Phys. Rev. **38**, 2265 (1931).

[6] S. R. de Groot and P. Mazur, *Non-Equilbrium Thermodynamics* (Dover, New York, 1984).

[7] K. E. Grew and T. L. Ibbs, *Thermal diffusion in gases* (Cambridge University Press, Cambridge, 1952).

[8] P. T. Cummings and D. J. Evans, Ind. Eng. Chem., **31**, 1237 (1992).

[9] D. MacGowan and D. J. Evans, Phys. Rev. A **34**, 2133, (1986).

[10] D. J. Evans and D. MacGowan, phys. Rev. A **35**, 5156, (1987).

[11] R. Vogelsang, C. Hoheisel, G. V. Paolini, and G. Ciccotti, Phys. Rev. A **36**, 3964 (1987).

[12] B. Hafskjold, T. Ikeshoji, and S. K. Ratkje, Mol. Phys. **80**, 1389 (1993).

[13] F. Müller-Plathe and P. Bordat, in *Novel Methods in Soft Matter Simulations*, Lecture Notes in Physics Vol. 584, edited by M. Karttunen, I. Vattulainen, and A. Lukkarinen (Springer, Heidelberg, 2004), p310.
[14] M. S. Green, J. Chem. Phys. **20**, 1281 (1952).
[15] R. Kubo, J. Phys. Soc. Japan **12**, 570 (1957).
[16] R. Zwanzig, J. Chem. Phys. **40**, 2527 (1963).
[17] Y. Zhou and G. H. Miller, J. Phys. Chem. **100**, 5516 (1996).
[18] H. Schmitz, R. Faller, and F. Müller-Plathe, J. Phys. Chem. B **103,** 9731 (1999).
[19] R. Zwanzig, Annu. Rev. Phys. Chem. **16**, 67 (1965).
[20] G. V. Paolini and G. Ciccotti, Phys. Rev. A **35**, 5156 (1987).
[21] B. Hafskjold, in *Thermal Nonequilibrium Phenomena in Fluid Mixtures*, Lecture Notes in Physics Vol. 584, edited by W. Köhler and S. Wiegand (Springer, Verlag, 2002) p3.
[22] J. H. Irving and J. G. Kirkwood, J. Chem. Phys. **18**, 817 (1950).
[23] D. Evans and G. Moriss, Comput. Phys. Rep. **1**, 297, (1984).
[24] A. Perronace, C. Leppla, F. Leroy, B. Rousseau, and S. Wiegand, J. Chem. Phys. **116**, 3718 (2002).
[25] F. Müller-Plathe, J. Chem. Phys. **106**, 6082 (1997).
[26] F. Müller-Plathe, Phys. Rev. E **59**, 4894 (1999).
[27] F. Müller-Plathe and D. Reith, Comput. Theor. Polym. Sci. **9**, 203 (1999).
[28] M. P. Allen and D. J. Tildesley, *Computer Simulation of Liquids* (Oxford University Press, Oxford 1987).
[29] C. Nieto-Draghi and J. B. Avalos, Mol. Phys. **101**, 2303 (2003).
[30] P. Bordat and F. Müller-Plathe, J. Chem. Phys. **116**, 3362 (2002).
[31] D. Bedrov and G. D. Smith, J. Chem. Phys. **113**, 8080 (2000).
[32] F. Müller-Plathe, Comput. Phys. Commun. **78**, 77 (1993).
[33] F. Müller-Plathe and D. Brown, Comput. Phys. Commun. **64**, 7 (1991).

3. Thermal conductivities in benzene-cyclohexane systems

3.1 Introduction

The reverse non-equilibrium molecular dynamics method (RNEMD) originally had been developed for the calculation of thermal conductivities in monatomic Lennard-Jones liquids [1]. Since then, its scope has been extended to the calculation of shear viscosities of atomic fluids [2, 3] and Soret coefficients of mixtures of Lennard-Jones particles [4,5]. The algorithm version for thermal conductivities has been used for Yukawa fluids [6], thin crystalline films [7], carbon nanotubes [8], and some molecular systems: Water [9], octahydro-1,3,5,7-tetranitro-1,3,5,7-tetrazocine [10] and DMSO-water mixtures [11]. The algorithm version for shear viscosities has been extended and validated for atomistic models of molecular liquids [12] and simple models of block copolymers [13], amphiphiles [14], and liquid crystals [15]. It has also been successfully combined with the dissipatitive particle dynamics equation of motion [16]. The method has recently been reviewed in detail [17]. Worries about convective heat transport as a source of error are unnecessary, because of the small dimensions. Estimates from instability theory [18] indicate that temperature differences of the order of 10^{17} K would be needed to drive convection on the scale of nanometers. In addition, for the single-component fluids, gravitation would be required to generate a Rayleigh-Benard instability.

This part of research implements the molecular exchange version of the RNEMD algorithm to study the thermal conductivities of realistic molecular fluids. The purpose is to extend the applicability of the algorithm to more molecular fluid systems. Benzene, cyclohexane and their mixtures of three different compositions are selected. Because they and their derivatives are widely used as solvents; of special interest are aromatic and aliphatic rings as these are two of the most popular elementary structures in polymers. For the first time, the algorithm is performed together with all-atom models of benzene and cyclohexane. The impacts of algorithm variants and simulation parameters, such as the exchange frequency (intensity of the perturbation), the presence or absence of thermostat, and the system size, are investigated. As the goal is mainly technical, the reproduction of known experimental thermal conductivities is a secondary issue here. We have mostly used tested and trustable force fields for the studied liquids, but made no attempt to tune them to give experimental thermal conductivities.

A critical issue for the calculation of transport coefficients by any equilibrium or non-equilibrium molecular dynamics method is thermostatting. In principle, any thermostat generates or destroys energy in the system. Energy is no longer a conserved property, and calculated heat fluxes may lose their significance. As a result, thermostats should be avoided altogether in the calculation of thermal conductivities. (As most thermostats do not conserve momentum either, analogous considerations apply in the calculation of shear viscosities [17].) However, calculations on realistic

molecular fluids may necessitate a thermostat, be it because *NVT* conditions are desired or be it to counteract slow temperature drifts due to round-off or cutoff noise. There is evidence from calculations on Lennard-Jones fluids that a gently coupled Berendsen thermostat does not significantly alter the calculated thermal conductivity λ [1]. This may be due to the uniform velocity scaling employed by this thermostat, which mainly shifts the entire temperature profile in a RNEMD simulation, but does not destroy it. As the temperature variation within the simulation is usually much smaller than the average temperature, the influence of the thermostat on the temperature gradient and, hence, the thermal conductivity is small, too. In this respect, the otherwise widely criticized Berendsen thermostat might have an advantage over alternatives. Thermostats, which apply individual velocity scaling based on local friction, are definitely not suited. In this work, we will therefore also investigate the effect of a Berendsen thermostat on calculated thermal conductivities for realistic molecular liquids.

3.2 Computational details

All molecular dynamics simulations were carried out with the YASP package [19], which uses the leap-frog algorithm [20] and orthorhombic periodic boundary conditions [20]. In leap-frog algorithm, the motion of each atom is predicted with:

$$\vec{v}_{n+1/2} = \vec{v}_{n-1/2} + \frac{\Delta t}{m}\vec{f}_n$$

$$\vec{r}_{n+1} = \vec{r}_n + \Delta t\,\vec{v}_{n+1/2} \tag{3.1}$$

where n and Δt are the number and the length of the time step, m the atom's mass, $\vec{v}$ its velocity vector, $\vec{r}$ its position vector and $\vec{f}$ the force vector acting on it. The subscripts indicate that velocities are evaluated at half steps and positions and forces at full steps.

The functional form for the force field used to calculate the potential energy E_{pot} of the system is [19]:

$$E_{\text{pot}} = \sum_{angles}(k_\Phi/2)(\phi-\phi_0)^2 + \sum_{torsions}(k_\varphi/2)(1-\cos p(\varphi-\varphi_0)) + \sum_{\substack{harmonic\\ dihedrals}}(k_\psi/2)(\psi-\psi_0)^2$$
$$+\sum_{i=1}^{N}\sum_{j=i+1}^{N}\left\{4\varepsilon_{ij}\left[(\sigma_{ij}/r_{ij})^{12}-(\sigma_{ij}/r_{ij})^{6}\right]+\frac{q_iq_j}{4\pi\varepsilon_0}\left(\frac{1}{r_{ij}}+\frac{\varepsilon_{\text{RF}}-1}{2\varepsilon_{\text{RF}}+1}\frac{r_{ij}^3}{r_{\text{cutoff}}^3}\right)\right\} \tag{3.2}$$

The force field shown in the equation consists of terms for the bonded and nonbonded molecular forces within the system. The bonded molecular force field potentials include the first three terms (Table 3.1): harmonic bond angle bending, periodic cosine-type torsional potentials (cyclohexane), harmonic dihedral potentials (benzene out-of-plane). In our simulations, constraints are used to maintain bond distances l rigid. In these three terms, ϕ the bond angle, φ the torsion dihedral angle, ψ the

Table 3.1. Geometry and force field parameters of benzene and cyclohexane [23-26][a)]

Atom	mass [amu]		
C	12.01		
H	1.00787		
Nonbonded[b)] benzene	ε [kJ mol^{-1}]	σ [nm]	Partial charge
C	0.294	0.355	-0.115
H	0.126	0.242	0.115
Nonbonded[b)] cyclohexane			
C (force field I)	0.299	0.328	0
H (force field I)	0.189	0.258	0
C (force field II)	0.276	0.35	-0.12
H (force field II)	0.125	0.25	0.06
Constraints	l_0 [nm]		
CH=CH (benzene)	0.139		
CH_2-CH_2 (cyclohexane)	0.1526		
C-H (benzene)	0.108		
C-H (cyclohexane)	0.109		
Bond angles	ϕ_0 [degree]	k_ϕ [kJ mol^{-1}rad^{-2}]	
C-C-C (benzene)	120	376.6	
C-C-H (benzene)	120	418.8	
C-C-C (cyclohexane)	109.5	335	
C-C-H (cyclohexane)	109.5	420	
H-C-H (cyclohexane)	109.5	290	
Torsions (cyclohexane)	φ_0 [degree]	k_φ [kJ mol^{-1}]	periodicity
C-C-C-C	180	10	3
Harmonic dihedrals (benzene)	ψ_0 [degree]	k_ψ [kJ mol^{-1} rad^{-2}]	
C-C-C-C	0	167.4	
C_2-C_3-C_1-H (on C_2)	0	167.4	

[a)] (Note a misprint in Table 2 of ref. 23: σ_C should read 0.355 nm).
[b)] All intramolecular nonbonded interactions have been excluded.

harmonic dihedral angle, subscript zero is the "reference" or "equilibrium" (strain free) values, and k the respective force constants. The last term describes the pair non-bonded potentials between atoms. Here the nonbonded potentials inside one molecule were excluded. This latter part includes the Lennard-Jones (LJ) potential for van der Waals interactions and the Coulomb potential for electrostatic interactions. In the Lennard-Jones potential, Lorentz-Berthelot mixing rules were implemented for unlike interactions to get the values of cross interaction potential ε_{ij} and atomic diameter

parameter σ_{ij}, where $\varepsilon_{ij} = \sqrt{\varepsilon_i \varepsilon_j}$, $\sigma_{ij} = (\sigma_i + \sigma_j)/2$. For the electrostatic potential, we employed a simplified model, the reaction field method. In this method, a sphere is constructed around the particle with a radius equal to the cutoff distance. The electrostatic potential of this charged particle can be regarded as the addition of two parts: One is the interaction with the other explicit charged ones inside the sphere; the other is that with a homogeneous dielectric medium beyond the sphere. In the last term, r_c denotes the cut-off radius, ε_{RF} the reaction field dielectric permittivity of the continuum, ε_0 the permittivity of the vacuum, q_i and q_j point charges, r_{ij} the distance between site i and j.

Nonbonded interactions were evaluated from a Verlet neighbour list, which was updated using a link-cell method [19, 20]. The cutoff lengths for both Lennard-Jones and electrostatic potential were of the same value. Specific settings of simulation parameters are reported below for the individual systems. We sampled the temperature profiles only in time steps, in which no velocity swaps were performed. Therefore, the sampling period is typically slightly different from the exchange period W or its multiples, for example $W + 1$ (see Section 2.2.3 for the meaning of W).

Bond constraints were solved for by the SHAKE method [21] to a relative tolerance of 10^{-6}. In the procedure of SHAKE,

$$\Delta\vec{r} = \vec{r} - \vec{r}' = \frac{d^2 - (\vec{r}' \cdot \vec{r}')}{2(\vec{r}' \cdot \vec{r}^{\,0})} \vec{r}^{\,0} \tag{3.3}$$

where d denotes the constrained distance between two atoms, $\vec{r}^{\,0}$ the final distance vector between the two atoms after the previous time step, $\vec{r}^{\,'}$ the intermediate distance vector between the two atoms after the unconstrained MD motion of the current time step, and $\vec{r}$ the final distance vector of the current time step after application of the constraints. The new positions of the two connected atoms $\vec{r}_i$ and $\vec{r}_j$ are given by:

$$\vec{r}_i = \vec{r}_i^{\,'} + \frac{M}{m_i}\Delta\vec{r}\,, \quad \vec{r}_j = \vec{r}_j^{\,'} + \frac{M}{m_j}\Delta\vec{r} \tag{3.4}$$

$\vec{r}_i^{\,'}$ and $\vec{r}_j^{\,'}$ are the intermediate unconstrained positions, and $M = \frac{m_i m_j}{m_i + m_j}$. In a system, there are many constraints, and satisfaction of one constraint may destroy the other one. Therefore a tolerance β is set which allows a slight difference between r and d in order to obtain a balance for all constraints:

$$\left|(\vec{r} \cdot \vec{r}) - d^2\right| \le 2\beta d^2 \tag{3.5}$$

The simulation cells were usually elongated in the z direction, in which the heat flow was imposed ($L_x = L_y = L_z/3$). Constant-temperature simulations can be performed with Berendsen's thermostat [22]. Constant temperature is implemented by a uniform scaling of the atom velocities,

$$\delta = \left[1 + \frac{\Delta t}{\tau_T} \left(\frac{T}{T_{bath}} - 1 \right) \right]^{1/2} \tag{3.6}$$

T is the system temperature, T_{bath} the target values or the values of the temperature bath, τ the coupling time which determines the intensity of the thermostat. A larger value of τ indicates a weaker coupling between the temperature bath and system. In this research, temperatures and densities were chosen at or close to ambient conditions, where experimental data are most abundant.

3.3 Result and discussion

3.3.1 Benzene

Benzene (645 molecules, density ρ = 874.9 kg/m^3, T = 308 K) was simulated at constant *NVE* conditions for 900 ps using a time step of 1 fs. A modified OPLS force field has been used (Table 3.1). Nonbonded interactions were truncated at cutoff length of 1.1 nm, the neighbour list (cutoff: 1.2 nm) was updated every 15 time steps. The reaction-field approximation was used for Coulombic interactions; the dielectric constant was 2.5. Molecular velocity swaps were performed every W = 150, 300 and 500 steps, and sampling of the temperature profile was done every 151, 301 or 501 time steps for the last 500 ps (W = 150) or 600 ps (W = 300, 500) of the simulation.

Benzene is a simple, relatively stiff molecule with small atomic partial charges. It can be run without coupling to a thermostat, if the reaction-field approximation is used: In the 900 ps simulation, only a small heating from 303 K to about 310 K has been observed, which is due to truncating the nonbonded interactions. The observed temperature profiles are linear, as are the concomitant density profiles (Figures 3.1 and 3.2). The fact that the temperature profile is linear means that ($\partial T / \partial z$) is constant across the system. As, by construction, the average heat flux is also constant across the system, it follows that also the thermal conductivity is independent of position (cf. Eq. 2.41). Therefore, the perturbations chosen here are small enough for λ not to depend on the distance from the exchange layers. This would be different if the perturbation were large enough to drive the system into nonlinear response. It may be noted in Figure 3.1 that the lowest temperature (W = 150) reached is ~260 K, which falls below the experimental freezing point of benzene (279 K). The benzene model used here is known to be liquid down to 240 K [27], so there are no complications from a two-phase situation. In addition, we have verified that the diffusion tensor is isotropic. Diffusion in the direction of heat flow would be significantly lower than perpendicular to it, if the cold slab formed a frozen or supercooled barrier. The convergence of the thermal conductivity to less than 10% uncertainty is shown in Figure 3.3 for a W of 500 by a cumulative average, the convergence being even faster for W values of 150 and 300 (Figures 3.4 and 3.5).

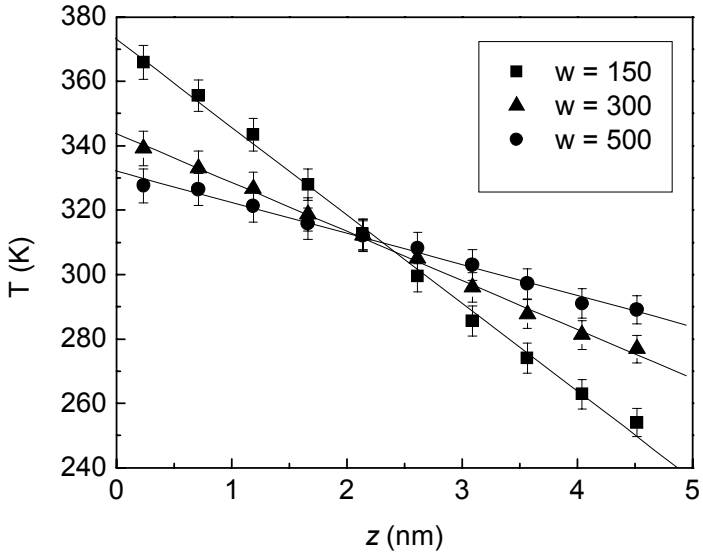

Figure 3.1. Temperature profiles in the RNEMD simulation of benzene for three perturbations (W = 150, 300, 500). The two symmetric sides of the simulation cells have been averaged. Linear least-squares fits to the data points are shown, too.

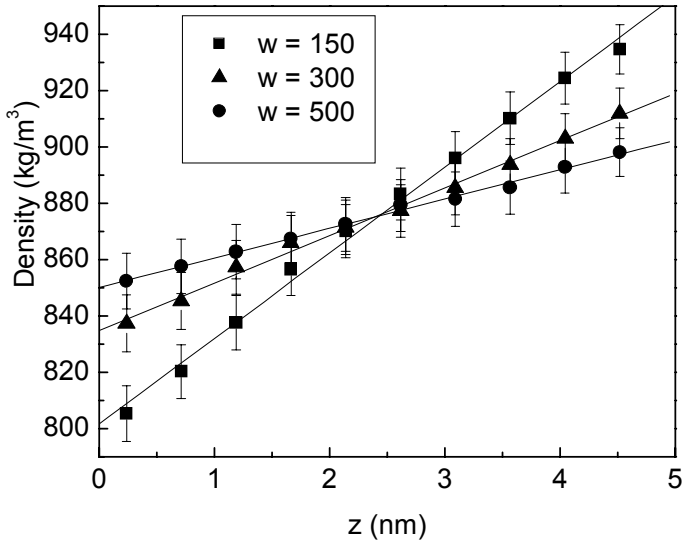

Figure 3.2. Density profiles in the RNEMD simulation of benzene for three perturbations (W = 150, 300, 500). The two symmetric sides of the simulation cells have been averaged. Linear least-squares fits to the data points are shown, too.

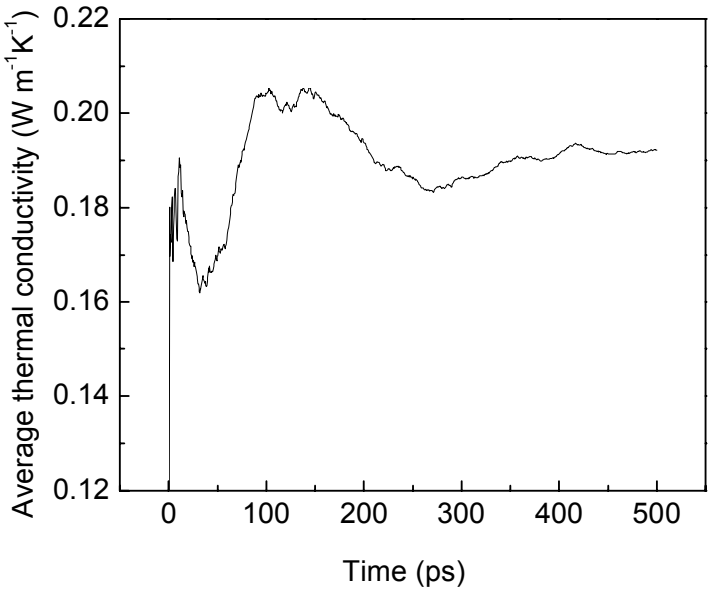

Figure 3.3. Cumulative average of the thermal conductivity of benzene at the smallest perturbation (W = 500). It shows the slowest convergence of all simulations in this contribution.

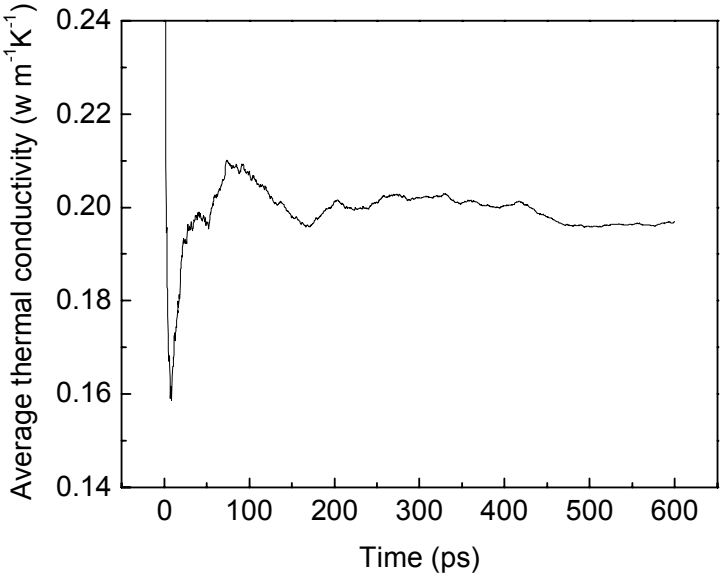

Figure 3.4. Cumulative average of the thermal conductivity of benzene at the intermediate perturbation (W = 300).

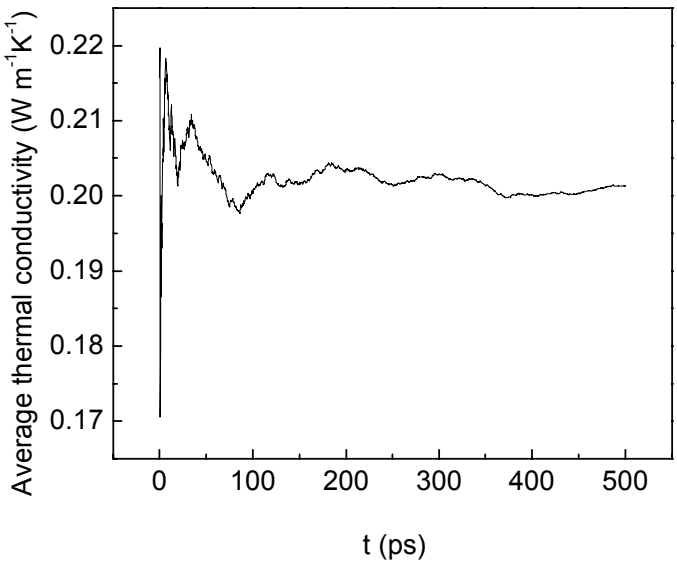

Figure 3.5. Cumulative average of the thermal conductivity of benzene at the strongest perturbation (W = 150).

The thermal conductivities are λ = 0.201, 0.197, and 0.192 W m^{-1} K^{-1} for W = 150, 300, and 500, respectively. These values agree well among each other, indicating that all chosen perturbation strengths (W) are in the linear-response domain. The smallest perturbation (W = 500) shows a decreasing statistical accuracy due to a lower signal-to-noise ratio (Figure 3.3). The calculated thermal conductivity is larger than the experimental one (0.141 W m^{-1} K^{-1} at 293 K) [28], the disagreement being small for a transport coefficient (the simulated self diffusion coefficient of this model is a factor of 2 lower than experiment) [24, 29]. Still, there could be other reasons for the disagreement apart from inaccuracies of the model or the experimental measurements: The model is semiflexible, and treats classically degrees of freedom like bond angles involving hydrogens. These are stiff enough to be quantum oscillators in their ground states in reality. As quantum oscillators they would not be available to transport energy, causing a lower λ.

The action of a thermostat (at constant NVT conditions) has been investigated. We have used a Berendsen thermostat [22] with a long coupling time of 10 ps. We have repeated the W = 150 (302 K) and W = 300 (301 K) calculations (simulation 600 ps, sampling 400 ps). Although forbidden in principle (see Section 3.1), the thermostat has little effect on λ, which are 0.20 (W = 150) and 0.191 W m^{-1} K^{-1} (W = 300).

In order to check for possible size effects on λ, we have repeated the calculations with smaller versions of the benzene system. They had the same extension in directions perpendicular to the heat flux (L_x and L_y), but in the direction of the flux (L_z) they were shortened to 1/3 and 2/3 of the original value. The thermal conductivity of the smallest system (L_z/3) was 0.27-0.29 W m^{-1} K^{-1}, i.e. significantly larger than the ~0.195 W m^{-1} K^{-1} found above. The intermediate system (2L_z/3), however, showed already a value (~0.20 W m^{-1} K^{-1}) not significantly different from that of the full

system. We, therefore, conclude that our system size of approximately 3.17 nm × 3.17 nm × 9.51 nm is large enough to observe a converged thermal conductivity. This should also hold for the other fluids studied here, as system dimensions and molecule sizes are similar. For safety, convergence with system size should be re-evaluated when much larger molecules are treated.

3.3.2 Cyclohexane

Cyclohexane (750 molecules, $\rho = 771.1$ kg/m^3, $T = 303$ K) was simulated at constant *NVE* conditions using a time step of 1 fs. An automatically optimized force field has been used (Table 3.1, force field I), which has no atomic partial charges. Nonbonded interactions were truncated at 1.1 nm, and the neighbour list (cutoff: 1.2 nm) was updated every 15 time steps. Molecular velocity swaps were performed every W = 150, 300 and 500 steps (simulation times: 500, 900, and 600 ps; sampling times 300, 600, and 400 ps, respectively), and sampling of the temperature profile was done every 151-501 time steps

Except the reasons mentioned in Section 3.1, cyclohexane has been chosen also because it can be described by a force field with only Lennard-Jones interactions, so no heating due to cutoff noise is to be expected, and thermostatting can be completely avoided. At the same time, it is slightly more flexible than benzene. Temperature and density profiles are linear for all perturbation strengths (Figures 3.6 and 3.7), λ is uniform across the system, and the cumulative average of λ shows convergence within a few hundred picoseconds (Figures 3.8, 3.9, and 3.10). The calculated thermal conductivities are 0.235 W m^{-1} K^{-1} (W = 150), 0.253 W m^{-1} K^{-1} (W = 300), and 0.238 W m^{-1} K^{-1} (W = 500), respectively, the mutual agreement showing that at all perturbation strengths linear response holds. All values are about twice as large as the experimental value (0.123 W m^{-1} K^{-1} at 298 K) [28]. The same considerations as with benzene (Section 3.3.1) apply: The deviation between experimental and calculated thermal conductivity is not too big for a transport property (the diffusion coefficient of this cyclohexane model is 36% below the experimental value), but there is the possibility that the classical description predicts a systematically too high λ. The fact that the overestimation is larger for cyclohexane than for benzene could then be due to the larger number of internal quantum degrees of freedom.

For cyclohexane, the influence of the Berendsen thermostat has also been investigated using *NVT* simulations. A quite short coupling time of 0.2 ps was used to accentuate its possible effects. We have repeated the W = 300 calculation (simulation 600 ps, sampling 400 ps). The result (0.234 W m^{-1} K^{-1}) shows the same conclusion made in the last section that thermostat has little effect on λ.

We have also investigated the sensitivity to the force field. We have repeated the W = 300 calculation (simulation 540 ps, sampling 360 ps, *NVT* conditions at $T = 299.9$ K) with nonbonded parameters from the OPLS model of cyclohexane (see Table 3.1 for nonbonded parameters, reaction-field dielectric constant is 2.0), with the same bonded terms as before. This changes the thermal conductivity to 0.182 W m^{-1} K^{-1}, in the direction of the experimental value, showing that the force field has an influence far

greater than that of either the exchange frequency W or the presence or absence of a thermostat. It should be mentioned that both force fields describe the same state of cyclohexane. Both pressures can be considered essentially zero, given the large pressure fluctuations.

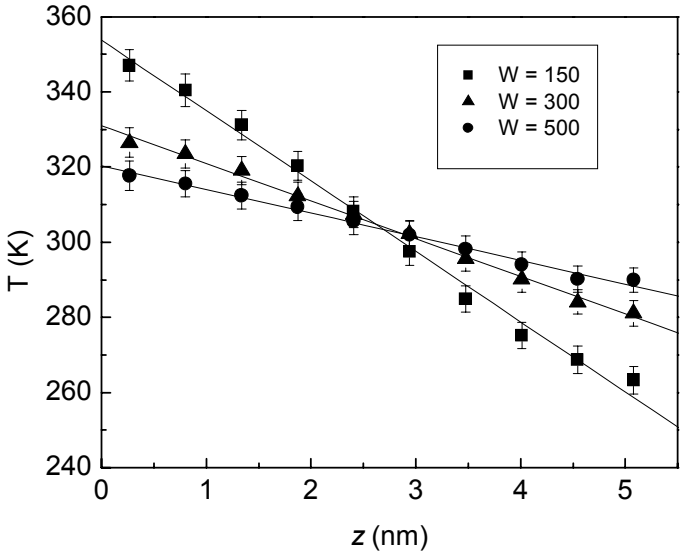

Figure 3.6. Temperature profiles in the RNEMD simulation of cyclohexane for three perturbations. The two symmetric sides of the simulation cells have been averaged. Linear least-squares fits to the data points are shown, too.

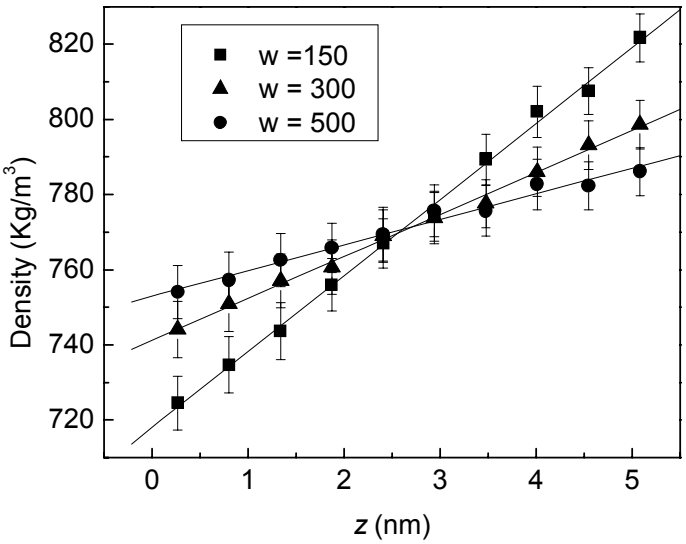

Figure 3.7. Density profiles in the RNEMD simulation of cyclohexane for three perturbations. The two symmetric sides of the simulation cells have been averaged. Linear least-squares fits to the data points are shown, too.

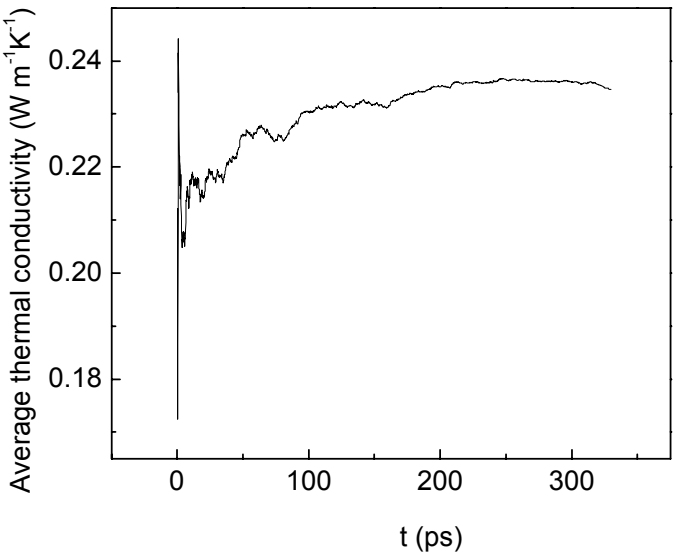

Figure 3.8. Cumulative average of the thermal conductivity of cyclohexane at the strongest perturbation ($W = 150$).

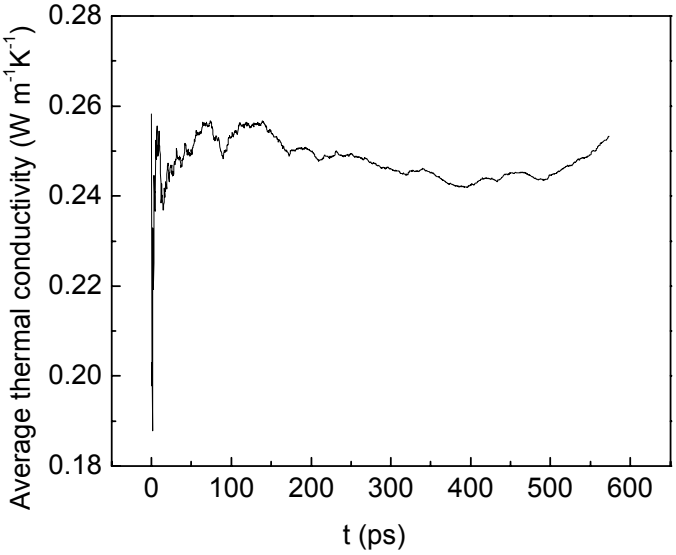

Figure 3.9. Cumulative average of the thermal conductivity of cyclohexane at the intermediate perturbation ($W = 300$).

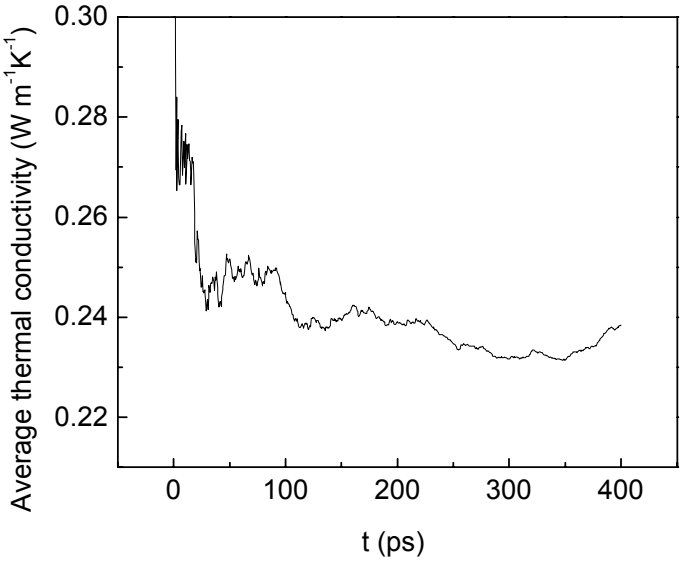

Figure 3.10. Cumulative average of the thermal conductivity of cyclohexane at the smallest perturbation (W = 500).

3.3.3 Mixtures of benzene and cyclohexane

Using the force fields and settings of Sections 3.3.1 and 3.3.2, mixtures of benzene and cyclohexane were simulated at constant *NVT* conditions (300 K using a very gentle thermostat with τ = 50 ps) and at three compositions: $x_{benzene}$= 0.25 (324 benzene, 972 cyclohexane, ρ=793.7 kg/m^3); $x_{benzene}$= 0.5 (645 benzene, 645 cyclohexane, ρ = 815.0 kg/m^3); $x_{benzene}$= 0.75 (645 benzene, 216 cyclohexane, ρ = 845.5 kg/m^3). A timestep of 2 fs was used, W was 100, sampling times were 1 ns ($x_{benzene}$= 0.25 and 0.5) and 950 ps ($x_{benzene}$= 0.75). Except for a constant temperature gradient, the steady state of these binary systems also requires a constant concentration gradient, which took much longer time (~2 ns) to reach. This will be discussed in more details in Section 4.

The force field was specifically selected for reproducing thermodynamic properties of benzene-cyclohexane mixtures [23], but not with thermal conductivities in mind. The thermal conductivity varies in a regular way and exhibits a shallow minimum at $x_{benzene}$= 0.75 (Figure 3.11). However, the variation of λ with composition is small; between $x_{benzene}$= 0.5 and $x_{benzene}$= 1, it is about the same as the variations due to different W, small differences in T, and whether or not a thermostat is used. Moreover, when compared to the absolute errors for the mixtures [30], the composition influence on λ is minimal. For a start, the experimental λ of benzene is higher than that of cyclohexane whereas the situation is reversed in the simulations. The only similarity between the two data sets is the negative deviation of λ for mixtures from a linear mixing rule. This points to a clear limitation of the calculation of thermal conductivities by molecular dynamics: The λ of different systems have to differ

significantly to be distinguishable by simulation. The present case of a mixture of two liquids with very similar λ is certainly not a problem usefully studied by MD. See, however, the discussion in the Conclusions (Section 3.4).

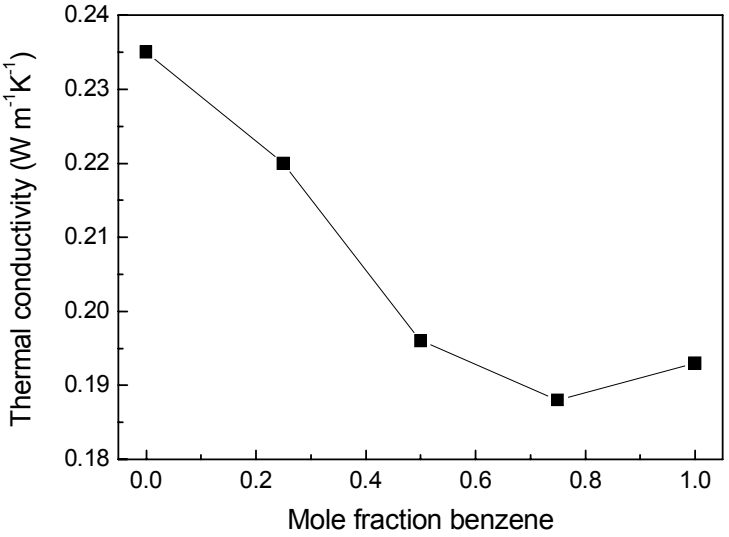

Figure 3.11. Calculated thermal conductivities of benzene-cyclohexane mixtures at around 300 K, $W = 150$ (pure fluids) and $W = 100$ (mixtures).

3.3.4 Equipartition of the kinetic energy

Figure 3.12 (benzene, $W = 500$), 3.13 (benzene, $W = 150$) and 3.14 (Cyclohexane, $W = 300$, coupling time 0.2 ps) display the profiles of temperatures calculated from the average kinetic energies of the different degrees of freedom (translation, rotation, and vibration, total). It shows that the kinetic energy is equipartioned between them, not only for the system as a whole, but also locally in the individual slabs. Exceptions are the exchange slabs, where the translational temperature deviates from the others, because the exchange of centre-of-mass velocities selectively influences this degree of freedom. The exchange slabs are excluded from the calculation of the temperature gradient. The three examples show the equipartition of kinetic energy of systems under three extreme situations: the weakest (Figure 3.12) and the strongest (Figure 3.13) perturbations, and the most intensive coupling between the system and the thermal bath (Figure 3.14). Similar equipartitioning has been found also for other molecular fluids (data not shown).

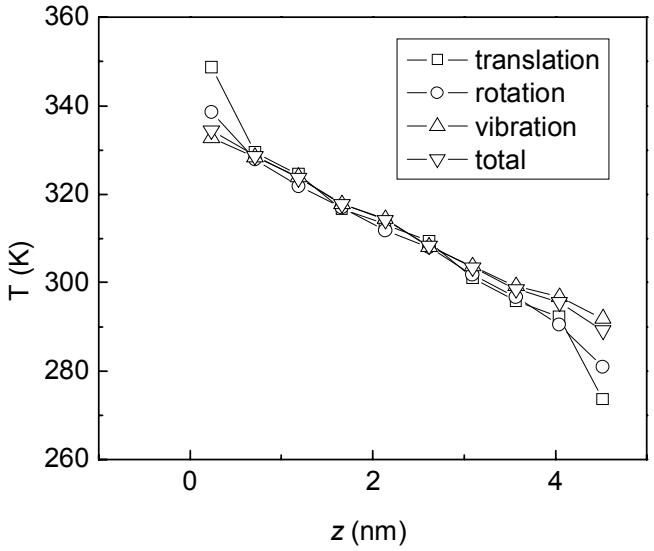

Figure 3.12. Temperature profiles for the different degrees of freedom for benzene at the weakest perturbation (W = 500, no thermostat, 308 K). The two symmetric sides of the simulation cells have been averaged.

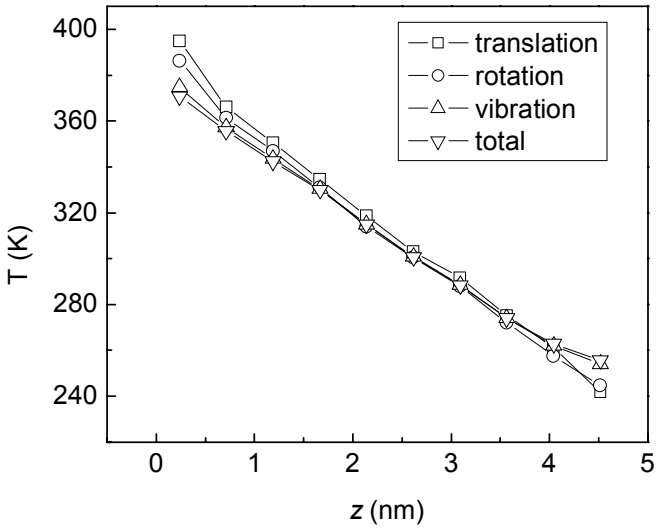

Figure 3.13. Temperature profiles for the different degrees of freedom for benzene at the strongest perturbation (W = 150, no thermostat, 308 K). The two symmetric sides of the simulation cells have been averaged.

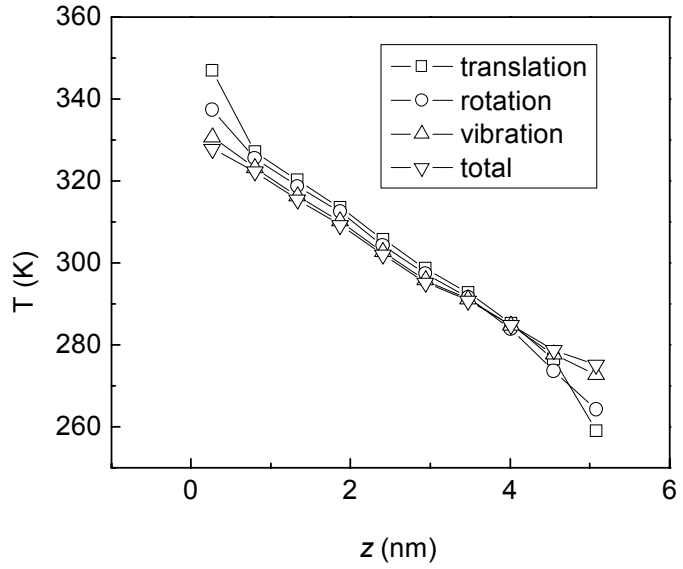

Figure 3.14. Temperature profiles for the different degrees of freedom for cyclohexane at the intermediate perturbation (W = 300, thermostat coupling time 0.2 ps, 300 K). The two symmetric sides of the simulation cells have been averaged.

3.4 Conclusions

The reverse non-equilibrium molecular dynamics method is suitable also for the calculation of thermal conductivities of molecular liquids. The calculated thermal conductivities are relatively insensitive to variations in the RNEMD parameters. In benzene and cyclohexane, λ changed by less than 7% when the exchange period W was varied. This is in line with results on the Lennard-Jones fluid [1] and shows that it is easy to keep the simulation in the linear-response regime. For all cases investigated, the linearity of the temperature profiles showed that the calculated λ is uniform across the system. The simulations also show that, for dense fluids of small to medium size molecules, system sizes of several hundred to some thousand molecules and several nanometers in length are sufficient to avoid size effects.

Despite the theoretical misgivings about thermostatting simulations aimed at the thermal conductivity, it has turned out that in calculations of practical interest a Berendsen thermostat is harmless. Even with an unrealistically short coupling time of 0.2 ps, the λ values calculated in the *NVT* ensemble differed less than 10% from that of an *NVE* simulation for cyclohexane. Normally, temperature-coupling times are at least one order of magnitude longer. Thus, any effect of the thermostat should be smaller. This finding, which is in keeping with previous results for the Lennard-Jones fluid [1] has important implications for future applications, as simulations often have to be thermostatted for a variety of technical or physical reasons.

From the few examples studied here, it appears that the force field potentially has the largest influence on the thermal conductivity. The results for the two cyclohexane

non-bonded parameter sets, one with atomic partial charges, the other without, differ by about 30%. More examples are needed to determine, to which force field parameters the thermal conductivity is most sensitive.

The present study has not been undertaken with the purpose of reproducing experimental thermal conductivities or of finding optimized force field parameters. Nonetheless, the results accumulated here allow some speculations about how a computer model of a molecular liquid must be designed, in order to reproduce or predict its thermal conductivity. It has already been noted (Section 3.3) that the thermal conductivity increases with the available degrees of freedom. All all-atom models (benzene, cyclohexane) produce thermal conductivities larger than experiment. The excess is +40% for benzene, +100% and +50% for the two cyclohexane models, respectively.

Degrees of freedom are removed by removing explicit atoms (united-atom model). Removing aliphatic and aromatic hydrogens and their bond and angle vibrations appears to be particularly useful. Their high frequencies make them quantum oscillators at room temperature, which are not available for heat conduction. This view is supported by previous simulations of Hoheisel et al.[31-33] They report equilibrium calculations of the thermal conductivities of cyclohexane, benzene and mixtures thereof using rigid united-atom Lennard-Jones models. They achieve better agreement with experiment than our work and their deviations are always negative: –15% and –6% for the two cyclohexane models [31, 32], –1% for benzene [32]. The encouraging implication of this speculation is that, for λ, cheap united-atom models may be the models of choice. On the other hand, there would be not one single model that describes the thermal conductivity as well as other properties. A united-atom benzene without an electric quadrupole moment, for example, does not reproduce the experimental liquid structure.

The need for constraining further degrees of freedom is not clear from the results. Luo and Hoheisel [32], on the other hand, achieve a similar agreement with experiment for their completely rigid benzene model. Our results on cyclohexane reveal that the choice of nonbonded parameters within the same functional form can have an effect much larger than that of constraining carbon-carbon bonds or not.

While the foregoing discussion of deviations between simulation and experiment is important for the selection of force fields, it must not be forgotten that the agreement is very good. The largest deviation found is a factor of 2 (cyclohexane). Smaller deviations, between 30 and 50 %, are much more typical. This makes molecular dynamics a useful predictive tool for thermal conductivities.

References

[1] F. Müller-Plathe, J. Chem. Phys. **106**, 6082 (1997).
[2] F. Müller-Plathe, Phys. Rev. E **59**, 4894 (1999).
[3] F. Müller-Plathe and D. Reith, Comput. Theor. Polym. Sci. **9**, 203 (1999)

[4] D. Reith and F. Müller-Plathe, J. Chem. Phys. **112**, 2436 (2000)
[5] P. Bordat, D. Reith, and F. Müller-Plathe, J. Chem. Phys. **115**, 8978 (2001)
[6] Z. Donkó and P. Hartmann, Phys. Rev. E **69**, 016405 (2004)
[7] S.-H. Choi and S. J. Maruyama, Kor. Phys. Soc. **45**, 897 (2004)
[8] C. W. Padgett and D. W. Brenner, Nano Lett. **4**, 1051 (2004)
[9] D. Bedrov and G. D. Smith, J. Chem. Phys. **113**, 8080 (2000)
[10] D. Bedrov, G. D. Smith, and T. D. Sewell, Chem. Phys. Lett. **324**, 64 (2000)
[11] C. Nieto-Draghi, J. Bonet Ávalos, and B. Rousseau, J. Chem. Phys. **119**, 4782 (2003)
[12] P. Bordat and F. Müller-Plathe, J. Chem. Phys. **116**, 3362 (2002)
[13] T. Soddemann, B. Dünweg, and K. Kremer, Eur. Phys. J. E **6**, 409 (2001)
[14] H. X. Guo, K. Kremer, and T. Soddemann, Phys. Rev. E **66**, 061503 (2002); C. Loison, M. Mareschal, K. Kremer, and F. Schmid, J. Chem. Phys. **119**, 13138 (2004); H. X. Guo and K. Kremer, J. Chem. Phys. **118**, 7714 (2003); H. X. Guo and K. Kremer, J. Chem. Phys. **119**, 9308 (2003).
[15] T. Soddemann, G. K. Auernhammer, H. X. Guo, B. Dünweg, and K. Kremer, Eur. Phys. J. E **13**, 141 (2004)
[16] T. Soddemann, B. Dünweg, and K. Kremer, Phys. Rev. E **68**, 046702 (2003)
[17] F. Müller-Plathe and P. M. Bordat, in *Novel methods in soft matter simulations*, Lecture Notes in Physics Vol. 640, edited by M. Karttunen, I. Vattulainen and A. Lukkarinen (Springer, Heidelberg, 2004) p310.
[18] C. Normand, Y. Pomeau, and M.G. Velarde, Rev. Mod. Phys. **49**, 581 (1993)
[19] F. Müller-Plathe, Comput. Phys. Commun. **78**, 77 (1993)
[20] M. P. Allen and D. J. Tildesley, *Computer Simulation of Liquids*, (Oxford University Press, Oxford, 1987).
[21] F. Müller-Plathe and D. Brown, Comput. Phys. Commun. **64**, 7 (1991)
[22] H. J. C. Berendsen, J. P. M. Postma, W. F. van Gunsteren, A. Di Nola, and J. R. Haak, J. Chem. Phys. **81**, 3684 (1984)
[23] G, Milano and F. Müller-Plathe, J. Phys. Chem. B **108**, 7415 (2004)
[24] F. Müller-Plathe, Macromolecules **29**, 4728 (1996)
[25] R. Faller, H. Schmitz, O. Biermann, and F. Müller-Plathe, J. Comp. Chem. **20**, 1009 (1999)
[26] H. Schmitz, R. Faller, and F. Müller-Plathe, J. Phys. Chem. B **103**, 9731 (1999)
[27] R. Witt, L. Sturz, A. Dölle, and F. Müller-Plathe, J. Phys. Chem. A **104**, 5716 (2000)
[28] D. R. Lide, (Ed.) *CRC Handbook of Chemistry and Physics 82nd Edition* (CRC Press, Boca Raton, 2001).
[29] F. Müller-Plathe, Chem. Phys. Lett. **252**, 419 (1996)
[30] Landolt-Börnstein, *Zahlenwerte und Funktionen*, Vol. II (Springer, Berlin 1969) Chapter 5.
[31] C. Hoheisel and A. Würflinger, J. Chem. Phys. **91**, 473 (1989)
[32] H. Luo and C. Hoheisel, J. Chem. Phys. **96**, 3173 (1992)
[33] H. M. Schaink, H. Luo, and C. Hoheisel, J. Chem. Phys. **99**, 9912 (1993)

4. Thermal diffusion in liquid benzene-cyclohexane mixtures

4.1 Introduction

If we use the mole fraction to replace the weight fraction, the Soret coefficient S_T in equation (2.42) can be expressed as:

$$S_T \equiv \frac{D_T}{D_{12}} = -\frac{1}{x_1(1-x_1)}\left(\frac{\partial x_1}{\partial z}\right)\left(\frac{\partial T}{\partial z}\right)^{-1} \tag{4.1}$$

Here a positive S_T means that the particles of species 1 prefer to move towards the cold side of the system. The advantage of this equation is that in RNEMD simulations, where the temperature gradient and the mole fraction gradient can be obtained easily, the Soret coefficient is calculated directly.

We have introduced in Section 1.2 that the magnitude and even the sign of the Soret coefficient sometimes change with the composition, which has been observed in water-alcohol [1-2], cyclohexane-cyclohexanol [3], toluene-hexane [4], benzene-cyclohexane mixtures [5], and even macromolecular solutions such as charged micellar salt solutions [6], colloidal particles [7] and poly (ethylene oxide) ethanol-water solutions [8]. However, research on the microscopic level is still essential to explain this phenomenon. As introduced in Section 1.2, the RNEMD or similar method has successfully simulated the thermal diffusion in Lennard-Jones fluids [9-11], as well as some molecular fluids, such as *n*-alkanes [12-15], and water-alcohol mixtures [16], yielding good results in each case. Due to the few examples in molecular fluids, we applied the RNEMD method to investigate the composition dependence of thermal diffusion in benzene-cyclohexane mixtures.

Recently, Debuschewitz and Köhler have made reliable measurements for the Soret coefficients of benzene-cyclohexane mixtures using the thermal diffusion forced Rayleigh scattering (TDFRS) method [5], making it convenient to compare our simulation results with the experimental data. The magnitude of the Soret coefficients of the mixtures is small (in the order of 10^{-3} K^{-1}), however sufficiently distinguishable at different mole fractions. The benzene-cyclohexane system is therefore a challenge to the algorithm and to the potential models of both molecules.

Hoheisel et al. [17] have already simulated the thermal diffusion of an equimolar benzene-cyclohexane mixture with equilibrium molecular dynamics (EMD) methods. Yet their results are insufficient as their correlation function did not converge. They employed six-center Lennard-Jones potential models, whereas we adopt an all-atom model with partial charges, which gives a better description of realistic molecular liquids.

This work is the first step of our research on the Soret effect of realistic liquids. The purpose is to test the precision of the algorithm when applied to molecular fluids and to test the influence of some algorithm parameters on the results. We use an all-atom force field, which describes the thermodynamics of benzene-cyclohexane mixtures very well [18]. Another objective is to study if and how well such a model is able to describe a small higher-order transport phenomenon such as the Ludwig-Soret effect.

4.2 Computational details

Three different mixtures of cyclohexane and benzene were simulated at temperatures and densities close to ambient conditions, where experimental data are available. The temperature was set as 300 K, unless specified otherwise. The details are summarized in Table 4.1. We used the YASP package [19] with the leap-frog algorithm [20] to run the molecular dynamics simulations, applying orthorhombic periodic boundary conditions. The cell was elongated in z direction, which is the direction of the imposed heat flow ($L_x = L_y = L_z/3$). Bonds were constrained by the SHAKE procedure [21] to a relative tolerance of 10^{-6}. Nonbonded interactions were evaluated from a Verlet neighbor list, which was updated each 15 time steps using a link-cell method. Nonbonded interactions within a molecule were excluded. The cutoff length for nonbonded interactions was r_c = 0.9 nm or 1.1 nm, as specified below, with the corresponding Verlet neighbor list cutoff length being 1.0 nm or 1.2 nm.

Table 4.1. Simulated systems

	x_{benzene}	$N_{\text{cyclohexane}}$	N_{benzene}	N_{total}	Density ρ (kg/m^3)	t^{sim} (ns)
1	0.25	972	324	1296	793.8	8
2	0.50	645	645	1290	815.0	16
3	0.75	216	675	891	845.0	25

See Table 3.1 for the details of the force field. The intramolecular force field contained constraints, harmonic bond angle bending, periodic cosine-type torsional potentials (cyclohexane), as well as harmonic dihedral potentials (benzene out-of-plane). For the intermolecular all-atom Lennard-Jones potential we employed Lorentz-Berthelot mixing rules for unlike interactions. For the treatment of electrostatic interactions we used the reaction-field method [19]. The force field parameters for benzene were modified from the OPLS model [18] (See Table 3.1). For cyclohexane we initially used an automatically optimized force field without partial charges on carbon and hydrogen [18]. In order to investigate the force field influence, also the OPLS nonbonded parameters for cyclohexane (see Table 3.1 force field II) were employed in one of the systems, x_{benzene} = 0.25.

The time step was 2 fs. All RNEMD simulations were carried out at constant *NVT* conditions to calculate the Soret coefficient S_T. The average temperature was kept constant by Berendsen's thermostat [22], with the temperature coupling time being τ_T

= 50 ps. The steady state was established in 2 ns, after which the sampling period started. The sampling time t^{sim} was varied from 8 ns to 25 ns for the three systems (Table 4.1).

The transport coefficients related to the Soret coefficients in equation (4.2) were estimated. The mutual and self- diffusion coefficients were obtained from 400 ps of EMD simulations at constant *NPT* conditions (300 K, 1 atm) for all the three systems. The self-diffusion coefficient is calculated via equation (2.24), and the mutual diffusion coefficient D_{12} is calculated from equation (2.25).The slope of the mean-square displacement vs. t was calculated in the linear regime, about from 30 ps to 170 ps for the self-diffusion coefficient and from 10 ps to 20 ps for the D_{12}. The error given is the standard deviation of the x, y and z components of the diffusion coefficient. The D_{12} values in the RNEMD simulations were also calculated. Since a temperature gradient is added in z-direction, we take the average of only the x and y components of the D_{12}. The difference between the two components is used as the error estimation of D_{12}. The slope of the mean-square displacement was calculated in the linear range of about 20-100 ps. The thermal diffusion coefficients D_T are obtained via equation (4.1).

4.3 Result and discussion

4.3.1 Preliminary study: Establishing the steady state

Time autocorrelation functions of the local temperature and the mole fraction in one slab, averaged over all slabs, show that the relaxation time for the temperature, which is around 100 ps (Figure 4.1), is significantly shorter than that of the concentration, which ranges from 1 ns to 2 ns (Figure 4.2). This indicates that the temperature gradient reaches the steady state faster than the concentration gradient. Comparing the three systems with different compositions we notice that the relaxation times of the temperature are very similar (Figure 4.1). The relaxation times of the mole fractions for the three systems are also of similar order. The small differences in the magnitude are regarded as statistical variations. We also observe that all the three concentration autocorrelation functions show a range where they are negative, albeit with small absolute values. At present, we are unable to explain this phenomenon or to attribute it unambiguously to insufficient statistics.

We also compare the auto correlation functions of local temperature and mole fraction for different perturbation intensities (exchange number W = 200 and W = 100) for $x_{benzene}$ = 0.25. There is no significant difference between the two relaxation times for the temperature (Figure 4.3), and for the concentration (Figure 4.4). This indicates that for both perturbation frequencies the temperature and concentration gradients reach steady state at approximately the same time. Thus a higher heat flux (higher perturbation) does not necessarily cause a faster convergence of the concentration and temperature gradient.

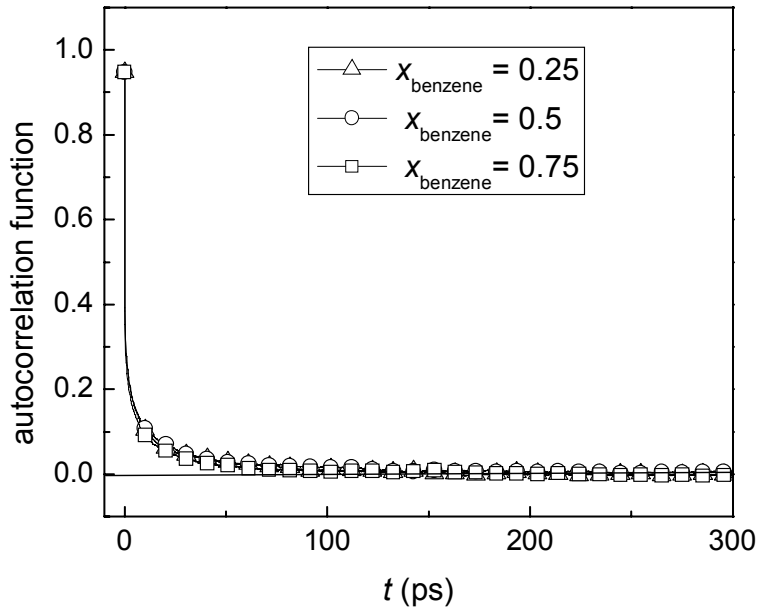

Figure 4.1. Time autocorrelation function of the local temperature in one slab, averaged over all slabs, for different concentrations ($x_{benzene}$ = 0.25, 0.50, 0.75) at 300 K and W = 100.

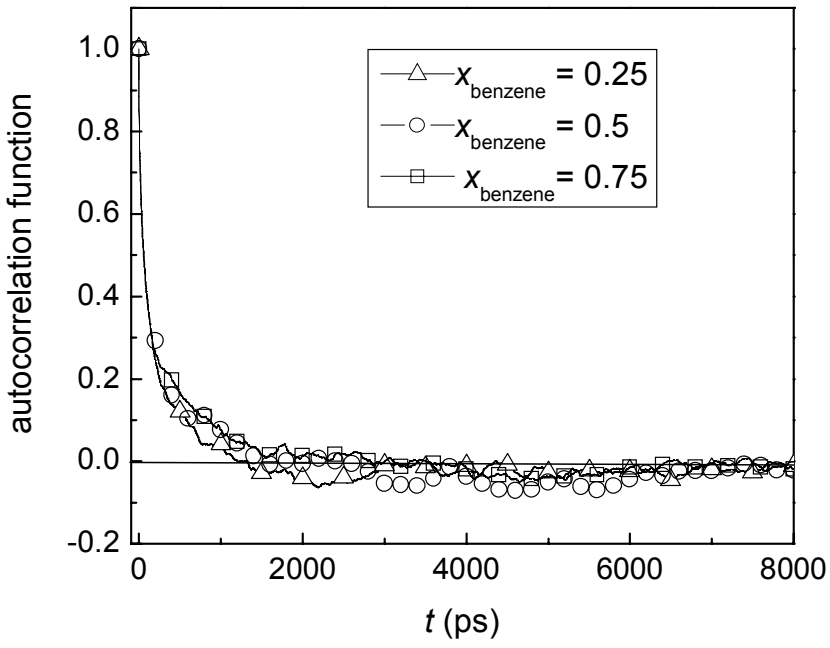

Figure 4.2. Time autocorrelation function of the local mole fraction in one slab, averaged over all slabs, for different concentrations ($x_{benzene}$ = 0.25, 0.50, 0.75) at 300 K, and W = 100.

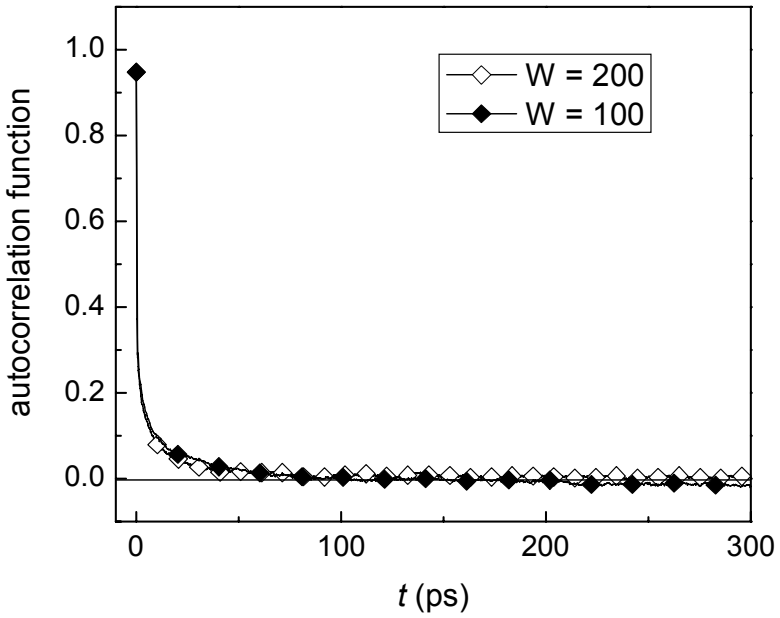

Figure 4.3. Time autocorrelation function of the local temperature in one slab, averaged over all slabs, for concentration $x_{benzene}$ = 0.25 at 324 K and different W (200 and 100).

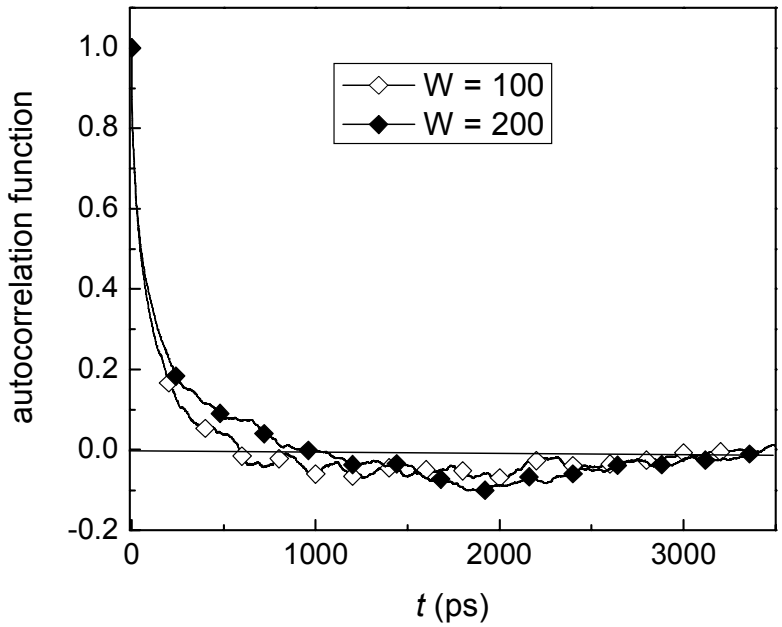

Figure 4.4. Time autocorrelation function of the local mole fraction in one slab, averaged over all slabs, for concentration $x_{benzene}$ = 0.25 at 324 K and different W (200 and 100).

4.3.2 Preliminary study: Sensitivity of the Soret effect to simulation parameters

Details of the force field such as the cutoff length may affect the efficiency of the algorithm and the results. To investigate the influence of the cutoff, we have carried out simulations in one system ($x_{benzene}$ = 0.25, 324 K, 1 atm, W = 100) for two different cutoff distances (0.9 nm and 1.1 nm). The long-range interactions do not affect the results to a great extent. Both the temperature gradient (Figure 4.5) and the concentration gradient (Figure 4.6) are the same for both cutoffs. The Soret coefficient is -6.1×10^{-3} K^{-1} in both cases.

While the applied perturbation should be kept small enough to ensure a linear response of the system, a higher perturbation intensity causes a better signal/noise ratio. We impose separately two perturbation intensities (W = 200 and W = 100) to the same system (cutoff = 1.1 nm) used for the cutoff influence test mentioned above. The good linearity of temperature gradient (Figure 4.7) and mole fraction gradient (Figure 4.8) for both perturbations indicates a linear response of the system. However, there is a significant difference between the calculated Soret coefficients of the two simulations. With the higher perturbation, the value of the Soret coefficient becomes $(-6.1 \pm 0.7) \times 10^{-3}$ K^{-1}, which is 65% higher than the experimental value -3.7×10^{-3} K^{-1} in magnitude. The Soret coefficient calculated at the lower perturbation is $(-9.7 \pm 1.1) \times 10^{-3}$ K^{-1}, thus overestimating the experimental values by a factor of 2.6. The better result obtained with W = 100 is probably due to the higher signal-to-noise ratio. Therefore the perturbation intensity W = 100 was used for the all following calculations on systems with different mole fractions.

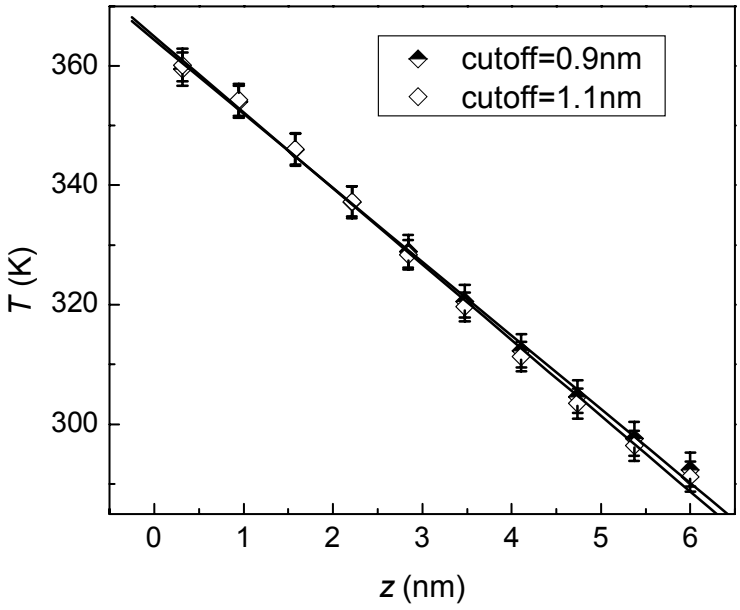

Figure 4.5. Cutoff dependence of the temperature profile for $x_{benzene}$ = 0.25 at 324 K, W = 100.

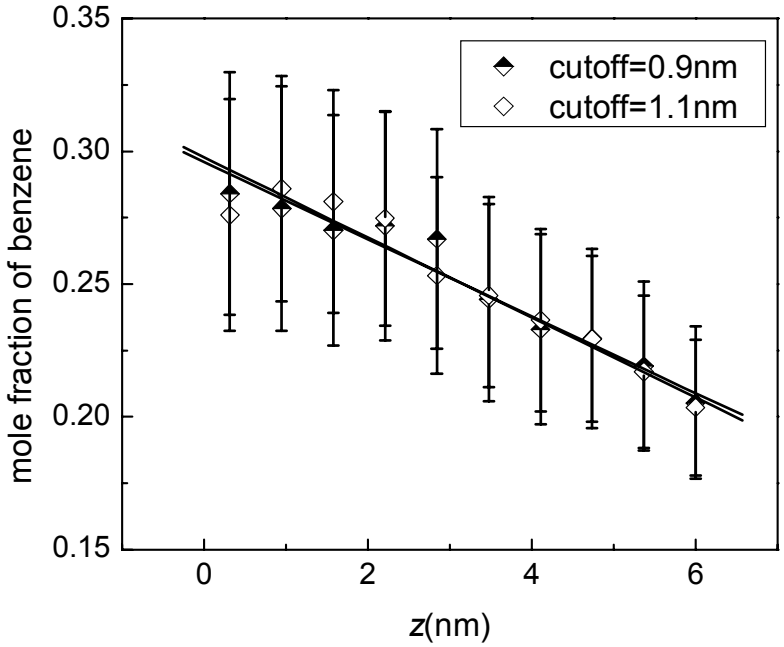

Figure 4.6. Cutoff dependence of the mole fraction profile for $x_{\text{benzene}} = 0.25$ at 324 K, $W = 100$.

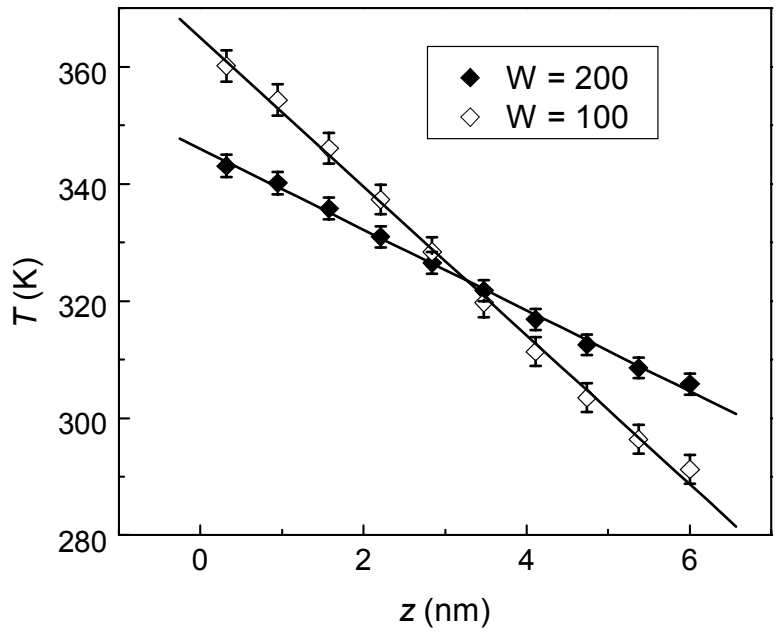

Figure 4.7. Dependence of the temperature profile on the velocity exchange frequency W for $x_{\text{benzene}} = 0.25$ at 324 K.

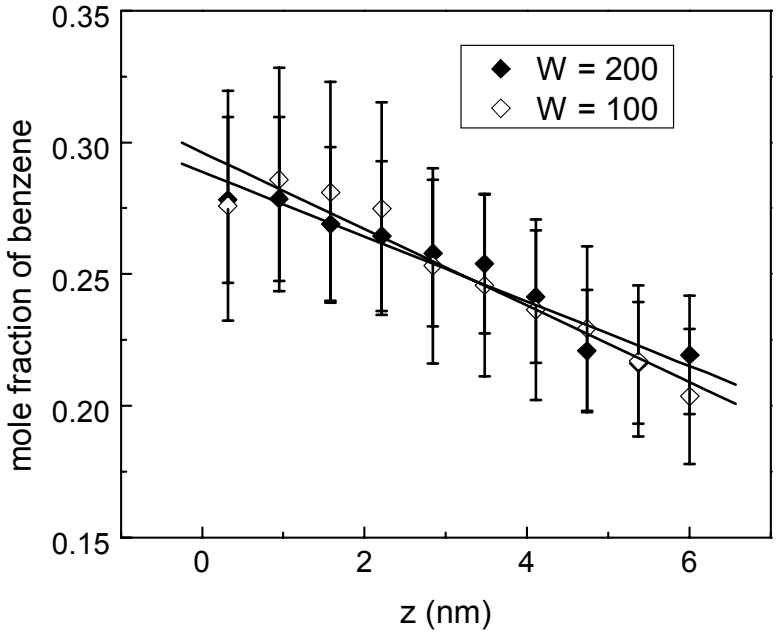

Figure 4.8. Dependence of the mole fraction profile on the velocity exchange frequency W for $x_{\text{benzene}} = 0.25$ at 324 K.

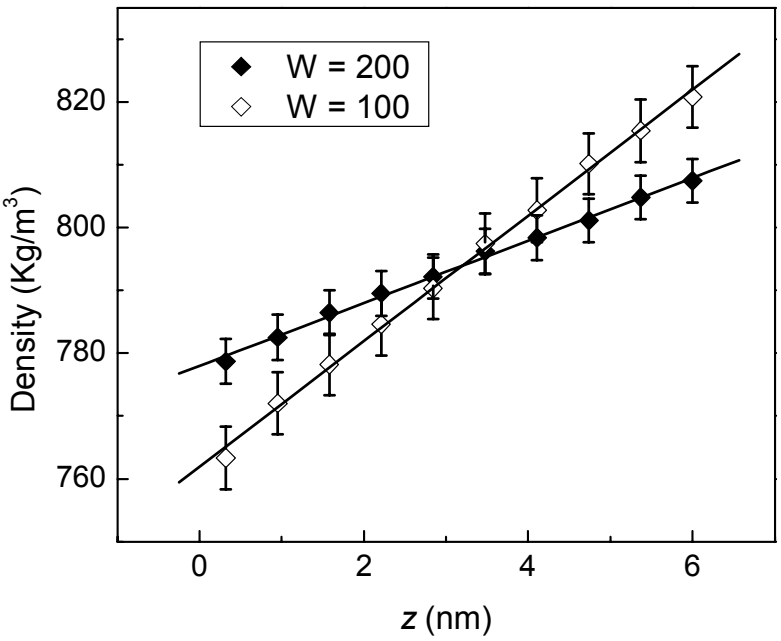

Figure 4.9. Density profiles for $x_{\text{benzene}} = 0.25$ at 324 K, cutoff = 1.1 nm, $W = 200$ and 100.

The temperature profile (Figure 4.7) shows that the temperature in the "hottest" slab is very close to the boiling point of benzene (353.1 K) and cyclohexane (353.7 K). In order to rule out the formation of a vapor phase, the density profile is plotted (Figure

4.9). It is linear throughout the entire system, and the mixture is liquid in every slab. Moreover, also the mutual diffusion coefficient of the system is that of an entirely liquid system, $(2.1 \pm 1.1) \times 10^{-5}$ cm^2 s^{-1}, confirming the absence of a gas phase. We did not try simulations with stronger perturbations, because that would increase the danger of a phase transition or a non-linear response.

4.3.3 Concentration dependence of the Soret coefficient

Three benzene-cyclohexane mixtures are used to test the applicability of the algorithm to the reproduction of the composition dependence of the Soret coefficient. Linearity of the temperature profile (Figure 4.10) and mole fraction profile (Figure 4.11) indicates that the system has reached the steady state. The standard deviation in each slab is around 5%-10% for the mole fraction, and less than 2 K for the temperature. The following values for the Soret coefficients were determined by simulations at around 300 K: $(-6.7 \pm 0.8) \times 10^{-3}$ K^{-1} ($x_{benzene} = 0.25$), $(-5.5 \pm 1.0) \times 10^{-3}$ K^{-1} ($x_{benzene} = 0.50$), $(-5.3 \pm 0.9) \times 10^{-3}$ K^{-1} ($x_{benzene} = 0.75$). Statistical errors range from 12% to 18% (Figure 4.12). The negative sign indicates the lighter component benzene moves to the hot side, as expected. Furthermore, the Soret coefficient increases when the benzene mole fraction increases from 0.25 to 0.75, which is also in agreement with experiment. The values at $x_{benzene} = 0.50$ and $x_{benzene} = 0.75$ are, however, very similar. Comparing our simulation results with the experimental data we observe a systematic error for the magnitude of the Soret coefficient, always being around $(3\text{-}5) \times 10^{-3}$ K^{-1} higher (Figure 4.12). We then estimated the diffusion and thermal diffusion coefficients to investigate the sources of the systematic error for the Soret coefficients. The self-diffusion coefficients of benzene and cyclohexane (Table 4.2) are 30% to

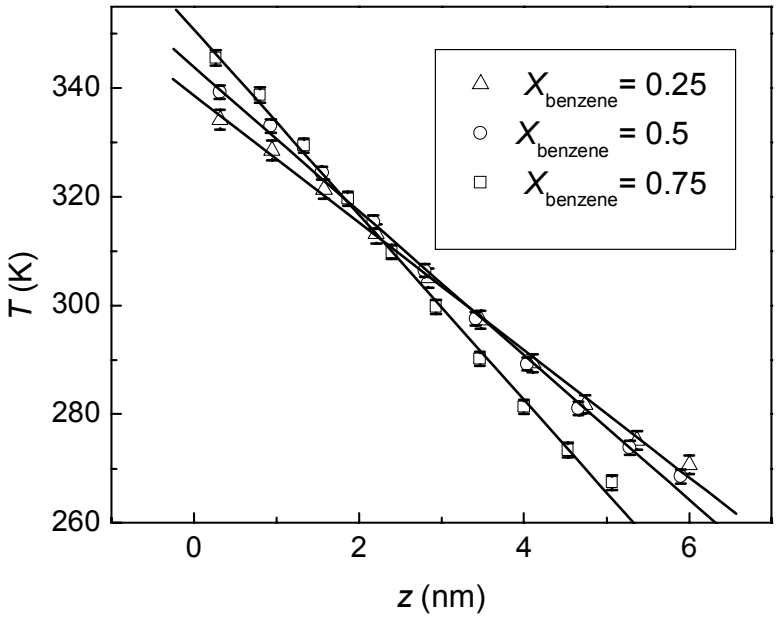

Figure 4.10. Temperature profiles for $x_{benzene} = 0.25$, 0.5, 0.75 at 300 K.

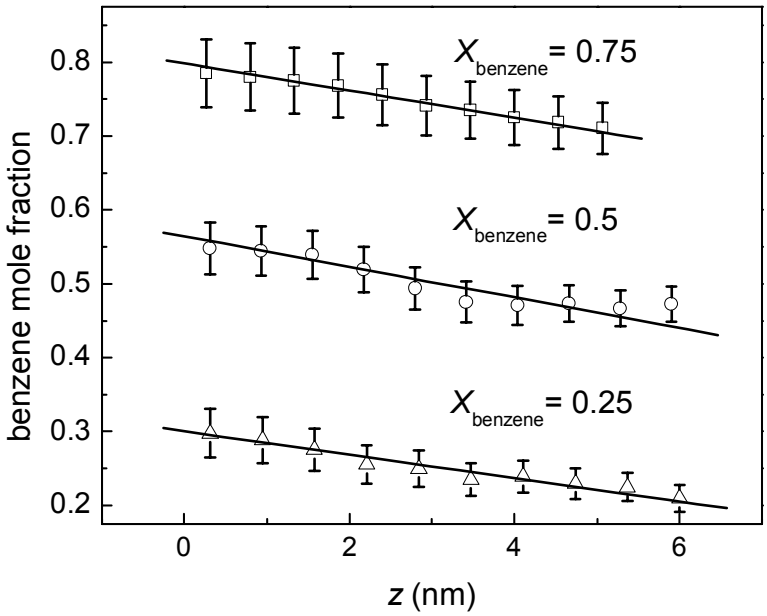

Figure 4.11. Mole fraction profiles for $x_{benzene}$ = 0.25, 0.5, 0.75 at 300 K.

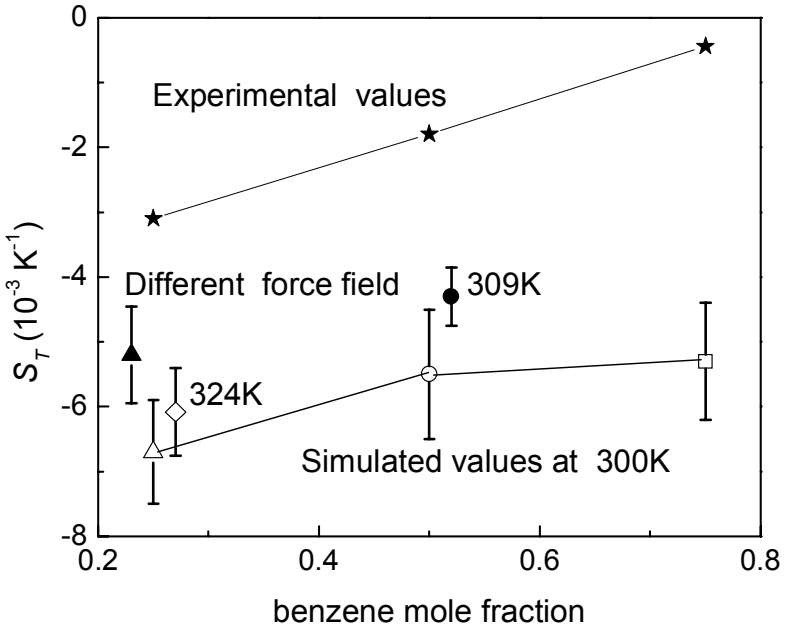

Figure 4.12. Soret coefficient for $x_{benzene}$ = 0.25, 0.50, 0.75. Experimental data are from Ref. 5.

60% lower than the experimental values [23]. The mutual diffusion coefficients D_{12} are in better agreement with the experimental values [23], but all being ~0.5 × 10^{-5} cm^2 s^{-1} lower (Table 4.2), and contributing positively to the systematic error for the Soret coefficient. The convergence of the D_{12} is not so good due to a too short

simulation time (400 ps). Since the computation is expensive, we tried to obtain a more precise D_{12} from the RNEMD runs which have much longer simulation times. Here only the mean-square displacement in x and y directions that are perpendicular to the heat flux have been used. Although it is physically not strictly correct, we intend to achieve a similar value of the D_{12} as in the EMD. However, the D_{12} obtained in the non-equilibrium systems are: $(2.1 \pm 0.1) \times 10^{-5}$ cm^2 s^{-1} ($x_{\text{benzene}} = 0.25$), $(2.5 \pm 0.1) \times 10^{-5}$ cm^2 s^{-1} ($x_{\text{benzene}} = 0.50$), and $(1.9 \pm 0.9) \times 10^{-5}$ cm^2 s^{-1} ($x_{\text{benzene}} = 0.75$), all much higher than those of the equilibrium systems. Thus we adopt the mutual diffusion coefficients of the equilibrium systems to calculate the thermal diffusion coefficients D_T. The magnitudes of the D_T (TABLE 4.2) are also systematically higher than the experimental ones, being around (4-7) $\times 10^{-8}$ cm^2 s^{-1} K^{-1}. The systematic errors could be due to the noise of the system, since we have obtained better results of S_T for simulations with higher perturbation. It is more likely, though, to be caused by the force field parameters, which were developed to reproduce the density and heat of vaporization [18] rather than transport properties.

Table 4.2. Calculated and experimental [a] self- and mutual diffusion coefficients (10^{-5} cm^2 s^{-1}, obtained from EMD simulations), Soret coefficients (10^{-3} K^{-1}), and thermal diffusion coefficients (10^{-8} cm^2 s^{-1} K^{-1}) of the benzene-cyclohexane mixtures (T = 300 K).

x_{benzene}	D_1	D_2	D_{12}	S_T	D_T
0.25	1.1±0.2(2.2)	0.8±0.1 (1.8)	1.4±0.5(1.8)	-6.7±0.8(-3.1)	-9.4±4.5(-5.6)
0.5	1.5±0.2(2.3)	1.2±0.2 (2.0)	1.3±0.7(1.8)	-5.5±1.0(-1.8)	-7.2±5.2(-3.2)
0.75	1.7±0.3(2.4)	1.5±0.3 (2.1)	1.4±0.9(1.9)	-5.3±0.9(-0.4)	-7.4±6.1(-0.8)

[a] In parenthesis, experimental values for self-diffusion and mutual-diffusion coefficients are from Ref. 23, and those for S_T and D_T are from Ref. 5. Experimentally, S_T is the primary measured property and D_T is derived.

An additional simulation using OPLS non-bonded force field parameters for cyclohexane ($x_{\text{benzene}} = 0.25$) supports our assumption above that the force field parameters might cause the systematic error of Soret coefficients. Under the same conditions (T = 300 K, ρ = 793.8 kg/m^3) the Soret coefficient of the additional simulation is $(-5.2 \pm 0.8) \times 10^{-3}$ K^{-1}, about 20% higher than the result with the previous force field (Figure 4.12), thus closer to the experimental value. Simulations with single-site Lennard-Jones models of benzene and cyclohexane with the same RNEMD method produced Soret coefficients with even a wrong sign [24]. Our result shows that the intermolecular interactions determine substantially the Soret effect. This is in agreement with previous studies of the Soret effect [11], which have shown that interaction details can affect the Soret effect significantly.

As described above, Hoheisel et al. [17] attempted to calculate the Soret coefficient of a benzene-cyclohexane mixture ($x_{\text{benzene}} = 0.5$, 313 K) using six-center Lennard-Jones potentials by equilibrium molecular dynamics (EMD). Because of the large statistical error, they roughly obtained the result as $(-3.7 \pm 2.0) \times 10^{-3}$ K^{-1}. Compared with this data, our result, $(-4.3 \pm 0.5) \times 10^{-3}$ K^{-1} (309 K), is in the range of the statistical variation. Thus our simulation results are in coincidence with this previous EMD

study. Due to the high variation of their data, we could not conclude here whether the force field causes the difference of the results or not.

Except for benzene-cyclohexane mixtures, studies on *n*-alkanes [12-14] and water-alcohol [16] binary mixtures using the same algorithm have showed a good quantitative agreement with experimental values. For *n*-alkane mixtures, due to their weak composition dependence of the Soret coefficient, it is difficult to say whether these simulations predict the right tendency or not, because the differences of the Soret coefficients were in the same order of magnitude as the uncertainty interval ~0.5 $\times 10^{-3}$ K^{-1}. For alcohol aqueous solutions, the Soret coefficients strongly vary with the composition around the concentration where the sign of S_T changes (>3 $\times 10^{-3}$ K^{-1}). The simulations reproduced exactly how the Soret coefficient changed with the mole fraction. The concentration dependence of our system was between that of *n*-alkane mixtures and alcohol aqueous solutions. Still, the algorithm reproduced the experimental differences of the Soret coefficients very well when the mole fraction of benzene varies between 0.25 and 0.5. The poorer differentiation between the remaining two compositions ($x_{benzene}$ = 0.50 and $x_{benzene}$ = 0.75) may be caused by the small magnitude of the Soret coefficient of the latter due to a lower signal/noise ratio. Our all-atom model is very close to the behaviour of realistic benzene-cyclohexane liquids and it is a great improvement over simpler models such as single-site Lennard-Jones models [24], or six-site Lennard-Jones models [17]. It is safe to say that the model is able to reproduce a difference of the Soret coefficient around 2 $\times 10^{-3}$ K^{-1} in realistic liquids. But it is difficult to study systems with too small absolute values of Soret coefficient, such as < 1 $\times 10^{-3}$ K^{-1}.

4.3.4 Temperature dependence of the Soret coefficient

Studies on systems such as Lennard-Jones particles [11, 25], methane-*n*-decane [15], and toluene-*n*-hexane [4], showed that the Soret effect decreases with the increase of the system temperature. Under the same volume, we observed the same trend in our simulations for systems of $x_{benzene}$ = 0.25 and 0.5 (Figure 4.12). Although there is no experimental or few reliable simulation data (in the section above, we have compared the result with that of the six-site Lennard-Jones model [17] for system $x_{benzene}$ = 0.5 at 309 K) available at higher temperature for comparison, the trend is in line with the previous studies concerning the temperature dependence of the Soret effect in other fluids. As the Soret coefficient of this realistic model takes a very long CPU time to converge, we refrained from undertaking a systematic investigation of the temperature influence.

4.4 Conclusions

We have applied a *molecular* exchange version of the reverse non-equilibrium molecular dynamics algorithm on a realistic all-atom model of benzene-cyclohexane mixtures. The auto-correlation functions of the temperature and mole fraction show that the temperature gradient establishes itself about ten times faster than the mole

fraction gradient. The perturbation strength has a small influence on the convergence time of the mole fraction.

Varying some algorithm parameters, we have found that, above a certain value, the cutoff distance has almost no influence on the Soret coefficient. This indicates a minor contribution of long-range interactions. The conclusion is also in accordance with previous studies on Lennard-Jones fluids [11], where the cutoff had nearly no influence on the Soret coefficients when it was above 2.5σ. In contrast, a stronger perturbation produces better results due to a better signal/noise ratio provided linear response holds.

We computed the concentration dependence of the Soret coefficient. The simulation results show the same tendency as the experimental values: the absolute value of S_T decreases with higher benzene content. However, both the simulated Soret coefficients and the thermal diffusion coefficients are systematically too large in magnitude. The error is most probably caused by the choice of the force field parameters. The method is able to differentiate Soret coefficients with an uncertainty of around 2×10^{-3} K^{-1}.

Further we investigated the temperature dependence of the Soret effect. The results show that the Soret effects decrease as the temperature increases, which is in agreement with previous studies. Most notably, it was shown that reverse non-equilibrium molecular dynamics can be applied to calculate the Soret coefficients in realistic molecular fluids.

While the calculated Soret coefficients overestimate the experiment by (3-5) $\times 10^{-3}$ K^{-1} in magnitude, this constitutes a substantial improvement over previous attempts to calculate the S_T of benzene-cyclohexane mixtures with simpler models. Some of these went as far as predicting the wrong sign. Also in view of thermal diffusion being a small, indirectly driven transport process (an off-diagonal term in the Onsager theory), it is reassuring that one can get so close to experiment using a force field, which has been parameterized to reproduce completely different liquid properties. Even for the direct transport coefficients, like the diffusion coefficient or the thermal conductivity, the disagreement with experiment are about to 50-100% for many well tested fluid models. It is, however, also evident from this work that the calculation of converged Soret coefficient requires considerable computational resources.

References

[1] L. J. Tichacek, W. S. Kmak, and H. G. Drickamer, J. Phys. Chem. **60**, 660 (1956).
[2] P. Kolodner, H. Williams, and C. Moe, J. Chem. Phys. **88**, 6512 (1988).
[3] I. Prigogine, L. De Brouckere, and R. Amand, Physica **16**, 851 (1950).
[4] K. J. Zhang, M. E. Briggs, R. W. Gammon, and J. V. Sengers, J. Chem. Phys. **104**, 6881 (1996).
[5] C. Debuschewitz and W. Köhler, Phys. Rev. Lett. **87**, 055901-1 (2001).

[6] R. Piazza and A. Guarino, Phys. Rev. Lett. **88**, 208302-1 (2002).
[7] B.-J. de Gans, R. Kita, B. Müller, and S. Wiegand, J. Chem. Phys. **118**, 8073 (2003).
[8] S. Wiegand, J. Phys.: Condens. Matt. **16**, R357 (2004).
[9] D. Reith and F. Müller-Plathe, J. Chem. Phys. **112**, 2436 (2000).
[10] B. Hafskjold, T. Ikeshoji, and S. K. Ratkje, Mol. Phys. **80**, 1389 (1993).
[11] P. Bordat, D. Reith, and F. Müller-Plathe, J. Chem. Phys. **115**, 8978 (2001).
[12] G. Galliéro, B. Duguay, J.-P. Caltagirone, and F. Montel, Fluid Phase Equ. **208**, 171 (2003).
[13] G. Galliéro, B. Duguay, J.-P. Caltagirone, and F. Montel, Phil. Mag. **83**, 2097 (2003).
[14] A. Perronace, C. Leppla, F. Leroy, B. Rousseau, and S. Wiegand, J. Chem. Phys. **116**, 3718 (2002).
[15] J.-M. Simon, D. K. Dysthe, A. H. Fuchs, and B. Rousseau, Fluid Phase Equilibria **150-151**, 151 (1998).
[16] C. Nieto-Draghi, *Transport and structural properties of aqueous solutions of organic solvents*, Thesis Universitat Rovira i Virgili, Tarragona, 2003.
[17] H. M. Schaink, H. Luo, and C. Hoheisel, J. Chem. Phys. **99**, 9912 (1993).
[18] G. Milano and F. Müller-Plathe, J. Phys. Chem. B **108**, 7415 (2004).
[19] F. Müller-Plathe, Comput. Phys. Commun. **78**, 77 (1993).
[20] M. P. Allen and D. J. Tildesley, *Computer Simulation of Liquids* (Oxford University Press, Oxford, 1987).
[21] F. Müller-Plathe and D. Brown, Comput. Phys. Commun. **64**, 7 (1991).
[22] H. J. C. Berendsen, J. P. M. Postma, W. F. van Gunsteren, A. Di Nola, and J. R. Haak, J. Chem. Phys. **81**, 3684 (1984).
[23] Landolt-Börnstein, *Zahlenwerte und Funktionen* (Springer, Berlin, 1969) p657.
[24] D. Reith, *Thermal diffusion in binary Lennard-Jones liquids*, Diploma thesis, University of Mainz and Max-Planck-Institute for Polymer Research, 1998.
[25] S. Yeganegi, J. Phys. Soc. Japan. **72**, 2260 (2003).

5. Thermal diffusion in dilute polymer solutions: Influence of chain length, chain stiffness, and solvent quality

5.1 Introduction

In most cases, polymer molecules migrate to the cold side of the solution due to their larger masses [1-5]. However, in some dilute polymer solutions under or close to poor solvent conditions, such as the poly (vinyl alcohol) in water at 25 ˚C [6], poly (*N*-isopropylacrylamide)-ethanol at temperatures lower than the critical solution point [7], poly (ethylene oxide) (PEO)-water-ethanol mixtures at certain water to ethanol ratios [8, 9], the macromolecules were observed to move to the warm side. A two-chamber lattice model shows that the Soret coefficient S_T of the polymer becomes less positive (i.e. the polymer has a smaller tendency to accumulate in the cold, or it even moves to the hot) in poorer solvent quality condition, and a mere change of the interactions between the polymer and the solvent can cause a sign change of S_T [10]. Here this kind of interactions between the unlike components, such as the monomer-solvent interactions, is called cross interaction. Similarly, the interactions between the same components, such as the monomer-monomer and solvent-solvent interactions are called pure interactions. Besides in the polymer solutions, the sign changes of S_T with composition were also observed in small molecule solutions, [11-14] mostly in associating liquids. Simulations of Lennard-Jones fluids also reveal that the variations of both the cross interactions and the mole fractions of the components can induce a sign change [15]. Altogether, the solvent quality, controlled by the relations between the cross interactions and the pure (like component) interactions, the mole fractions of the components, as well as the temperature, affect the sign of the Soret coefficient.

Measurements of the thermal diffusion coefficient D_T disclosed another interesting behavior of thermal diffusion which has been introduced in Section 1.2: D_T of polymer chains does not depend on the degree of polymerization. This is widely observed for polymer solutions, such as polystyrene and its derivatives in different solvents [3, 2, 5], polystyrene in ethyl acetate [3], and aqueous poly (ethylene glycol) solutions [4]. It has also been found that the shortest chain needed to achieve a constant D_T is determined by the properties of both the polymer and the solvent. Sometimes a dimer [4] or a trimer [16] already has the same D_T as infinite chains. In order to explain microscopically this chain length independence of D_T in dilute polymer solutions, several theories have expressed the idea that D_T is determined by local interactions between the solvent and the polymer segments, and not with the entire chain. One needs to notice that a polymer segment consists of one or several monomers. For instance, according to Brochard and De Gennes's explanation [17], in a dilute polymer solution where there is no hydrodynamic coupling between polymer segments, the heat flux under a concentration gradient arises from the local friction between the polymer segments and the solvent around. As a result, the heat flux associated with mass flux (the Dufour effect) is independent of the number of the segments for one polymer chain. According to Onsager reciprocity relation, the mass

flux associated with heat flux (thermal diffusion) should also be independent of that number. Khazanovich derived a segmental theory for highly dilute polymer solutions [18] on the base of Smoluchowski equation for diffusion, where the probability density in configurational space is defined as a function of the friction and diffusion constant of the polymer segment. He predicted that D_T is related to the diffusion coefficient and the friction coefficient activation energy of the segments. According to the Stokes law, the friction coefficient activation energy is equal to that for solvent viscosity, hence he obtained the equation $D_T = D_{seg}U_s/RT^2$, where D_{seg} is the segmental diffusion coefficient, U_s the solvent activation energy for viscous flow, R the gas constant, and T the temperature. This equation shows that the thermal diffusion of the entire polymer chain is only determined by the segmental mobility. Therefore the flexibility of the chain which affects the segmental mobility can also affect the thermal diffusion of the polymers. The segmental theory predicted that D_T was independent of the polymer molecular weight. But it was not possible for the theory to yield quantitative data because the isothermal diffusion coefficient for segment can only be estimated from that for monomer or oligomer [4]. Most recently, Schimpf and Semenov proposed the thermophoresis theory [19], which is based on the same concept as the segmental theory that D_T of polymer in dilute solutions is related to the segmental mobility under the temperature gradient. Instead of the segmental diffusion coefficient, this theory uses the properties of the solvent, the effective segmental size, as well as the segment-solvent interactions to express the segmental mobility:

$$D_T = -\frac{16\alpha r_m^2 A}{27\eta v_0} \tag{5.1}$$

r_m is the segmental radius, α the thermal expansion factor of the solvent, η viscosity of the solvent, v_0 the specific volume occupied by a solvent molecule. A is the Hamaker constant for the interaction potential between the solvent and the polymer segments. There is no direct data for A, so it is estimated from the Hamaker constants of the pure monomer ($A_{m\text{-}m}$) and the pure solvent ($A_{s\text{-}s}$) by $A = \sqrt{A_{m\text{-}m}A_{s\text{-}s}}$. Note the equation (5.1) is derived only for nonelectrolyte solvents. The model is able to qualitatively predict D_T. For example, for two polymers of polymethylmethacrylate and polystyrene, the model predicted the general trends how D_T changed with the solvents; however, it overestimated the values of D_T by a factor of 2-4 [17]. Besides the theoretical explanations, several experiments have obtained a scaling law for some polymers of above 100 monomers in dilute solutions: S_T and D_{12} are reciprocally proportional to the polymer molecular mass with a power of 0.53, which results in a constant value of D_T [4, 20].

The purpose of this research is to test the applicability of the RNEMD method in polymer thermal diffusion simulations. A generic bead-spring model of a polymer in a generic solvent is built to study the thermal diffusion in dilute polymer solutions. In the first part, the influence of the solvent quality is investigated. One can tune the solvent quality by changing the cross interactions between solvent and solute. The variation of S_T with the monomer-solvent cross interactions in solutions of 8-mers is studied qualitatively. In addition, a symmetric binary non-ideal Lennard-Jones fluid is employed to investigate generically the sign change of S_T in different solvent conditions. In the second part, the chain length (in)dependence of D_T is studied. The

first step of this part is to find out whether this phenomenon can be reproduced by such a simple model; further more it is interesting to see the influence of the local structure of the polymer chains. The stiffness of the chain is varied to yield different local structures. Finally, the influence of the monomer mole fraction on the polymer thermal diffusion is also investigated in order to test whether the concentration used is sufficiently low.

5.2 Computational details

Reduced units were used with the Lennard-Jones parameters of argon (ε = 1 kJ/mol, σ = 0.3405 nm, m = 39.95 g/mol) as reference (see reference 21 for reduced units). Simulations were all carried out at T^* = 0.8, ρ^* = 0.9, P^* ~ 0.017. The monomers of the polymers of various chain lengths (denoted as "monomer" in the following) had the same nonbonded interaction parameters as the solvent atoms (denoted as "solvent"). The mole fraction of the monomers was fixed at 0.1 for all systems irrespective of the chain length. The solvent consisted of 6480-8640 atoms. The monomer had a mass m^* of 1 and a particle diameter σ^* of 1, so do the solvent atoms. The monomer-monomer interaction parameter ε_{11}^* and the solvent-solvent interaction parameter ε_{22}^* were always kept at 1, and the cross monomer-solvent interaction parameter ε_{12}^* was varied. In the bead-spring model, adjacent monomers were connected by harmonic potentials. The equilibrium bond length l_b^* was 0.58, nearly half of the particle diameter. The reduced bond force constant k^* was 25770 which was sufficiently large to ensure that under T^* the vibrational displacement of the bond length was one order less than l_b^*. The values of l_b^* and k^* chosen could avoid the cross between the chains, at the same time, k^* was sufficiently small to provide a large time step which reduced the CPU time. The persistence length l_p, which is defined via the decay of the bond direction correlation function along the chain backbone [22], was set to 2.5, 4.2, and 7.9 (the unit here is l_b^*). The larger the l_p, the more rigid is the polymer chain. This was accomplished by varying the treatment of bond angles between three neighbouring beads: the 1-2 and 1-3 non-bonded interactions were excluded for chains of l_p = 2.5; only 1-2 non-bonded interactions were excluded for chains of l_p = 4.2; and a linear angle potential ($V_{linear-angle} = \sum_{angles} k_l(1+\cos\phi)$, k_l^* = 52.53) was used for chains of l_p = 7.9 to keep three neighbouring beads in a nearly linear arrangement. The number of monomers in the monodisperse polymer chains was varied from 4 to 20. The cutoff length was 2.9 σ, with the related Verlet neighbour list cutoff being 3.2 σ.

All simulations were carried out with the YASP package [23]. Equilibrium molecular dynamics (EMD) was carried out under *NPT* conditions both to obtain a well equilibrated initial system for RNEMD, and to calculate the mutual diffusion coefficient D_{12} [24]. RNEMD simulations were carried out under *NVT* conditions. The average temperature was kept constant using Berendsen's thermostat [25]. The temperature coupling time t^*_{coup} was 46.5 for RNEMD simulations, and 0.23 for EMD ones. The time step Δt^* of the leap-frog algorithm [26] was set to 0.0023. The production time was 1.2-4 × 10^6 time steps for D_{12}, and 4-12 × 10^6 time steps for S_T (after ~12-30 × 10^6 time steps of establishing the steady state). In order to produce

heat flux in RNEMD simulation, atomic velocity swaps were imposed each W = 50-600 time steps, depending on the magnitude of the Soret coefficient; the larger the magnitude is, the larger the W is. Periodic boundary conditions were applied. The Soret coefficient was calculated with a rectangular box ($L^* \times L^* \times 3L^*$) elongated in the z direction, where the temperature gradient was imposed. The L^* depended on the particle numbers to keep the same density. A cubic box was used to calculate the D_{12}, as compared to the rectangular box, it convergences faster in all three directions. In order to test the influence of the box size, the D_{12} of one 16-mer solution (l_p = 4.2) was calculated with three different box sizes. The calculated reduced mutual diffusion coefficients D_{12}^* were (4.9 ± 0.7) × 10^{-3} (L^*~ 17.8, solvent consists of 4608 atoms), (4.6 ± 0.1) × 10^{-3} (L^*~20.4, solvent consists of 6912 atoms), (4.7 ± 0.6) × 10^{-3} (L^*~22.5, solvent consists of 9216 atoms). The differences of the D_{12}^* between the last two systems are ~2%. Therefore a medium size box (L^*~20.4) was used to calculate the D_{12} of all other systems.

5.3 Result and discussion

5.3.1 Influence of solvent quality

In order to tune the solvent quality, we adjusted the cross interaction ε_{12}^* in the 8-mer solutions (l_p = 4.2). For good solvent conditions, all cross interactions ε_{12}^* were larger than the pure interactions (ε_{11}^* = ε_{22}^* = 1). The calculated values of S_T^* (calculated with equation $S_T^* = S_T \varepsilon / k_B$) are positive and the magnitude increases with ε_{12}^*: 9.4 ± 0.4 (ε_{12}^* = 1.41), 18.2 ± 1.1 (ε_{12}^* = 2.0), and 33.4 ± 2.6 (ε_{12}^* = 2.45), denoting that the 8-mer prefers the cold region in better solvent conditions (Figure 5.1). Previous research with lattice models showed the same tendency that the S_T of polymer in dilute solutions is more positive in a better solvent condition [10]. In order to explain this phenomenon, we refer to the theory of Hafskjold et al. [27], which assumes the heat transfer in the cold region is dominated by the molecular interactions, while the kinetic energy is more responsible for the heat transfer in the hot region. In our case, the cross interaction is larger than the pure interaction, hence, the higher concentration of the minority component on the cold side will enlarge the heat transfer from molecular interaction potentials; and the smaller proportion of this component on the hot side will increase the mobility of the particles. Consequently, a larger ε_{12}^* promotes the minority component to move to the cold region for a better heat transfer. When the ε_{12}^* is increased to 2.83, the Soret effect is strong enough to lead to a phase separation (Figure 5.2) at the same temperature gradient ($\partial T^*/\partial z^*$ = 0.025) as in the system of ε_{12}^* = 2.45 (atomic velocity swaps were imposed every 500 time steps). This phase separation in good solvent conditions at a high temperature gradient was also observed experimentally in a polystyrene-polybutadiene-dioctyl- phthalate solution [28].

As mentioned before, the sign of the Soret coefficient can change when the solvent quality changes. Thus, we reduced the solvent quality from good to poor to study this question. The ε_{12}^* was set to 1 for the same 8-mer system as above. Unfortunately, phase separation happened in this system already in equilibrium MD, as oligomer chains attract each other. This is a complication due to the polymeric nature of the

solute. So we chosen a symmetric binary Lennard-Jones fluid, i.e. the solute and solvent consist of the same single particles. In this system, the mole fraction of the

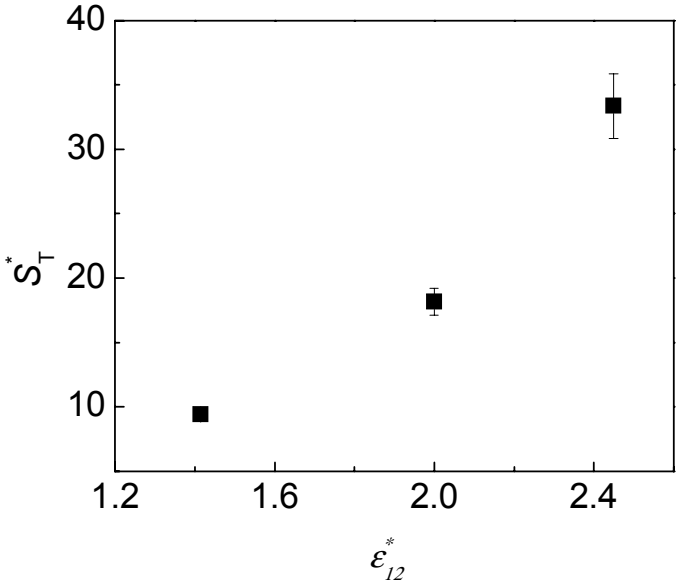

Figure 5.1. The dependence of the Soret coefficient on solvent-monomer interactions for 8-mer solutions. A positive S_T means that the polymer moves to the cold region.

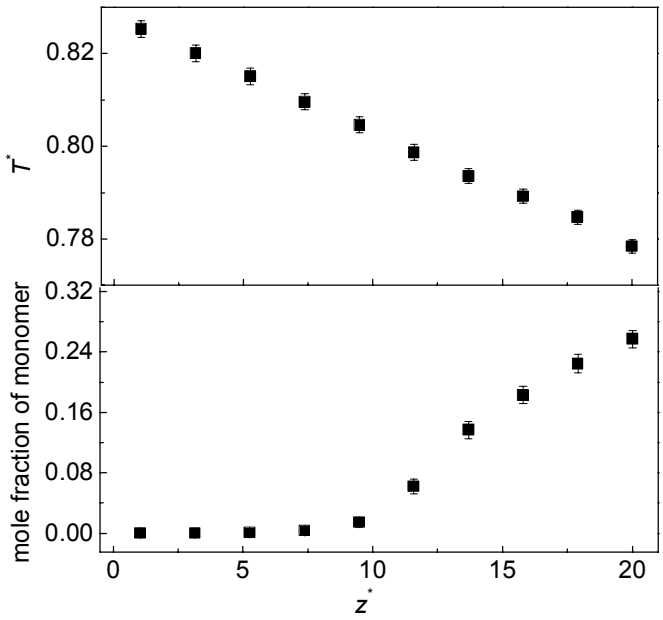

Figure 5.2. Phase separation at a temperature gradient of $\partial T^* / \partial z^* = 0.025$ for 8-mer solution with $\varepsilon_{12}{}^*$ of 2.83.

"solute" was also fixed at 0.1, but the solute atoms are less localized and more difficult to assemble compared to the longer chain systems with monomer mole fraction of 0.1. The pure interactions ε_{11}^* and ε_{22}^* were equal to 1. However, the interaction ε_{12}^* between "solute" atoms and "solvent" atoms was altered between 0.90 and 3.33. The calculated S_T^* are -0.49 ± 0.04 (ε_{12}^* = 0.90), 1.10 ± 0.05 (ε_{12}^* = 1.41), and 2.4 ± 0.1 (ε_{12}^* = 3.33). A sign change was observed: the minority component migrated to the warm side in poor solvent condition, but behaved inversely in good solvent condition. The Lennard-Jones solutions are non-ideal, for the ε_{12}^* are not of the values calculated with Lorentz-Berthelot mixing rule ($\varepsilon_{12}^* = \sqrt{\varepsilon_{11}^* \varepsilon_{22}^*}$). Hence, a special repulsive interaction between solvent and solute exists for ε_{12}^* smaller than 1, so does the attractive interaction for ε_{12}^* larger than 1. Our result confirms the conclusions of lattice model simulations [10, 15] that the cross interaction variations due to the specific interactions affect the magnitude and the sign of S_T dramatically. It also explains why this sign change of S_T due to cross interaction changes were mostly observed experimentally in associating solutions [11-13], where the specific interactions, such as hydrogen bonding or electrostatic interactions, exist. They do, however, also indicate that hydrogen bonding is not necessary to achieve a sign change. Our model is no associating fluid and yet its non-ideality of mixing is sufficient to cause a sign change.

The results above remind us that too high values of ε_{12}^* are not suitable for further simulation studies of polymer thermal diffusion, since the temperature gradient must be kept quite small to prevent phase separation. This may cause an unsatisfactory signal-noise ratio [29]. On the other hand, long chains tend to agglomerate when the ε_{12}^* is small enough, and it becomes hard to calculate the Soret coefficient. Therefore, ε_{12}^* is set to 2.0 for the following simulations.

5.3.2 Influence of chain length and chain stiffness

Solutions of polymers with different lengths and three chain stiffness were simulated. The independence of D_T of the chain length was observed for all three stiffnesses for long enough chains (Table 5.1). The stiffness of the chain affects D_T substantially. The chain length where D_T becomes constant is between 8 to 16 monomers, depending on the persistence length (Table 5.1, see Section 5.2 for the adjustment of the different l_p in our model). The general tendency is that for the more flexible chains, constancy of D_T is reached at a smaller number of monomers. This suggests that there may be a systematic dependence of the cross-over length on the persistence length. In Figure 5.3, D_T is shown as a function of multiples of the persistence length. The figure indicates that D_T becomes constant when the chain length is around 2-3 l_p in spite of different types of stiffness. Experimentally, the D_T of poly(ethylene glycol) in aqueous solutions is constant above the trimer [4], which is of around 1.5 to 2 l_p (l_p ~ 0.4 to 0.5 nm, corresponding to 1.5 to 2 monomers) [30]; the D_T of polystyrene in toluene solutions is constant above the 14-mer [31], which is around 3.5 l_p (l_p~1 nm, or 4 monomers) [31]. Our result agrees well with these two experimental values. However, the thermal diffusion behaviour of styrene oligomers (16, 3, 2) in ethyl acetate is quite different, where D_T becomes constant above the dimer [16]. The different thermal diffusion behaviour of polystyrene in two solvents suggests that it

would be of further interest to study the solvent effect on the chain length independence of D_T in polymer solutions. In addition, Rauch and Köhler found that the butyl end groups affected the D_T of the shorter chains more than the longer chains in polystyrene toluene solutions, due to their higher mass weight in the shorter chains [31]. Although the butyl end groups contributes only ~10% to the total values of D_T of polystyrene , it would be another interest to study the influence of different end groups on the thermal diffusion of the entire polymer chains, especially for shorter chains.

Table 5.1. Calculated chain length (in)dependence of the reduced mutual diffusion coefficient D_{12}^* ($D_{12}^* = D_{12}\sqrt{m}/\sigma\sqrt{\varepsilon}$), the Soret coefficient S_T^*, and the thermal diffusion coefficient D_T^* for polymers with different persistence length l_p.

l_p (l_b^*)	M	D_{12}^* (10^{-2})	S_T^*	D_T^*
2.5	4	1.2±0.2	8.0±0.4	0.10±0.02
	6	0.87±0.05	14.6±0.9	0.13±0.02
	8	0.71±0.04	21.9±0.9	0.15±0.02
	12	0.56±0.03	27.9±1.7	0.16±0.02
4.2	4	1.1±0.1	7.5±0.5	0.08±0.02
	6	0.84±0.17	11.9±0.4	0.10±0.03
	8	0.66±0.05	17.9±0.6	0.12±0.02
	12	0.58±0.02	29.7±1.2	0.17±0.02
	16	0.46±0.01	36.0±3.3	0.17±0.02
7.9	4	0.95±0.06	8.3±0.5	0.08±0.01
	6	0.75±0.07	15.2±1.1	0.12±0.02
	8	0.71±0.10	19.6±1.1	0.14±0.03
	12	0.57±0.04	39.4±1.6	0.22±0.03
	16	0.45±0.02	55.0±2.8	0.25±0.03
	20	0.43±0.02	60.6±3.2	0.26±0.03

Figure 5.3 also shows another tendency, especially for longer chains, namely that the magnitude of D_T increases with l_p. If we suppose that the effective size of a "segment" grows as the persistence length, the result qualitatively agrees with Schimpf and Semenov's thermophoresis theory [22] which states that D_T is proportional to the effective radius of the segment when the solvent situation is kept constant. The values of S_T are proportional to the reduced molecular mass M of the polymer (Figure 5.4). The magnitude of S_T, like that of D_T, also tends to increase with the persistence length for longer chains, as is most obvious for the most rigid system (l_p = 7.9). The mutual diffusion coefficient D_{12} is inversely proportional to M (Figure 5.5). We are unable to obtain quantitatively the scaling laws [4, 20] for the M dependence of S_T and D_{12} due to the relatively short chains studied here, but the calculated D_{12} and S_T should reciprocally depend on M for D_T to become constant.

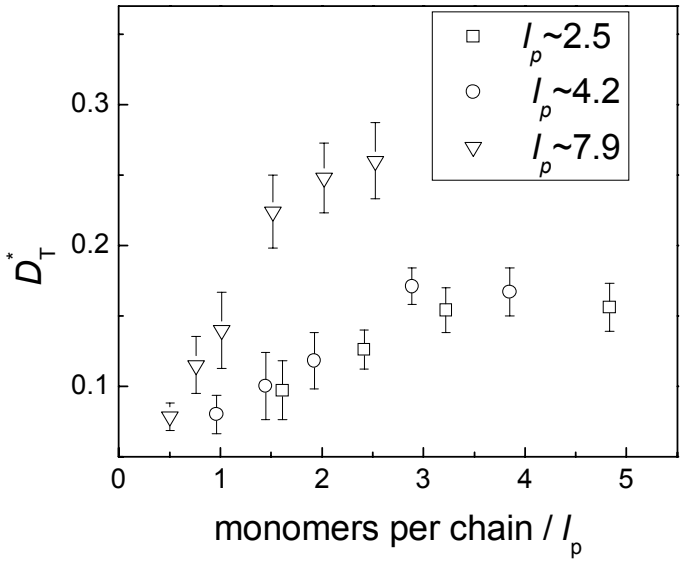

Figure 5.3. Dependence of the thermal diffusion coefficient on chain length (in terms of multiples of the persistence length) for three different chain stiffnesses.

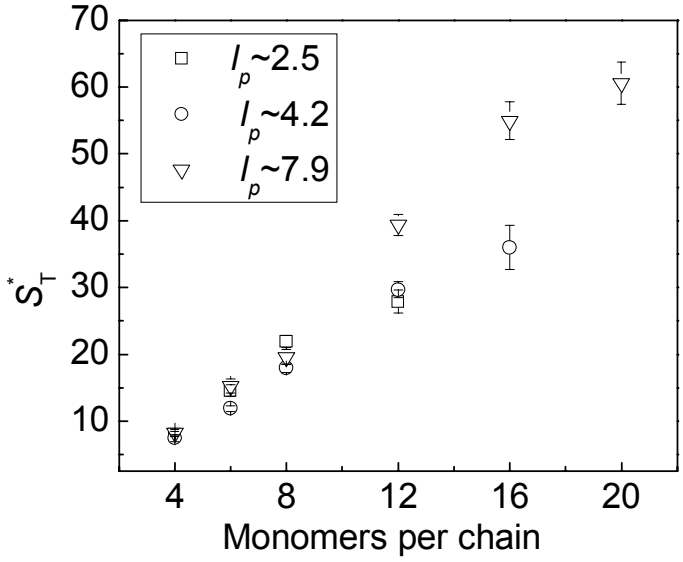

Figure 5.4. Dependence of the Soret coefficient on chain length for three different chain stiffnesses.

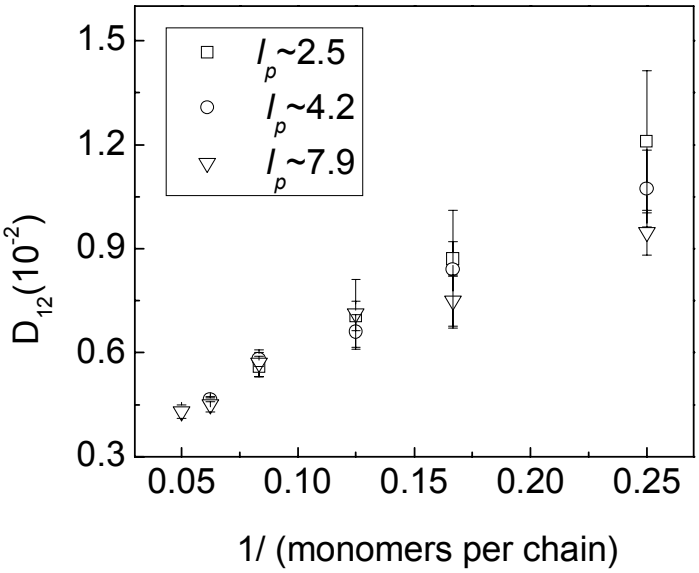

Figure 5.5. Dependence of the mutual diffusion coefficient on chain length for three different chain stiffnesses.

5.3.3 Influence of the monomer mole fraction

A monomer mole fraction of 0.1 is close to the lowest limit where simulations yield a good statistics with a suitable system size. A more dilute solution would need a larger number of solvent particles and much longer simulation times. But is it sufficiently low to reproduce the thermal diffusion behaviour found experimentally for polymers in dilute solutions?

Therefore, the thermal diffusion of a solution of 8-mers (l_p = 4.2) was simulated at three different monomer mole fractions (0.075, 0.1, 0.125, Table 5.2). The D_T^* barely changes with concentration: the interpolated value at infinite dilute solution is 0.13, the difference between which and the D_T^* of monomer fraction 0.10 is smaller than the error bar. When the concentration rises, the S_T^* has a small tendency to increase, while D_{12}^* softly decreases. Previous experimental studies showed that the concentration had almost no influence on D_T, D_{12} and S_T in dilute polymer solutions, whereas it affected D_T, D_{12} and S_T significantly when approaching the concentrated solutions [5, 20, 31-32]. In our results, only small changes of D_T, D_{12}, and S_T were observed when the monomer fraction varied 25% from 0.1, indicating a thermal diffusion behaviour for polymers in dilute solutions. In addition, the pronounced molecular mass dependence of S_T and D_{12} (Figure 5.4, 5.5) shown in Section 5.3.2 also proves that not only the 8-mer solution but all other systems, too, are not in the concentrated regime, where S_T and D_{12} are independent of the molecular mass [5, 20, 32]. We can not determine whether the systems are in dilute or semi-dilute regime only by the thermal diffusion behaviours for the polymers of such small molecular masses; for some experiments showed that the polymers of small molecular masses had similar thermal diffusion behaviours in both regimes [5, 31]. However, we can

conclude that in the simulations, a monomer mole fraction of 0.1 is able to reproduce the thermal diffusion behaviour found experimentally for polymers in dilute solutions.

Table 5.2. Calculated reduced values of the mutual diffusion coefficient D_{12}^*, the Soret coefficient S_T^*, and the thermal diffusion coefficient D_T^* in a solution of 8-mers (l_p = 4.2) at three different monomer mole fractions.

Monomer mole fraction	D_{12}^* (10^{-2})	S_T^*	D_T^*
0.075	0.77±0.08	15.8±0.6	0.12±0.02
0.1	0.66±0.05	17.9±0.6	0.12±0.02
0.125	0.61±0.05	17.5±0.6	0.11±0.02

5.4 Conclusions

We have used a generic bead-spring model to investigate the thermal diffusion in dilute polymer solutions by means of reverse non-equilibrium molecular dynamics. All systems are simulated with a fixed monomer mole fraction of 0.1. Studies of an 8-mer solution show a big influence of the solvent quality on the Soret coefficient, which is more positive (higher affinity of the polymer to the cold region) in better solvent condition. This phenomenon that the minority component (8-mer) prefers more the cold side in better solvent conditions agrees with previous simulations [15], and can be explained by Hafskjold et al.'s heat transfer mechanism [27]. A sign change of the Soret coefficient has been observed in a symmetric non-ideal binary Lennard-Jones fluid with the minority component designated as solute. When the mixed interaction is larger than the pure interactions, the minority component is inclined to stay in the cold side, and vice versa. This confirms that specific interactions, such as the hydrogen bonding and electrostatic interactions, may bring about a sign change by effectively altering the solvent quality. However, changes in the solvent quality due to other mechanisms should lead to similar sign changes.

Moreover, the experimentally known chain-length independence of D_T in dilute polymer solutions is reproduced by this simple computer model; more flexible chains are observed to achieve constant D_T at shorter chain lengths compared to rigid chains. If the chain length is described in terms of the persistence length l_p, D_T becomes constant when the chain length is of around 2-3 l_p for all chain stiffnesses. This agrees well with most of the experimental results. It is also found that a higher stiffness of the chain increases both the Soret coefficient and the thermal diffusion coefficient substantially, especially for longer chains. This founding qualitatively agrees with Khazanovich's theory that the flexibility of the polymer chain can affect the thermal diffusion of polymers in dilute solutions. The mutual diffusion coefficient, however, is not so sensitive to the chains stiffness. The reverse non-equilibrium molecular dynamics is shown to be a useful tool for the study of the thermal diffusion of polymer in conjunction with such a generic model.

Additional simulations in a solution of 8-mers at three different monomer mole fractions prove that the monomer mole fraction of 0.1 is sufficiently low for studying the thermal diffusion behaviours for polymers in dilute solutions. The thermal diffusion coefficient of the polymer at monomer fraction of 0.1 is found to be very close to that of infinitely dilute solution.

References

[1] M. Schimpf and J. Giddings, Macromolecules **20**, 1561 (1987).
[2] M. Schimpf and. J. Giddings, J. Polym. Sci. **B 27**, 1317 (1989).
[3] P. Rossmanith and W. Köhler, Macromolecules **29**, 3203 (1996).
[4] J. Chan, J. J. Popov, S. Kolisnek-Kehl, and D. G. Leaist, J. Solution Chem. **32**, 197 (2003).
[5] J. Rauch and W. Köhler, J. Chem. Phys. **119**, 11977 (2003).
[6] M. Giglio and A. Vendramini, Phys. Rev. Lett. **38**, 26 (1977).
[7] R. Kita, G. Kircher, and S. Wiegand, J. Chem. Phys. **121**, 9140 (2004).
[8] B. J. de Gans, R. Kita, S. Wiegand, and J. Luettmer-Strathmann, Phys. Rev. Lett. **91**, 245501 (2003).
[9] B. J. de Gans, R. Kita, B. Müller, and S. Wiegand, J. Chem. Phys. **118**, 8073 (2003).
[10] J. Luettmer-Strathmann, J. Chem. Phys. **119**, 2892 (2003).
[11] L. J. Tichacek, W. S. Kmak, and H. G. Drickamer, J. Phys. Chem. **60**, 660 (1956).
[12] P. Kolodner, H. Williams, and C. Moe, J. Chem. Phys. **88**, 6512 (1988).
[13] I. Prigogine, L. De Brouckere, and R. Amand, Physica (Amsterdam) **16**, 851 (1950).
[14] G. Wittko and W. Köhler, J. Chem. Phys. **123**, 014506 (2005).
[15] B. Rousseau, C. Nieto-Draghi, and J. Bonet Avalos, Europhys. Lett. **67**, 247 (2004).
[16] S. Wiegand, J. Phys.: Condens. Matter **16,** R357 (2004).
[17] M. E. Schimpf, in *Thermal Nonequilibrium Phenomena in Fluid Mixtures*, Lecture Notes in Physics Vol. 584, edited by W. Köhler and S. Wiegand (Springer, Verlag, 2002) p 285.
[18] T. N. Khazanovich, J. Polym. Sci. C **16,** 2463 (1967).
[19] M. E. Schimpf and S. N. Semenov, J. Phys. Chem. B **104,** 9935 (2000).
[20] J. Rauch and W. Köhler, Phys. Rev. Lett. **88**, 185901-1 (2002).
[21] D. Reith and F. Müller-Plathe, J. Chem. Phys. **112**, 2436 (2000).
[22] R. Faller, F. Müller-Plathe, and A. Heuer, Macromolecules **33**, 6602 (2000).
[23] F. Müller-Plathe, Comput. Phys. Commun. **78,** 77 (1993).
[24] H. Schmitz, R. Faller, and F. Müller-Plathe, J. Phys. Chem. B **103**, 9731 (1999).
[25] H. J. C. Berendsen, J. P. M. Postma, W. F. van Gunsteren, A. Di Nola, and J. R. Haak, J. Chem. Phys. **81**, 3684 (1984).
[26] M. P. Allen and D. J. Tildesley, *Computer Simulation of Liquids* (Oxford University Press, Oxford, 1987).
[27] B. Hafskjold, T. Ikeshoji, and S. K. Ratkje, Mol. Phys. **80**, 1389 (1993).
[28] J. Kumaki, T. Hashimoto, and S. Granick, Phys. Rev. Lett. **77**, 1990 (1996).

[29] M. Zhang, E. Lussetti, L. E. S. De Souza, and F. Müller-Plathe, J. Phys. Chem. B. **109**, 15060 (2005).
[30] J. Brandrup, E. H. Immergut, and E. A. Grulke (Ed.), *Polymer Handbook 4th edition* (John Wiley & Sons Inc. USA, 1999).
[31] J. Rauch and W. Köhler, Macromolecules **38**, 3571 (2005).
[32] K. J. Zhang, M. E. Briggs, R. W. Gammon, and J. V. Sengers, J. Chem. Phys. **111**, 2270 (1999).

6. Summary

The application of the reverse non-equilibrium molecular dynamics method to study the heat conduction and matter transfer is extended to the molecular fluids: benzene, cyclohexane, and their mixtures, as well as to dilute polymer solutions. An all-atom model is used to mimic realistic molecular fluids, and a generic bead-spring model is used for the polymer.

The first part of this work is devoted to the molecular fluids. Firstly, we investigate the influence of different variants of the molecular dynamics algorithm and their combinations with other system parameters on the thermal conductivity, the Soret coefficient, and the mutual diffusion coefficient (equilibrium molecular dynamics is used).

It is found that, in the linear response region, the perturbation intensity has a small impact on the thermal conductivity, while a stronger perturbation produces better results for the Soret coefficient. The steady state of the non-equilibrium system is characterized by a linear gradient of temperature and concentration. The temperature gradient is found to establish itself ten times faster than the concentration gradient, and the CPU time required for calculating the Soret coefficient is much longer than for the thermal conductivity. This is because the thermal conduction is a much more pronounced effect (diagonal transport effect in the Onsager theory) than thermal diffusion (off-diagonal effect) and it has a much better signal-to-noise ratio. The weak signal-to-noise ratio of the thermal diffusion also makes it impossible to calculate a value of the Soret coefficient less than 1×10^{-3} K^{-1}, which is close to the minimum magnitude measurable for the experimental techniques.

Above a certain value, the cutoff length for nonbonded interactions has almost no influence on the Soret coefficient. This indicates a minor contribution of long-range interactions. A system of several hundred to some thousand molecules and of several nanometers in length is large enough to avoid finite-size effects when the thermal conductivity and the mutual diffusion coefficient for dense fluids of small to medium size molecules are calculated. Although it is forbidden in principle, applying a Berendsen thermostat does not significantly alter the calculated thermal conductivity. Therefore, a very gentle thermostat is assumed to be harmless in the calculation of the Soret coefficients. As simulations often have to be thermostatted for a variety of technical or physical reasons, this finding has important implications for future applications. Our conclusions about the perturbation intensity, the cutoff length, and the Berendsen thermostat are in accordance with previous simulations of Lennard-Jones fluids [1].

Secondly, the influence of the force field was also studied. The force field potentially has the largest influence on the thermal conductivity and the Soret coefficient. Two groups of force fields slightly different in the non-bonded parameters, produces the

thermal conductivity for cyclohexane with a 30% disagreement with each other, and lead to about 20% deviation for the Soret coefficient of benzene-cyclohexane mixture. The degrees of freedom of the model are found to affect the heat transfer significantly. Our all-atom models overestimate the experimental thermal conductivities mostly by 30-50% (by 100% only for one system), while the united atom models used by Hoheisel et al. [2, 3] in equilibrium molecular dynamics simulations underestimated the experimental values by around 15%. Although their model is not able to reproduce the realistic structure of benzene, their thermal conductivities are closer to experiment. The overestimation of the thermal conductivity for an all-atom model can be explained by the fact that the vibration of aliphatic and aromatic hydrogens contribute to the heat conduction in the simulations, while in real situation these atoms act as quantum oscillators at room temperature, which are not available for heat conduction.

The all-atom models chosen were parameterised for reproducing the density and the enthalpy of vaporization, not for transport properties. They are known to underestimate the self-diffusion coefficients by a factor of ~2. With these models, most computed thermal conductivities had around 30-50% deviations from the experimental values. This magnitude of the deviations is quite common in the calculations of transport coefficients. Although the Soret coefficients were $(3\text{-}5) \times 10^{-3}$ K^{-1} larger than the experimental values, our simulation has yielded the best results compared to previous simulations [3, 4]. Furthermore, our results have reproduced the tendency of the mole fraction dependence and the temperature dependence of the Soret coefficients. It is also safe to say that the method is able to reproduce a difference of the magnitude of the Soret coefficient of $\sim 2 \times 10^{-3}$ K^{-1}. Altogether, our simulations validated the applicability of the RNEMD method on investigating the heat conduction and the thermal diffusion for molecular fluids as complicated as benzene and cyclohexane.

The discussions above leads to two suggestions: first, a force field parameterised to reproduce the direct transport coefficients such as self-diffusion coefficient may yield better results for the thermal conductivity and the Soret coefficient; second, a model with fewer degrees of freedom than the all-atom models may reproduce the thermal conductivity better. The suggestions can be used in the future to investigate the microscopic mechanism of the thermal diffusion in molecular fluids. For example, it has been recently observed in experiments that the temperature dependence of the Soret coefficients depends on the compositions. This phenomenon happens in molecular fluids such as alkane-benzene [5] and isotopically substituted benzene-cyclohexane mixtures [6]. No microscopic explanation has been proposed.

The second part of this work is to investigate the thermal diffusion in dilute polymer solutions with the RNEMD method. The simulation proves that a simple generic-bead spring model is useful for the study of thermal diffusion in polymer solutions. The model has not only reproduced the chain length independence of the thermal diffusion coefficient, but also yielded a critical range of chain lengths (around 2-3 times the persistence length) where the thermal diffusion coefficient becomes constant. This is largely independent of chain stiffness. This value of the range is supported by several experimental results [7, 8]. It also provides evidence for the theory that it may be the segment, not the entire chain, which decides the thermal diffusion behaviour of a polymer in dilute solution.

The influence of the solvent quality has also been studied. In good solvent conditions, a better solvent quality induces a higher affinity for the polymer to the cold region. This may even go to thermal-diffusion-induced phase separation. However, it is hard to study the thermal diffusion for polymers in poor solvent condition, as the polymer chains start to aggregate in this case. Therefore, we use symmetric non-ideal Lennard-Jones atomic fluids to study the thermal diffusion in different solvent conditions further. A sign change is observed in these fluids when the solvent quality switches from good to poor, which confirms that specific interactions, such as the hydrogen bonding and electrostatic interactions, may bring about a sign change by effectively altering the solvent quality.

For future work to investigate the solvent quality effect on the thermal diffusion of polymers in more detail, the study of the thermal diffusion in poor solvent quality is necessary. It is possible to keep the polymer chains separated in poor solvent conditions when their concentration is reduced with the temperature kept constant. The monomer mole fraction we use is close to the lowest limit where simulations yield good statistics with a suitable system size. A more dilute solution would need a larger number of solvent particles and much longer simulation times. Increasing the temperature might be an alternative way to suppress the phase transition at poor solvent condition with the same monomer fraction. We did not try to simulate at different temperatures in this work due to the limitation of CPU time. Specific questions to be addressed in order to detect the solvent quality effect are: a) what is the molecular reason to determine the migration direction of the macromolecules in different solvent quality? and b) how does the solvent quality affect the critical number of monomers above which the thermal diffusion coefficient is constant?

References

[1] F. Müller-Plathe, J. Chem. Phys. **106**, 6082 (1997).
[2] H. Luo and C. Hoheisel, J. Chem. Phys. **96**, 3173 (1992)
[3] H. M. Schaink, H. Luo, and C. Hoheisel, J. Chem. Phys. **99**, 9912 (1993).
[4] D. Reith, *Thermal diffusion in binary Lennard-Jones liquids*, Diploma Thesis, Max-Planck-Institute, Mainz, 1998.
[5] P. Polyakov and S. Wiegand, in *Thermodiffusion: Basics & Applications*, Edited by M. M. Bou-Ali and J. K. Platten (Mondragon Unibertsitatea, 2006), p399.
[6] G. Wittko and W. Köhler, in *Thermodiffusion: Basics & Applications* (Edited by M. M. Bou-Ali and J. K. Platten (Mondragon Unibertsitatea, 2006), p399.
[7] J. Chan, J. J. Popov, S. Kolisnek-Kehl, and D. G. Leaist, J. Solution Chem. **32**, 197 (2003).
[8] J. Rauch and W. Köhler, Macromolecules **38**, 3571 (2005).

Simulation Tools

This research is one of the projects for SPP1155 “Molecular Modelling and Simulation in Chemical Engineering” of the Deutsche Forschungsgemeinschaft and by the Fonds der Chemischen Industrie.

Molecular dynamics simulations of this research were implemented on the cluster of “transtec” PJ-OPT/HPCF nodes in Prof. Dr. Florian Müller-Plathe’s group, on IBM p690 computers in the Hochschulrechenzentrum of the Technische Universität Darmstadt, and on IBM p690 computers at the John von Neumann Institute for Computing at the Forschungszentrum Jülich.

The simulation software package YASP was developed by Professor Dr. Florian Müller-Plathe’s theoretical physical chemistry group. The package was parallelized by Konstantin Tarmyshov using openMP for shared-memory parallel programming.

Publication Lists

[1] M. Zhang and F. Müller-Plathe, *The Soret effect in dilute polymer solutions: influence of chain length, chain stiffness and solvent quality*, J. Chem. Phys. **125**, 124903 (2006).

[2] M. Zhang and F. Müller-Plathe, *Thermal diffusion studies in realistic molecular liquids and model polymer solutions via reverse non-equilibrium molecular dynamics*, in the proceedings of 7th International Meeting on Thermodiffusion (Mondragon Unibertsitatea, Donostia-San Sebastian, Spain, 2006).

[3] M. Zhang and F. Müller-Plathe, *Reverse non-equilibrium molecular dynamics calculation of the Soret coefficient in liquid benzene/cyclohexane mixtures,* J. Chem. Phys. **123**, 124502 (2005).

[4] M. Zhang, E. Lussetti, L.E.S. de Souza and F. Müller-Plathe, *Thermal conductivities of molecular liquids by reverse non-equilibrium molecular dynamics*, J. Phys. Chem B **109**, 15060 (2005).

Meimei Zhang
Darmstr. 29
64287 Darmstadt

Darmstadt, den 11. Dezember 2006

Eidesstattliche Erklärung

Ich erkläre hiermit an Eides Statt, dass ich meine Dissertation selbständig und nur mit den angegebenen Hilfsmitteln angefertigt habe.

(Meimei Zhang)

Meimei Zhang
Darmstr. 29
64287 Darmstadt

Darmstadt, den 11. Dezember 2006

Erklärung

Ich erkläre hiermit, noch keinen Promotionsversuch unternommen zu haben.

(Meimei Zhang)

Lebenslauf

Name:	**Meimei Zhang**
Date of Birth:	**17. 12. 1976**
Place pf Birth:	**Zhe Jiang, China**
Nationality:	**China**

School

1982 – 1987	**DongFangHong primary school, Zhe Jiang, China**
1987 – 1990	**ChenGuanZhen Junior high school, Zhe Jiang, China**
1990 – 1993	**XinChang high school, Zhe Jiang China**

Study for Bachelor's Degree in Chemistry

1993-1998	**Department of Applied Chemistry, University of Science & Technology of China, Hefei, China**

Study for Master's Degree in Organic Chemistry

1998- 2001	**Research Center for Eco-Environmental Science, The Chinese Academy of Science, Beijing, China**

Study for Master's Degree in Computational Chemistry

2001- 2003	**Department of Chemistry, Science School of Purdue University, Indianapolis, USA**

Study for Doctor's Degree in Physical Chemistry

2003-2005	**School of Engineering and Science, International University Bremen, Germany**
2005-2006	**Department of Chemistry, Technische Universität Darmstadt, Germany**

(Meimei Zhang) **Darmstadt, den 11. Dezember 2006**